BIOMASS VALORIZATION FOR THE PRODUCTION OF VALUE-ADDED CHEMICALS AND BIO-FUELS

DOCTORAL THESIS

Università degli Studi di Messina (Home Institution)

&

L'École Nationale Supérieure de Chimie de Montpellier (Host Institution)

&

TOTAL Research and Technology Feluy (Industrial Partner)

SINCHEM - Sustainable and Industrial Chemistry

Erasmus Mundus - Joint Doctoral Research program

Dottorato di XXIX ciclo in

Ingegneria e Chimica dei Materiali e delle Costruzioni

Coordinatore: Prof. Signorino Galvagno

SSD: CHIM/04, ING-IND/25

Supervisor (Home): Prof.ssa Siglinda PERATHONER

Supervisor (Host): Prof. Francesco DI RENZO

Co-Supervisor (Host): Dr. Nathalie TANCHOUX

by

Atıf Emre DEMET

2014-2017

THÈSE

Pour obtenir le grade de

Docteur

Délivré par **ECOLE NATIONALE SUPERIEURE DE CHIMIE DE MONTPELLIER**

Préparée au sein de l'école doctorale Sciences Chimiques Balard

Et de l'unité de recherche **UMR 5253 CNRS-UM-ENSCM**

Spécialité: **Chimie et Physico Chimie de Matériaux**

Présentée par **ATIF EMRE DEMET**

BIOMASS VALORIZATION FOR THE PRODUCTION OF VALUE-ADDED CHEMICALS AND BIO-FUELS

Soutenue le 03/04/2017 devant le jury composé de

M. Francesco DI RENZO, Directeur de recherche, ICGM-ENSCM	Directeur de thèse
Mme. Siglinda PERATHONER, Professeur, Università di Messina	Directeur de thèse
Mme. Alessandra QUADRELLI, Directeur de recherche, CPE-LYON	Rapporteur
Mme. Sabine VALANGE, Maître de conférences, Université de Poitiers	Rapporteur
M. Gabriele CENTI, Professeur, Università di Messina	Examinateur
M. Francesco BASILE, Professeur, Università di Bologna	Examinateur

The Jury Committee

Prof. Francesco DI RENZO, *ICGM-ENSCM*	Supervisor
Prof. Siglinda PERATHONER, *Università di Messina*	Supervisor
Prof. Alessandra QUADRELLI, *CPE-LYON*	Referee
Prof. Sabine VALANGE, *Université de Poitiers*	Referee
Prof. Gabriele CENTI, *Università di Messina*	Examiner
Prof. Francesco BASILE, *Università di Bologna*	Examiner

The external referees required by Italian regulations;

Prof. Massimo MIGLIORI, *Università di Calabria*	Referee
Prof. Giuseppe Fornasari, *Università di Bologna*	Referee

aileme ve ülkeme...

à ma famille et mon pays...

to my family and my country...

alla mia famiglia e il mio paese...

Acknowledgements

This European PhD project was co-funded through a Sustainable Industrial Chemistry (SINCHEM) Grant. SINCHEM is a Joint Doctorate programme selected under the Erasmus Mundus Action 1 Programme (FPA 2013-0037). The Education, Audiovisual and Culture Executive Agency (EACEA), Erasmus Mundus SINCHEM PhD programme consortium, Universita` degli Studi di Messina, Italy (UniME) as the home institution, L'Ecole Nationale Superieure de Chimie de Montpellier, France (ENSCM) as the host institution and TOTAL Research & Technology Feluy, Belgium (TRTF) as the industrial partner are acknowledged. As a matter of fact, what makes an institution different than a building are the people working there and the culture they build. Therefore, I would like to acknowledge people who I owe my sincere thanks to.

Very special thanks to

DEMET family,

Siglinda Perathoner, Francesco Di Renzo,

Nathalie Tanchoux, Françoise Quignard, Gabriele Centi,

Stefania Albonetti,

Walter Vermeiren, Jean-Pierre Dath, Rita De Luca,

<u>For the administrative assistance;</u>

Francesca Pollicino, Angela Garozzo, Francesca Scribano,

Vasile Hulea, Didier Tichit, Isabelle Girard,

For the technical assistance and trainings;

Paola Lanzafame and Katia Barbera (experimental supports), Salvatore Abate (TPR), Giorgia Papanikolaou (GC), Serena Gentiluomo (AAS),

Gwendoline Gravé (MRS), Olinda Gimello and Pascale Guiffrey (HPLC), Thomas Cacciaguerra (TEM, EDX and XRD), Nathalie Marcotte (UV-VIS), Hugo Petitjean (FT-IR), Géraldine Layrac (Nitrogen Adsorption), Mourad Guermache (IT), Jérémy Rodriguez and Manon Gand (chemicals),

For the fruitful ambiance;

Bhanu Chandra Marepally, Chalachew Mebratu, Maria Freni, Chiara Genovese, Rosalba Passalacqua, Maria Grazia Salvaggio, Leone Frusteri, Claudio Ampelli, Roberto Pizzi, Gianfranco Giorgianni, Shiming Chen, Paolo Delia, Francesco Tavella,

Bilel Said, İsmail Can Oğuz, Chemseddine Menakbi, Erwin Fernandez, Youcef Didi, Elena Voznuik, Gabriele Azzalin, Dilan Karapınar, Nadia Toumi, Claudia Cammarano, Issam Dabbabi, Iqra Zubair Awan, Lotfi Boudjema, Asja Pettignano, Elodie Wan, Laura Vaugon, Arnaud Chaix, Sébastien Blanquer, Oussama Gantassi, Alysson Duarte Rodrigues, Paolo Boscaro, Emilie Molina, Tzonka Mineva and Hazar Guesmi,

Philippe Bodart, Jean-Christophe Raboin, Luis Robles, Laurent Duranel, Pascal Petteau, Alessandro Chieregato, Jean Mazurelle,

Sant'Anna Maria Casella,

Thank you!

Grazie!

Merci!

Teşekkürler!

Abstract (extended)

The ‘energy’ is a paramount term in the micro and macro scale and has a very broad concept. The wealth level and entire economic activities of humankind strongly depend on energy. It drives all the advanced systems that frontier technology has already reached today as it meets our basic needs such as heating, cooling, and lighting. Since the industrial revolution, the demand and supply for energy has been snowballing dramatically and this trend will be continued owing to the increasing world population, and new technologies.

The overwhelming majority of energy supplies come from diminishing fossil fuels that brings several economic, social and environmental problems together. Therefore, the research and technological development in alternative energy sources in particular biomass and biofuels have been increasing, with the goal of providing an alternative, sustainable and renewable source of energy and chemicals.[1] Through bio-refinery, many value added chemicals and fuels can be obtained from biomass.[2] Hence, the transformation of abundant biomass resources into chemicals is quite significant and attractive from the viewpoint of sustainable chemistry.

Annually, 170 billion metric tons of biomass is produced in nature by photosynthesis and composition of terrestrial biomass, which consists of three main components of lignocellulose; cellulose (40–50%), hemicellulose (25–35%) and lignin (15–20%). [3],[4],[5] The kind of biomass used is important for the biofuel categorization, which refers to the first, second, and third generation biofuels, as well as the technique involved in the processing and the final target molecule.[6] In contrast to first and second

generation, the third generation refers to a technology where the entire biomass is saccharified to its sugar components and later sugars by enzymatic and/or catalytic routes to obtain not only bio-ethanol but also an array of many other value-added molecules such as levulinic acid and 5-hydroxymethylfurfural (HMF). Depending on their characteristics, those biomass derived products are considered in three class; directly replaceable (competes against the existing oil-derived ones), novel (possesses new or enhanced properties) and platform molecules (provides diverse portfolio of products from a single intermediate).

Among other primary renewable building blocks, HMF is considered a key versatile platform molecule, for the production of for plastics, pharmaceuticals, fine chemicals, and liquid fuel due to its rich chemistry and potential availability from carbohydrates.[7],[8] In particular, what makes HMF crucial is its oxidation reaction to 2,5-furandicarboxylic acid (FDCA), which is one of the top 12 value added bio-based chemicals suggested by U.S. Department of Energy.[9],[10],[11] FDCA can serve as a substitute for petroleum-derived terephthalic acid in the production of poly (ethylene terephthalate) (PET) plastics due to its similar structure, and the market for virgin PET is currently around 50 million tons per year.[12],[13]

Although HMF and its oxidation products are not manufactured in high volumes yet due to their high production costs, the synthesis and utilization of them are being studied extensively owing to their commercial potential in biorefining strategies.[10],[14] While several methods have been published, efficient conversion of lignocellulosic materials to fuel and value added biochemicals are still to day a challenging proposition.[15],[16] Thus it is imperative to develop the efficiency of existing processes and supply systems for biomass conversion in order biomass-derived chemicals and fuels to be competitive with the cost of ones derived from petroleum.[17],[18],[19] Thus, catalysis is regarded as a key enabling technology for biomass conversion in general.[20]

Although homogeneous catalysts are effective for this reaction, because of the drawback of homogeneous catalytic systems, heterogeneous catalysts can be

employed.[21] In the literature, the use of noble metal based catalysts are more common than non-noble metal catalysts. Nevertheless, more research with non-noble transition metals for the HMF oxidation reactions need to be conducted to understand their catalytic mechanism and also to develop higher performance catalysts with abundant non-noble metals owing to their cheaper price and environmentally benign.

Inorganic materials with spinel structures with are versatile compounds offering tunable composition, structural stability and possibility for bifunctional redox properties. The general formula for spinel compounds is AB_2O_4, in which A^{2+} metal ions occupy the tetrahedral (t_d) sites while the B^{3+} metal ions occupy the octahedral (O_h) sites within the fcc oxygen sublattices in a cubic crystal system.[22] The occupation of metals at T_d and O_h sites have an influence on the spinel properties such as magnetic behavior, conductivity, and catalytic activity etc.[23]

Co-Fe spinels have been shown to be effective oxidation catalysts, for instance for the oxidation of benzyl alcohol to benzaldehyde[24] and the oxidative decomposition of organic pollutants.[25] Cu-Mn spinels have been proposed as catalysts for oxygenate reforming[26],[27] and water gas shift reaction.[28]

In this work, two series of mixed oxide catalysts with nominal composition $M^1_{3-x}M^2_xO_4$ have been synthesized with non-noble metals, wherein M^1=Co and M^2=Fe or M^1=Cu and M^2=Mn, by cost effective co-precipitation method. Each serie consists of 5 catalysts with the cation fractions $M^2/(M^1+M^2)$ of 0.00, 0.33, 0.50, 0.67, 1.00. The catalysts have been characterised using XRD, EDX, N_2 physisorption, FT-IR, UV-VIS, TEM and TPR techniques, then employed in the successive oxidation reactions of biomass derived HMF, to several value added chemicals, which have a diverse portfolio of applications in various industries, including maleic anhydride (MA), 2,5-furandicarboxaldehyde (DFF), 5-Hydroxymethyl-2-furancarboxylic acid (HMFCA), 5-formyl-2-furancarboxylic acid (FFCA) and FDCA, which is essential for future generation of bio-plastics. The oxidation reaction products of HMF were analyzed by HPLC then kinetics study has been performed. The ultimate goal is not only to investigate the correlations between physicochemical properties and catalytic

performances of the aformentioned catalysts on the complex cascade HMF to FDCA oxidation process but also to make a humble contribution to the scientific literature for a sustainable, renewable and greener world.

Mixed oxide catalysts in the Fe-Co and Cu-Mn series were prepared by coprecipitation and calcined at 450 °C. In the Co-Fe system, cubic spinel solid solutions were formed throughout the composition field except for the formation of α-Fe_2O_3 in the absence of cobalt. In the Cu-Mn system, the phase composition evolved with the manganese content from CuO to $Cu_{1.5}Mn_{1.5}O_4$ cubic spinel and Mn_3O_4 tetragonal spinel. Amorphous manganese oxides were present in several Cu-Mn samples and minor Mn_5O_8 was observed in the absence of copper.

Monitoring the products of HMF oxidated by aqueous t-BuOOH in acetonitrile at several temperature levels and retention times allowed to measure activation energies and reaction rates of the individual steps of the oxidation cascade.

As observed in other aqueous-organic mixed solvents, the rates of oxidation of carbonyl and alcohol groups proceed at quite similar rates for the HMF reagent and the primary intermediates. However, the oxidation of carbonyl requires a slightly higher activation energy than the activation of alcohol and the activation energy is much higher for the final reaction, the oxidation of the carbonyl group of the electron-poorer FFCA. Lower activation energies are observed for the unwanted parallel reaction paths, like as the oxydecarbonylation to maleic anhydride and the condensation to oligomers and ultimately to humins. This last process has been shown to follow a complex hydration-condensation path and its global rate is related to the concentration of all carbonyl-bearing species, suggesting that the process is controlled by propagation of the oligomer chain.

Single-component oxides showed a poor specific activity in our conditions with the exception of CuO, itself hampered by its low surface area. Mixed oxides performed significantly better, confirming the importance of internal redox coupling in oxidation catalysts. In the Cu-Mn system, the $Cu_{1.5}Mn_{1.5}O_4$ spinel proved an effective catalyst but the role of residual CuO and amorphous Mn oxides is worth further investigation.

In the Fe-Co system, the high activity of Co-rich mixed spinels is clearly related to their peculiar cation distribution.

Mixed oxides of easily available transition metals are effective heterogeneous catalysts of HMF. The comparison of the activation energies of the different steps of the reaction cascade provides suggestions for the optimal conduction of the biorefinery process.

Keywords: Biomass, valorisation, 5-hydroxymethylfurfural, HMF, 2,5-furandicarboxylic acid, FDCA, spinel, cobalt-iron, copper-manganese

Riassunto (esteso)

"Energia" è un termine di importanza capitale su tutte le scale e rappresenta un concetto molto vasto. Il livello di ricchezza e tutte le attività economiche dipendono dall'energia. Questa indirizza tutti i sistemi e le tecnologie avanzate oltre a sodisfare alle necessità basilari quali riscaldamento, condizionamento e fornire la luce necessaria a tutte le attività umane. A partire dalla revoluzione industriale la rihiesta e la fornitura di energia è stata variabile in funzione anche dell'avvento delle nuove tecnologie nelle diverse parti del mondo.

La situazione odierna dominante per la fornitura di energia deriva dalla diminuzione della richiesta di combustibili fossili. Quindi la ricerca è lo svluppo tecnologico per lo sfruttamento di fonti energetiche alternative è in crescita, specialmente nel campo delle biomasse.[1] L'obiettivo finale è quello di fornire una fonte energetica alternativa e sostenibile sia per l'energia che per la chimica.[2] L'implementazione della bioraffineria nello schema classico di raffineria tradizionale permette quindi di introdurre sia combustibili che intermedi per la chimica fine dalle biomasse.

Annualmente 170 bilioni di tonnellate di biomasse sono prodotte attraverso la fotosintesi clorofilliana. La composizione delle biomasse terrestri (lignocellulosa) consite di 3 componenti principali: Cellulosa (40-50%), emicellulosa (25-35%) e lignina (15-20%).[3],[4],[5] Il tipo di biomassa è fondamentale per la catalogazione dei bio-combustibili ottenuti in bio-combustibili di prima,seconda e terza generazione.[6] A contrario dei primi due metodi di produzione di combustibili, le biomasse di 3° generazione permettono la trasformazione principale in saccaridi e successivamente

la loro trasformazione con metodi enzimatici o catalitici in bio-etanolo ed al molecole ad alto valore aggiunto come per esempio il 5-idrossimetilfurfurale (HMF) o l'acido levulinico. A seconda delle loro caratteristiche questi prodotti derivanti dalle biomasse possono essere catalogate a loro volta in tre classi: direttamente sostituibili (in competizione con prodotti derivanti dal petrolio), innovativi (con proprietà innovative e superiori) e "molecole piattaforma" (permettono da una singola molecola diverse vie di produzione di prodotti ad alto valore aggiunto).

Tra i componenti base rinovabili primari l'HMF è considerato il più versatile per la produzione di materiali polimerici, prodotti farmaceutici e di chimica fine e combustibili liquidi, grazie alla sua versatilità di produzione da carboidrati.[7],[8] Di particolare importanza è l'ossidazione dell'HMF a FDCA, che viene considerato dall'U.S. Department of Energy uno dei 12 più importanti composti ad elevato valore aggiunto prodotto da biomasse.[9],[10],[11] L'FDCA rappresenta un importante sostituto dell'acido tereftalico per la preparazione di plastiche come il PET, il cui mercato si aggira a 50 Milioni di tonnellate annue.[12],[13]

Sebbene l'HMF ed i suoi prodotti di ossidazione non siano ancora preparati su larga scala a causa degli alti costi di produzione, la loro sintesi ed il loro utilizzo rappresentano un potenziale economico nelle strategie di bio-raffineria.[10],[14] Mentre molte metodologie di sintesi sono state pubblicate, un'efficiente conversione di materiale ligno-cellulosico a combustibili ed intermedi per la produzione chimica rappresentano tutt'ora una sfida.[15],[16] Quindi è di fondamentale importanza l'aumento dell'efficienza dei processi esistenti per rendere competitivi i prodotti derivanti dalla trasformazione delle biomasse con quelli derivanti dal petrolio. La catalisi viene considerata quindi la chiave del successo.[20]

Possono essere utilizzati sia catalizzatori omogenei che eterogenei ed in letteratura vengono riportati come attivi e selettivi principalmente catalizzatori a base di metalli nobili.[21] Nonostante questa evidenza, c'è attualmente la necessità di focalizzare l'attenzione sull'utilizzo di metalli di transizione non-nobili, possibilmente

"abbondanti" sulla crosta terrestre e di basso impatto per l'ambiente ed il contatto umano.

A tal proposito, materiali inorganici a struttura spinello rappresentano una classe interessante di composti con composizione modulabile, stabilità strutturale e possibilità di avere proprietà redox bifunzionali. La formula generale per un composto a struttura spinello è AB_2O_4, per la quale lo ione metallico A^{2+} occupa una posizione tetraedrica (T_d), mentre lo ione metallico B^{3+} occupa la posizione ottaedrica (O_h) all'interno del reticolo cristallino in un sistema cubico.[22] La presenza di metalli bi-e trivalenti in posizione tetraedrica ed ottaedrica influenzano in particolare le proprietà magnetiche, di conducibilità e catalitiche di questi materiali.[23]

Le strutture a spinello a base di Co-Fe sono note come catalizzatori di ossidazione, per esempio nell'ossidazione dell'alcol benzilico a benzaldeide[24] e nella decomposizione ossidativa di inquinanti organici.[25] Gli spinelli Cu-Mn sono invece stati proposti come catalizzatori per il reforming[26],[27] e per la WGSR.[28]

In questa tesi, due serie di catalizzatori a base di ossidi misti con composizione nominale $M^1_{3-x}M^2_xO_4$ sono stati sintetizzati con metalli non nobili, in cui M^1=Co e M^2=Fe o M^1=Cu e M^2=Mn, con il metodo della co-precipitazione. Ogni serie è composta da 5 catalizzatori con rapporti tra i cationi pari a $M^2/(M^1+M^2)$ 0.00, 0.33, 0.50, 0.67, 1.00. I catalizzatori sono stati caratterizzati attraverso tecniche XRD, EDX, fisisorbimento di N_2, FT-IR, UV-VIS, TEM e TPR, e successivamente testati nelle reazioni di ossidazione del 5-idrossimetilfurfurale (HMF) derivante da biomasse a diversi intermedi ad elevato valore aggiunto, che hanno importanti applicazioni in vari settori dell'industria chimica, tra cui l'anidride maleica (MA), la 2,5-furandicarboxaldeide (DFF), l'acido 5-idrossimetil-2-furancarbossilico (HMFCA), e l'acido 5-formil-2-furancarbossilico (FFCA) e l'acido 2,5-furandicarbossilico (FDCA), che è importante come un sostituto alternativo all'acido tereftalico derivato da materie prime fossili per la produzione di polietilenetereftalato (PET). I prodotti di reazione derivanti dall'ossidazione del HMF sono stati analizzati mediante HPLC ed è stato eseguito un approfondito studio cinetico. L'obiettivo finale è stato non solo

quello di trovare una correlazione tra proprietà fisico-chimiche ed attività catalitica dei catalizzatori presi in esame per la complessa trasformazione dell'HMF a FDCA, ma anche quello di dare un contributo consistente ai processi chimici industriali alla base di uno sviluppo sostenibile della società.

Gli ossidi misti delle due serie a base di Fe-Co e Cu-Mn sono stati preparati per coprecipazione, essicati e calcinati a 450 °C. Per i sistemi Fe-Co si è potuta rilevare in tutto il campo di composizione la presenza della struttura spinello cubica, eccetto per il catalizzatore preparto in assenza di Co, dove si è invece osservata la fase alfa-Fe_2O_3. Invece nel sistema Cu-Mn la composizione delle fasi ha mostrato un'evoluzione in funzione del contenuto di manganese da CuO a $Cu_{1.5}Mn_{1.5}O_4$ come spinello cubico e Mn_3O_4 come spinello tetragonale. In più ossidi di Mn amorfi sono stati rivelati in molti campioni Cu-Mn come anche minori quantità di Mn_5O_8 sono state osservate nei campioni senza rame.

Rilevando i prodotti di ossidazione dell' HMF in soluzione acquosa di t-BuOOH e acetonitrile a diverse temperature ha permesso di calcolare le energie di attivazione e le velocità di reazione per ogni step di reazione.

Come osservato per altri solventi misti acqua/organico le velocità di ossidazione dei gruppi carbonilici ed alcolici procedono in maniera simile per la trasformazione dell'HMF che per gli intermedi primari. Anche se l'ossidazione dei carbonili richiede una maggiore energia di attivazione dei gruppi alcolici, l'energia di attivazione maggiore è riportata per la reazione finale.

Gli ossidi a singoli componenti hanno mostrato in ogni caso una minore attività specifica nelle nostre condizioni, con eccezione del CuO, nonostante la sua basse area superficiale. Gli ossidi misti hanno mostrato un'attività decisamente superiore, confermando l'importanza delle coppie redox interne a catalizzatori di ossidazione. Nel sistema Cu-Mn lo spinello $Cu_{1.5}Mn_{1.5}O_4$ ha mostrato un'attività elevata nonostante la presenza di CuO residuo e di ossidi di manganese amorfi debba essere chiarita

ulteriormente. Nei sistemi Fe-Co l'attività degli spinelli misti ricchi in Co dipende chiaramente dalla peculiare distribuzione cationica.

Ossidi misti contenenti metalli di transizione non critici hanno dimostrato di essere catalizzatori attivi nell'ossidazione dell'HMF. Il confronto delle energie di attivazione per i singoli stadi del complesso "processo a cascata" permette di ottenere utili informazioni per una conduzione ottimale del processo di bio-raffineria.

Parole chiave: valorizzazione, biomassa, 5-idrossimetilfurfurale, HMF, acido 2,5-furandicarbossilico, FDCA, catalizzatori a struttura spinello, cobalto-ferro, rame-manganese.

Résumé (étendu)

L'énergie est un terme primordial à l'échelle micro et macro et a un concept très large. Le niveau de richesse et les activités économiques entières de l'humanité dépendent fortement de l'énergie. Elle est le moteur de tous les systèmes avancés développés grâce aux technologies de pointes car il répond à nos besoins fondamentaux tels que le chauffage, le refroidissement et l'éclairage. Depuis la révolution industrielle, la demande et l'offre d'énergie ont changé de façon spectaculaire et cette tendance se poursuivra en raison de la croissance de la population mondiale et des nouvelles technologies.

L'écrasante majorité des approvisionnements énergétiques proviennent de la consommation des combustibles fossiles qui impliquent plusieurs problèmes économiques, sociaux et environnementaux. Par conséquent, la recherche et le développement technologique des sources d'énergie alternatives, en particulier la biomasse et les biocarburants, ont augmenté, dans le but de fournir une source d'énergie renouvelable et alternative, et de produits chimiques.[1] Grâce à la bio-raffinerie, de nombreux produits chimiques et combustibles à valeur ajoutée peuvent être obtenus à partir de la biomasse.[2] Par conséquent, la transformation des ressources en biomasse abondantes en produits chimiques est assez importante et attrayante du point de vue de la chimie durable.

Annuellement, 170 milliards de tonnes de biomasse sont produites dans la nature par la photosynthèse et décomposition de la biomasse terrestre, qui se compose de trois composantes principales de lignocellulose: cellulose (40-50%), hémicellulose (25-35%) et lignine (15-20%).[3],[4],[5] Le type de biomasse utilisé est important pour la catégorisation des biocarburants, qui se réfère aux biocarburants de première, deuxième et troisième génération, ainsi que la technique impliquée dans le traitement et la molécule cible finale.[6] Contrairement à la première et à la deuxième génération, la troisième génération fait référence à une technologie où la biomasse entière est saccharifiée à ses composants sucres et sucres postérieurs par des voies enzymatiques et / ou catalytiques pour obtenir non seulement du bioéthanol mais aussi un panel de beaucoup d'autres produits à valeur ajoutée comme l'acide lévulinique et le 5-hydroxyméthylfurfural (HMF). Selon leurs caractéristiques, ces produits dérivés de la biomasse sont considérés dans trois catégories; directement substituable (rivalisant avec les dérivés issus du pétrole existant), nouvelles (possédant des propriétés nouvelles ou améliorées) et des molécules plates-formes (offrant un portefeuille diversifié de produits à partir d'un seul intermédiaire).

Parmi les autres blocs de construction renouvelables primaires, le HMF est considéré comme une molécule plate-forme polyvalente, pour la production de matières plastiques, de produits pharmaceutiques, de produits chimiques fins et de carburant liquide en raison de sa richesse chimique et de sa disponibilité potentielle à partir des hydrates de carbone.[7],[8] En particulier, ce qui rend le HMF crucial, c'est sa réaction d'oxydation en acide 2,5-furandicarboxylique (FDCA), qui est l'un des 12 principaux produits chimiques à valeur ajoutée bio suggérés par le Département américain de l'énergie.[9],[10],[11] Le FDCA peut servir de substitut à l'acide téréphtalique dérivé du pétrole dans la production de plastiques poly (éthylène téréphtalate) (PET) en raison de sa structure similaire et le marché du PET vierge est actuellement d'environ 50 millions de tonnes par an.[12],[13]

Bien que le HMF et les produits de son oxydation ne soient pas encore fabriqués à des volumes élevés, en raison de leurs coûts de production élevés, la synthèse et l'utilisation de ceux-ci font l'objet d'études approfondies en raison de leur commercialisation potentiel dans les stratégies de bioraffinage.[10],[14] Alors que plusieurs méthodes ont été publiées, la conversion efficace des matériaux lignocellulosiques en carburant et en produits biochimiques à valeur ajoutée est encore aujourd'hui une proposition difficile [15],[16]. Il est donc impératif de développer l'efficacité des procédés existants et des systèmes d'approvisionnement pour la conversion de la biomasse afin que les produits chimiques dérivés de la biomasse et les combustibles soient compétitifs par rapport au coût des produits dérivés du pétrole.[17],[18],[19] Ainsi, la catalyse est considérée comme une technologie clé facilitant la conversion de la biomasse en général.[20]

Bien que des catalyseurs homogènes soient efficaces pour cette réaction, en raison de l'inconvénient des systèmes catalytiques homogènes, on peut utiliser des catalyseurs hétérogènes.[21] Dans la littérature, l'utilisation de catalyseurs à base de métaux nobles est plus fréquente que les catalyseurs métalliques non nobles. Néanmoins, de plus amples recherches avec des métaux de transition non nobles pour les réactions d'oxydation de HMF doivent être conduites pour comprendre leur mécanisme catalytique et aussi pour développer des catalyseurs de performance supérieure avec des métaux non nobles abondants en raison de leur prix moins élevé et respectueux de l'environnement.

Matériaux inorganiques avec des structures de spinelle avec sont des composés polyvalents offrant composition réglable, la stabilité structurelle et la possibilité de propriétés rédox bifonctionnelles. La formule générale des composés spinelles est AB_2O_4, dans laquelle les ions métalliques A^{2+} occupent les sites tétraédriques (t_d) tandis que les ions métalliques B^{3+} occupent les sites octaédriques (O_h) dans les sous-réseaux d'oxygène fcc dans un système de cristaux cubiques.[22] L'occupation des métaux aux sites Td et Oh a une influence sur les propriétés des spinelles telles que le comportement magnétique, la conductivité et l'activité catalytique, etc...[23]

On a montré que les spinelles de Co-Fe sont des catalyseurs d'oxydation efficaces, par exemple pour l'oxydation de l'alcool benzylique en benzaldéhyde [24] et la décomposition oxydante des polluants organiques [25]. Les spinelles Cu-Mn ont été proposés comme catalyseurs pour le reformage oxygéné [26],[27] Et réaction de changement de gaz d'eau.[28]

Dans ce travail, deux séries de catalyseurs à oxyde mixte de composition nominale $M^1_{3-x}M^2_xO_4$ ont été synthétisées avec des métaux non nobles, dans laquelle M^1=Co et M^2=Fe ou M^1=Cu et M^2=Mn, par une méthode de co-précipitation rentable. Chaque série se compose de 5 catalyseurs avec les fractions cationiques $M^2/(M^1+M^2)$ de 0,00, 0,33, 0,50, 0,67, 1,00. Les catalyseurs ont été caractérisés en utilisant les techniques XRD, EDX, N_2 physisorption, FT-IR, UV-VIS, TEM et TPR, puis utilisés dans les réactions d'oxydation successives de la HMF dérivée de biomasse, en plusieurs produits chimiques à valeur ajoutée, (DFF), l'acide 5-hydroxyméthyl-2-furancarboxylique (HMFCA), l'acide 5-formyl-2-furancarboxylique (FFCA) et le FDCA, Ce qui est essentiel pour la future génération de bio-plastiques. Les produits de réaction d'oxydation de HMF ont été analysés par CLHP puis une étude cinétique a été réalisée. Le but ultime est non seulement d'étudier les corrélations entre les propriétés physico-chimiques et les performances catalytiques des catalyseurs mentionnés sur le processus d'oxydation en cascade complexe de HMF à FDCA, mais aussi d'apporter une contribution modeste à la littérature scientifique pour un monde durable, renouvelable et plus vert.

Des catalyseurs d'oxydes mixtes dans les séries Fe-Co et Cu-Mn ont été préparés par coprécipitation et calcinés à 450 °C. Dans le système Co-Fe, des solutions solides de spinelle cubique ont été formées dans tout le champ de la composition sauf pour la formation d'α-Fe_2O_3 en l'absence de cobalt. Dans le système Cu-Mn, la composition de phase a évolué avec la teneur en manganèse de CuO en spinelle cubique $Cu_{1.5}Mn_{1.5}O_4$ et en spinelle tétragonale Mn_3O_4. Des oxydes de manganèse amorphes étaient présents dans plusieurs échantillons de Cu-Mn et des Mn5O8 mineurs ont été observés en l'absence de cuivre.

La surveillance des produits de HMF oxydés par du t-BuOOH aqueux dans de l'acétonitrile à plusieurs niveaux de température et de temps de rétention, permet de mesurer les énergies d'activation et les vitesses de réaction des différentes étapes de la cascade d'oxydation.

Comme on l'a observé dans d'autres solvants mixtes aqueux-organiques, les taux d'oxydation des groupes carbonyle et alcool ont lieu à des vitesses tout à fait semblables pour le réactif HMF et les intermédiaires primaires. Cependant, l'oxydation du carbonyle nécessite une énergie d'activation légèrement supérieure à celle de l'activation de l'alcool et l'énergie d'activation est beaucoup plus élevée pour la réaction finale, c'est à dire l'oxydation du groupe carbonyle du FFCA plus pauvre en électrons. Des énergies d'activation inférieures sont observées pour les chemins de réaction parallèles indésirables, tels que l'oxydécarbonylation en anhydride maléique et la condensation en oligomères et finalement aux humines. On montre que ce dernier processus suit une voie d'hydratation-condensation complexe et sa vitesse globale est liée à la concentration de toutes les espèces porteuses de carbonyles, ce qui suggère que le procédé est contrôlé par propagation de la chaîne oligomère.

Les oxydes monocomposants présentaient une mauvaise activité spécifique dans nos conditions, à l'exception de CuO, lui-même entravé par sa faible surface. Les oxydes mixtes se sont révélés significativement meilleurs, confirmant l'importance du couplage rédox interne dans les catalyseurs d'oxydation. Dans le système de Cu-Mn, la spinelle de $Cu_{1.5}Mn_{1.5}O_4$ s'est révélée être un catalyseur efficace, mais le rôle du CuO résiduel et des oxydes de Mn amorphes mérite d'être approfondi. Dans le système Fe-Co, la forte activité des spinelles mixtes riches en Co est clairement liée à leur distribution de cations particulière.

Les oxydes mixtes de métaux de transition facilement disponibles sont des catalyseurs hétérogènes efficaces de HMF. La comparaison des énergies d'activation des différentes étapes de la cascade de réaction fournit des suggestions pour la conduction optimale du procédé de bioraffinage.

Mots-clés: Biomasse, valorisation, 5-hydroxyméthylfurfural, HMF, acide 2,5-furandicarboxylique, FDCA, spinelle, cobalt-fer, cuivre-manganèse

Contents

List of Figures

List of Tables

Chapter 1 Introduction

1.1 Overview to biomass valorisation

Energy is at the heart of all economic activity of humankind and drives transport, communication and computer systems in addition to our basic needs such as heating.[29] Due to the increasing energy demand as seen in Figure 1.1, the research and technological development in biomass and biofuels have been increasing in the last decades, with the ultimate goal of providing an alternative, sustainable and renewable source of energy and chemicals for a greener world. [30]

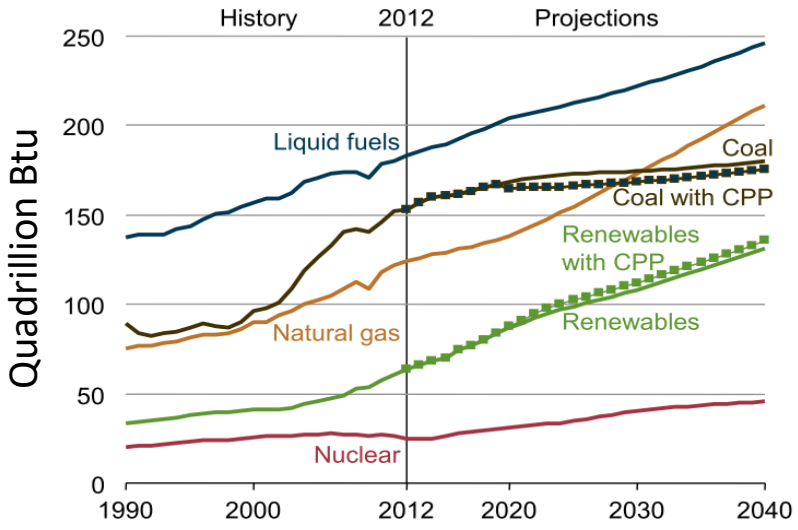

Figure 1.1. Total world energy consumption in quadrillion Btu by energy source, 1990–2040. (Dotted lines show projected effects of the U.S. Clean Power Plan.) [30]

Notwithstanding biomass energy in different ways has been utilizing since ancient times, its significance has recently re-discovered due to the economic, political and environmental concerns associated with diminishing fossil fuel reserves.[31] The

potential threat posed by climate change, due to high emission levels of greenhouse gases, has become a major stimulus for renewable energy sources in general.[1] Thus, biomass represents an abundant carbon-neutral renewable resource and its enhanced use would address several challenges.[32] Through bio-refinery, many value added chemicals and fuels can be obtained from biomass.[2] Hence, the transformation of abundant biomass resources into chemicals is quite significant and attractive from the viewpoint of sustainable chemistry.

Being sustainable means emitting roughly the same amount of carbon during conversion as is taken up during plant growth. As illustrated in Figure 1.2, the use of biomass neither affect the natural C-CO_2 cycle nor contribute to a build-up of CO_2 in the atmosphere; while fossil fuels do, and so add to the increase in greenhouse gases.

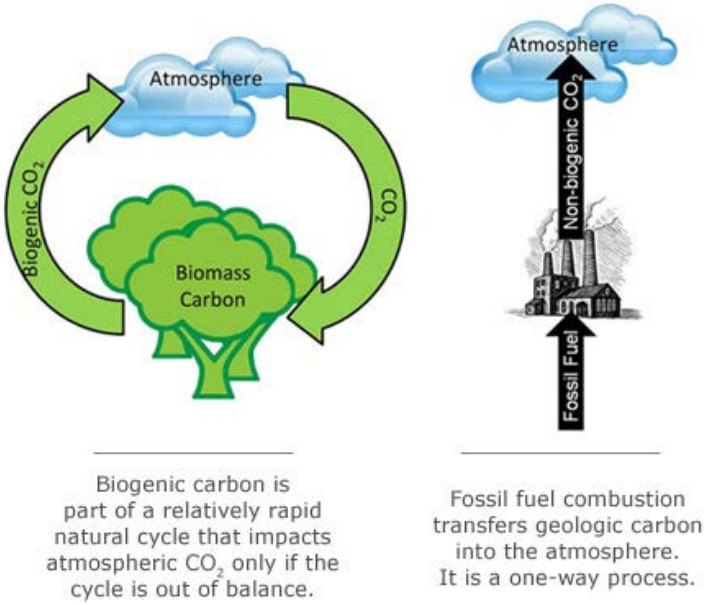

Figure 1.2. The natural C-CO_2 cycle (Washington Forest Protection Association)

In addition, a major advantage of biomass is that it can be produced almost everywhere in the world depending on the crops and agricultural waste of each region. This characteristic can be specifically important for the sustainability of developing economies which can reduce transportation costs and become self-sufficient.[33]

Annually, 170 billion metric tons of biomass is produced in nature by photosynthesis and composition of terrestrial biomass consists of carbohydrates (sugars, cellulose and hemicellulose), lignin, proteins and lipids (oils and fatty acids). The three main components of lignocellulose are cellulose (40–50%), hemicellulose (25–35%) and lignin (15–20%) as illustrated in Figure 1.3, with the relative proportions of the three dependent on the material source as presented in Table 1.1.[3],[4],[5]

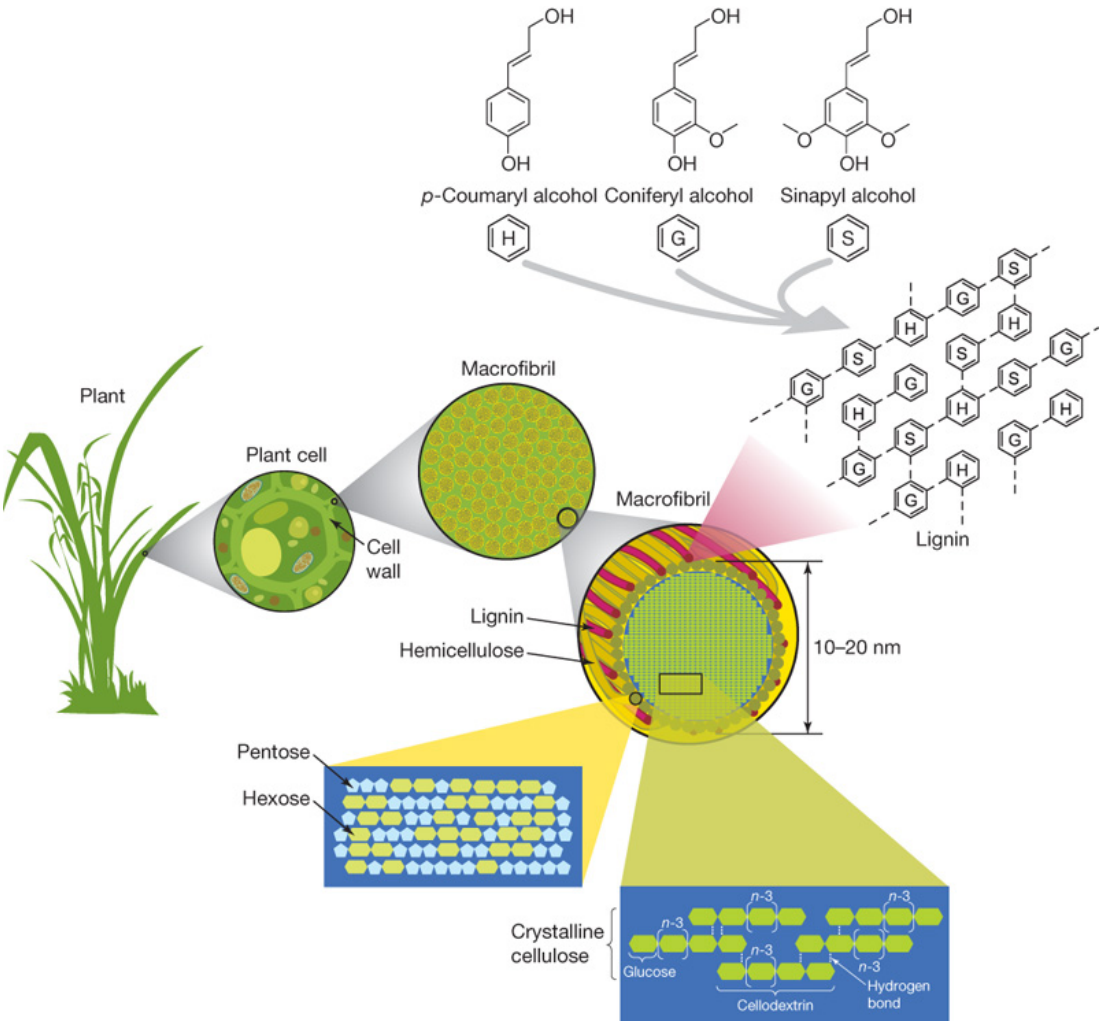

Figure 1.3. The structure of lignocellulose [4]

Table 1.1. Composition of various lignocellulosic feedstock [11]

Material	Cellulose	Hemicellulose	Lignin
Grasses	25–40	25–50	10–30
Hardwoods	45 ± 2	30 ± 5	20 ± 4
Hardwood barks	22–40	20–38	30–55
Softwoods	42 ± 2	27 ± 2	28 ± 3
Softwood barks	18–38	15–33	30–60
Cornstalk	39–47	26–31	3–5
Wheat straw	37–41	27–32	13–15
Chemical pulp	60–80	20–30	2–10
Sorghum stalks	27	25	11
Corn stover	38–40	28	7–21
Coir	36–43	0.15–0.25	41–45
Bagasse	32–48	19–24	23–32
Rice straw	28–36	23–28	12–14
Wheat straw	33–38	26–32	17–19
Barley straw	31–45	27–38	14–19
Sorghum straw	32	24	13

The kind of biomass used is important for the biofuel categorization, which refers to the first, second, and third generation biofuels, as well as the technique involved in the processing and the final target molecule.[6] In contrast to first and second generation, the third generation refers to a technology where the entire biomass is saccharified to its sugar components and later sugars by enzymatic and/or catalytic routes to obtain not only bio-ethanol but also an array of many other value-added

molecules such as levulinic acid and 5-hydroxymethylfurfural (HMF) as seen in Figure 1.4. Depending on their characteristics, those biomass derived products are considered in three class; directly replaceable (competes against the existing oil-derived ones), novel (possesses new or enhanced properties) and platform molecules (provides diverse portfolio of products from a single intermediate).

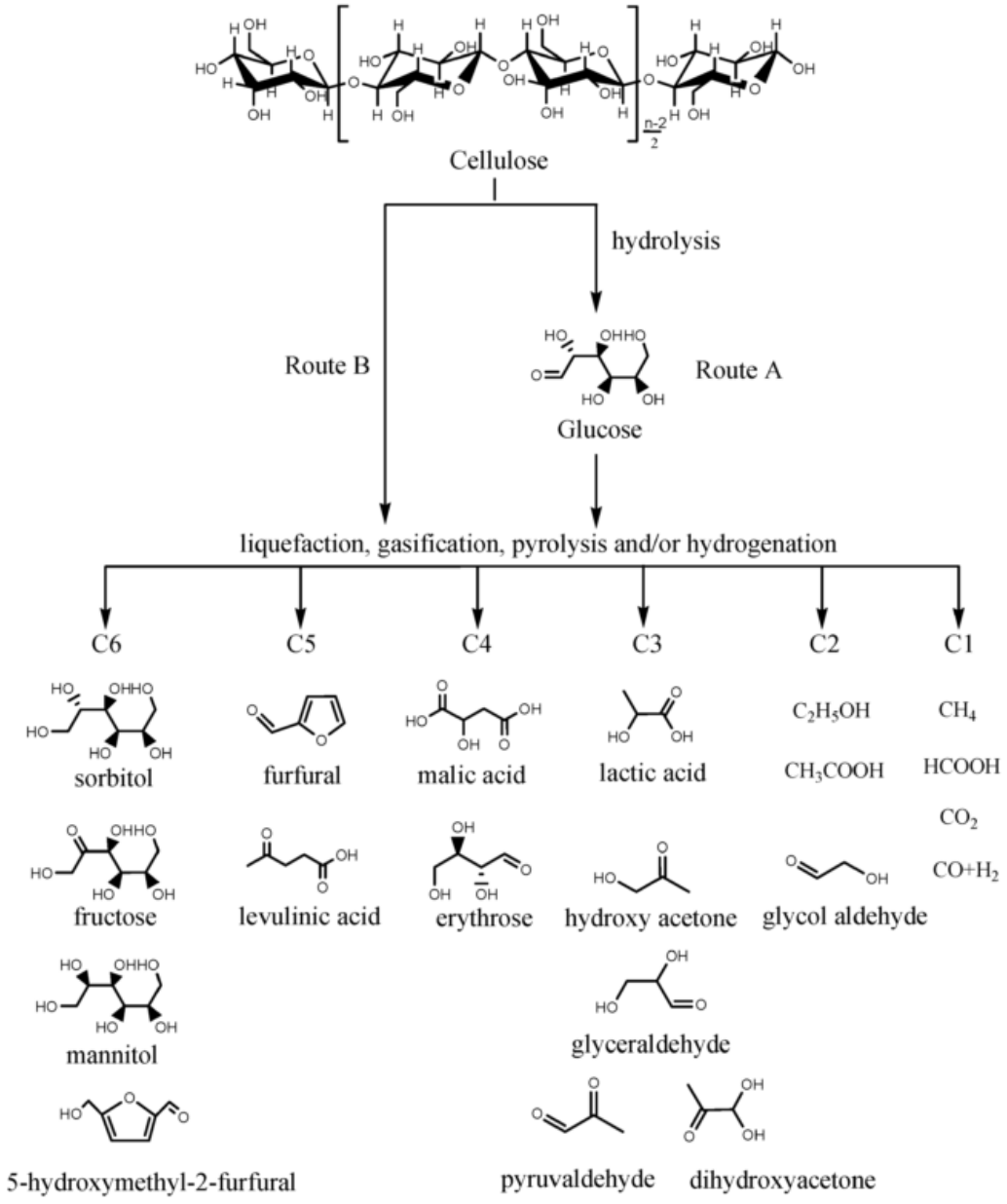

Figure 1.4. Potential chemicals and fuels from the catalytic conversion of cellulose.[34]

Figure 1.5 depicts an analogous model of a biobased product flow-chart for biomass feedstock obtained by effective screening tool using the concepts employed in traditional petrochemical industry.[9] This comprehensive flow-chart assist to apprehend the importance of biomass conversion process from feedstocks to end products used in various industries.

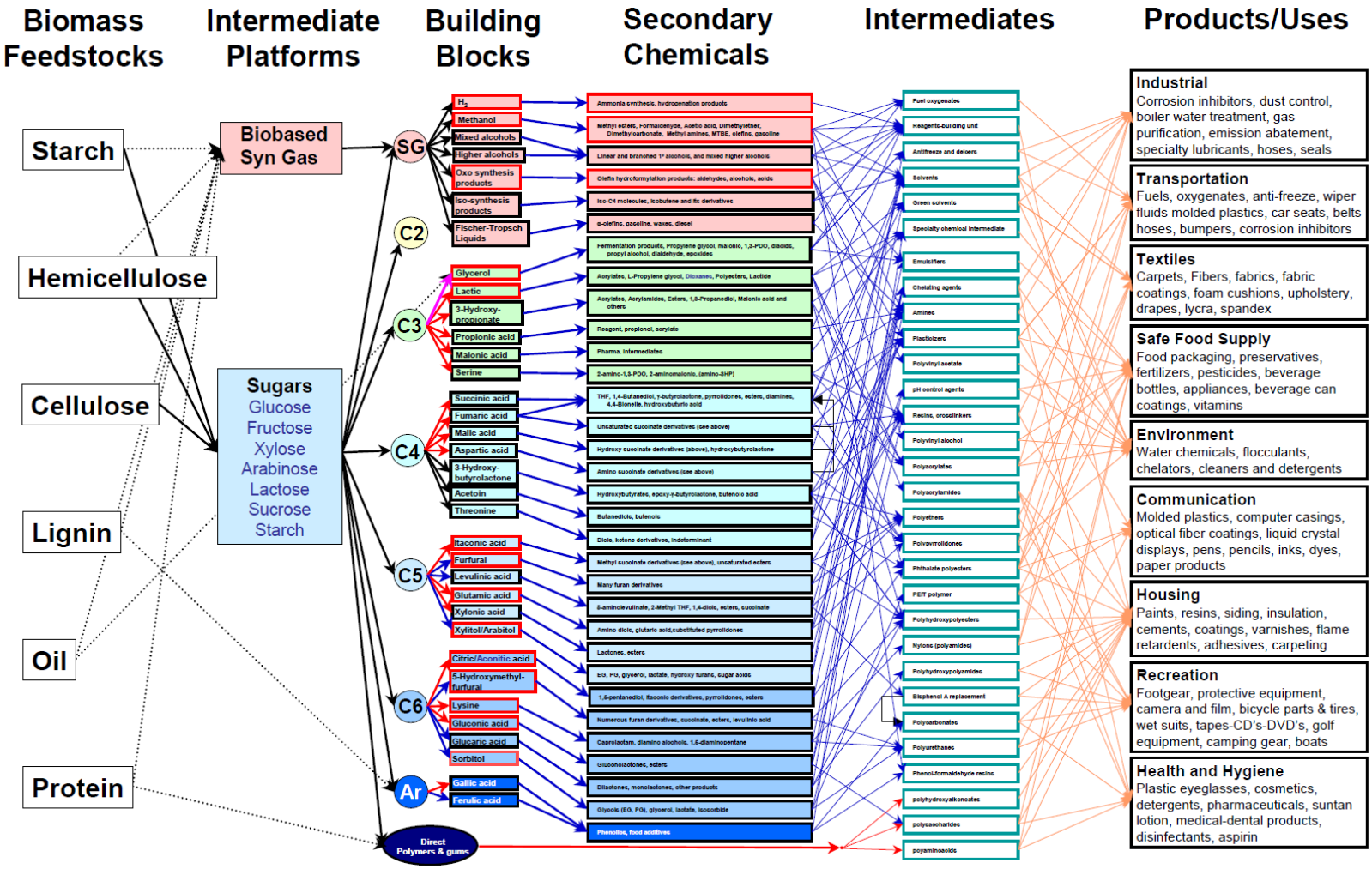

Figure 1.5. Analogous model of a biobased product flow-chart for biomass feedstock [9]

1.2 Big data approach on patent literature in catalytic conversion of lignocellulosic biomass

In this section, due to the confidentiality issues only limited number of results, are presented, belong to the PhD candidate's work that has been conducted for TOTAL Research and Technology Feluy, Belgium during the 3 months of professionalization period.

A patent is an intellectual property right for a technical invention in any field of technology and is issued by authorized bodies to inventors to make use of, and exploit their inventions for a limited period of time. The usefulness of patent literature for many researcher is either unknown or underestimed.[35] Contrarily, patent literature is a huge pool of technical knowledge as big as non-patent literature. According to World Intellectual Property Indicators 2016, the number of worldwide patent application in 2015 reached to 2.8 millions with 7.8 % of growth rate in comparison to the previous year and statistics in the field of chemistry is shown in Figure 1.6.[36] On the other hand, it is also a worthy source used for in order to understand the trends of a specific technology and to provide intelligence which can assist to improve future strategies for key stakeholders in small and large companies and academia.

Field of technology	2005	2010	2014	Share (%), 2014	Average growth (%), 2005-14
Chemistry					
Organic fine chemistry	56,673	54,383	58,235	2.5	0.3
Biotechnology	38,550	39,275	50,423	2.1	3.0
Pharmaceuticals	73,295	71,423	90,242	3.8	2.3
Macromolecular chemistry, polymers	27,610	28,527	41,096	1.7	4.5
Food chemistry	23,066	28,277	57,365	2.4	10.7
Basic materials chemistry	38,720	44,598	70,519	3.0	6.9
Materials, metallurgy	29,329	37,642	58,033	2.5	7.9
Surface technology, coating	27,874	33,073	40,498	1.7	4.2
Micro-structural and nano-technology	2,161	3,446	4,710	0.2	9.0
Chemical engineering	33,636	37,301	53,183	2.2	5.2
Environmental technology	21,021	25,918	36,955	1.6	6.5

Figure 1.6. Patent applications worldwide by field of chemical technologies [36]

"Big data" refers to datasets whose size is beyond the ability of typical database software tools to capture, store, manage, and analyze.[37] Therefore, Big Data approach, with a fairly large number of (250-10,000) articles, can help identify emerging trends, improve business decision making and develop new revenue-making strategies.[38],[39]

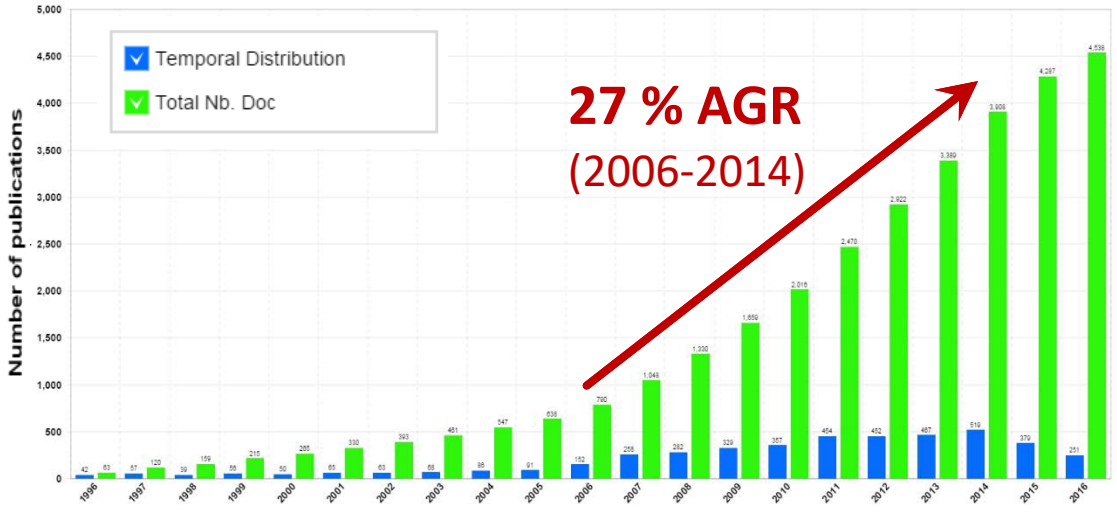

Figure 1.7. Number of patent families per earliest priority year (1996-2016)

A big data IP study on catalytic conversion of lignocellulosic biomass (CCLB) has been conducted with 4,538 of patents over the last two decades. In Figure 1.7 and Figure 1.8, respectively, illustrate the temporal distribution and geographic coverage of patenting activity related to the patent families included in the selected dataset of CCLB. Due to the delay between the filing of patents and the publication by patent offices, usually taking place 18 months later, the last complete year of information is 2014.[40] Therefore, it can be said that the interest in CCLB has been continuously increasing. The annual growth rate (AGR) between 2006 and 2014 is about 27 %.

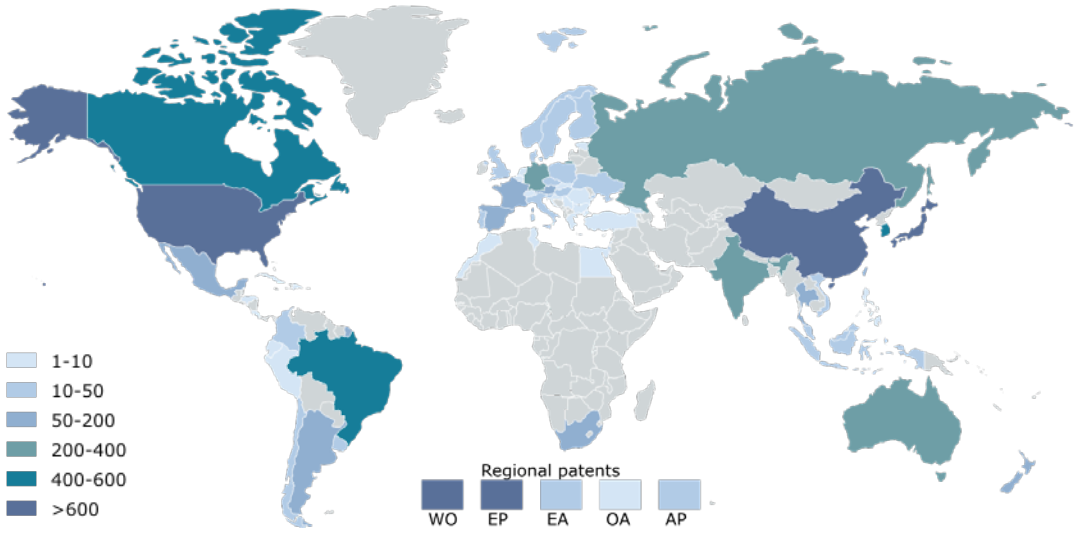

Figure 1.8. Geographic coverage of patent families in the field of LBCC

The most frequent 20 industrial processes for catalytic conversion of lignocellulosic biomass routes are ranked in Figure 1.9. The most frequent process is pyrolysis which deals with whole lignocellulosic biomass leading to upgradeable platforms such as syn-gas and bio-oil.[5] The importance of oxidation, condensation and hydrolysis processes can be considered as crucial for CCLB.

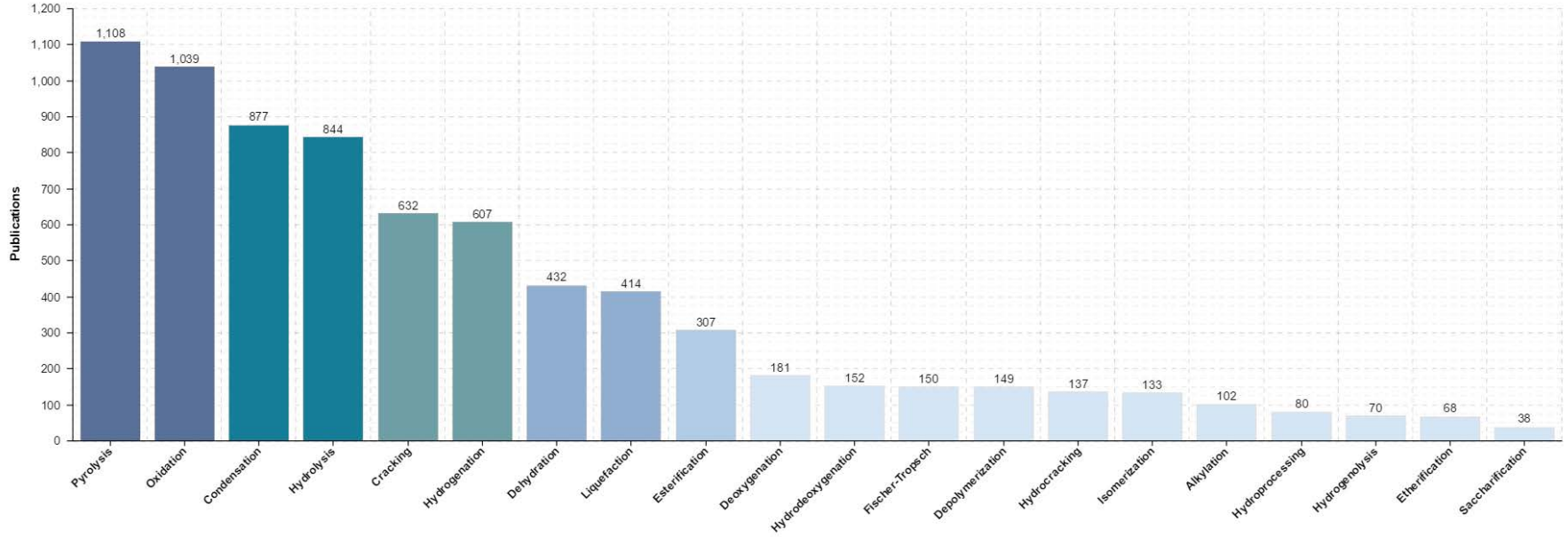

Figure 1.9. The most frequent 20 processes for catalytic conversion of lignocellulosic biomass

Figure 1.10 shows the number of patent families related to the top 30 intermediate platforms and building blocks with different carbon atoms. Considering that aromatic products possibility remain with greater than a 60-billion-pound market, it is not unexpected to be ranked first among the biomass derived products.[41] However it is interesting to observe that furfurals related to an equivalent number

of publications as glucose, which is one of the most important main sugars. In addition to other sugars, presence of an array of platform molecules like, such as hydroxymethylfurfural (HMF), levulinic and succinic acids, sorbitol, among those top 30 products highlights the significance of platform molecules. In the meanwhile, the attention on ethylene glycol and 2,5-furandicarboxylic acid (FDCA), which are polyethylene furanoate (PEF) made from, implies that new generation of bio-polymers will outperform fossil fuel derived conventional PET polymers in the very near future. [42],[43]

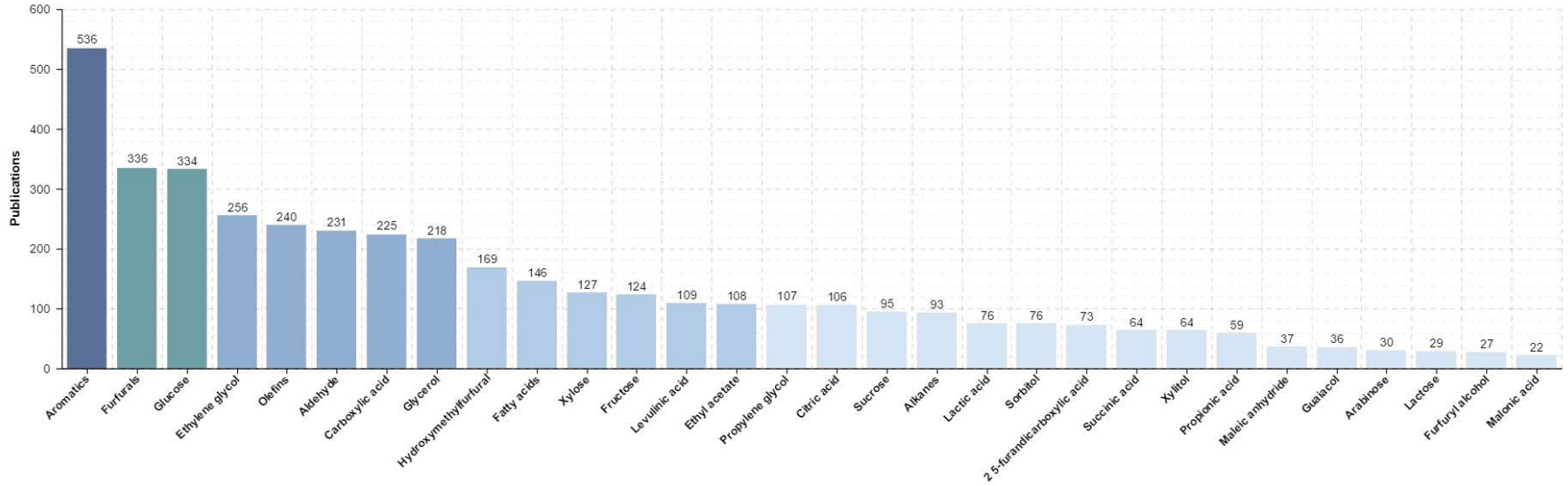

Figure 1.10. The top 30 biomass derived products obtained by CCLB

Figure 1.11 displays the most commonly used 30 transition metals which are contained in catalysts for lignocellulosic biomass conversion. The attention on non-noble metals such nickel, iron, cobalt, copper and manganese rather than many nobel metals is quite positive for the green chemistry.

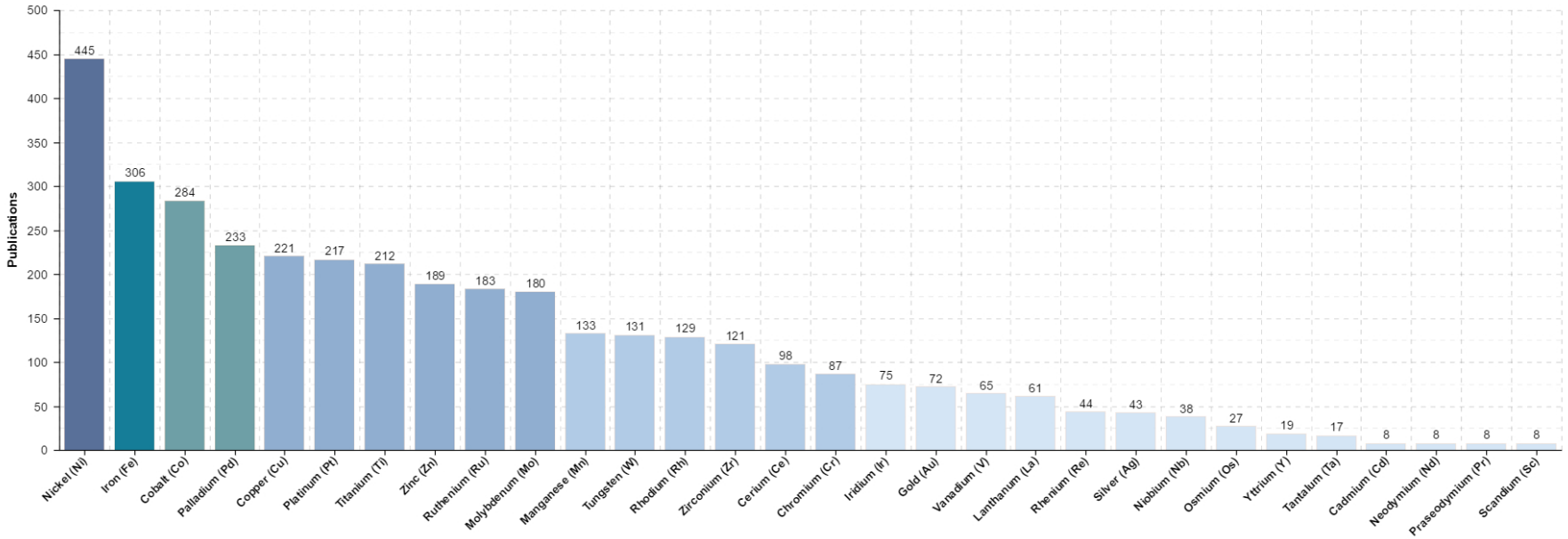

Figure 1.11. The most frequent 30 transition metals which are contained in catalysts for lignocellulosic biomass conversion

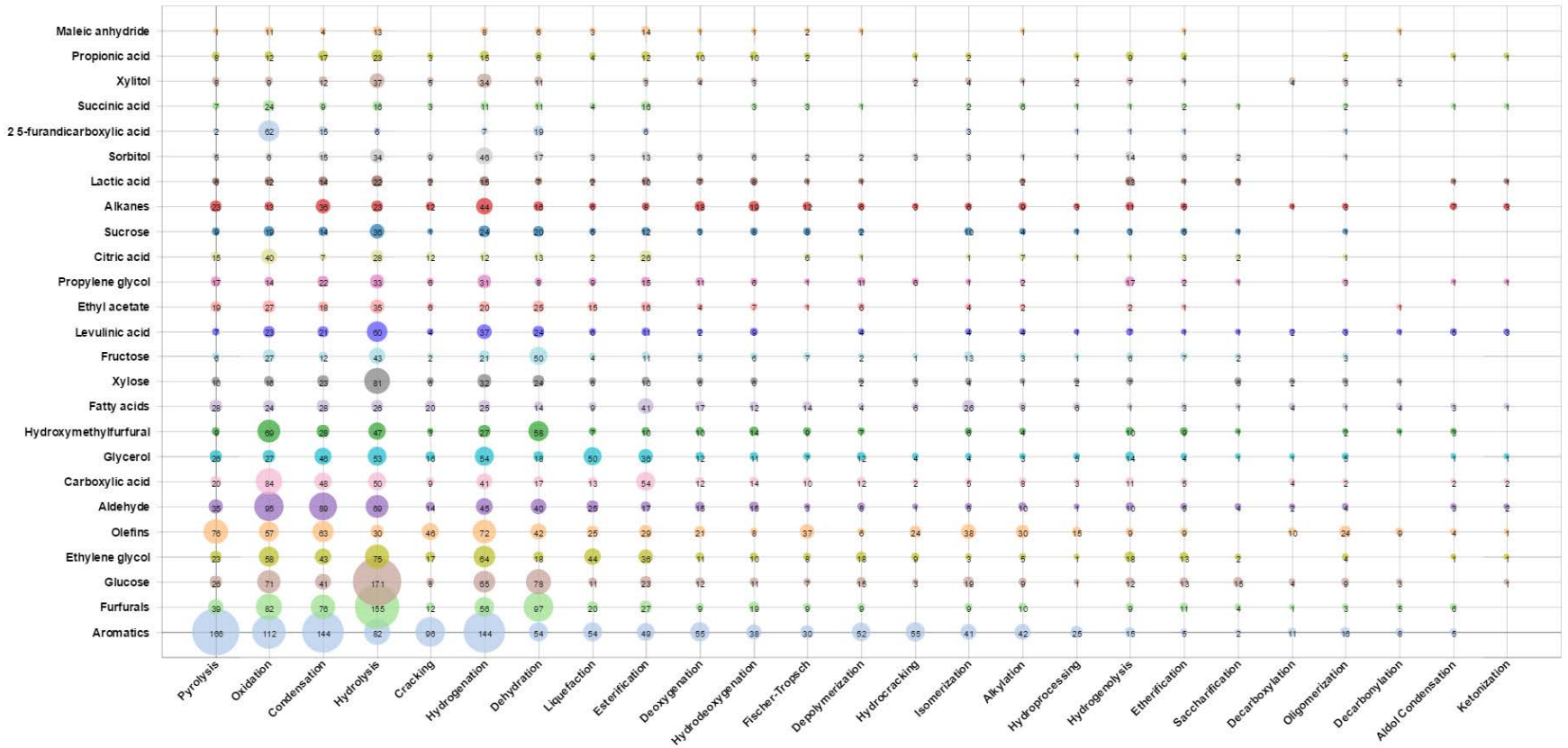

Figure 1.12. The top 25 biomass conversion processes (x-axis) versus the top 25 biomass derived products (y-axis)

Figure 1.12 not only illustrates the relation between the top 25 biomass conversion processes (x-axis) versus the top 25 biomass derived products (y-axis) but also explains the relation, which is between two important bio-products HMF and FDCA, is oxidation.

Figure 1.13 and Figure 1.14 provide a general idea about the correlations between the type of biomass conversion processes (or biomass derived products) and transition metals contained in the catalysts used for those processes.

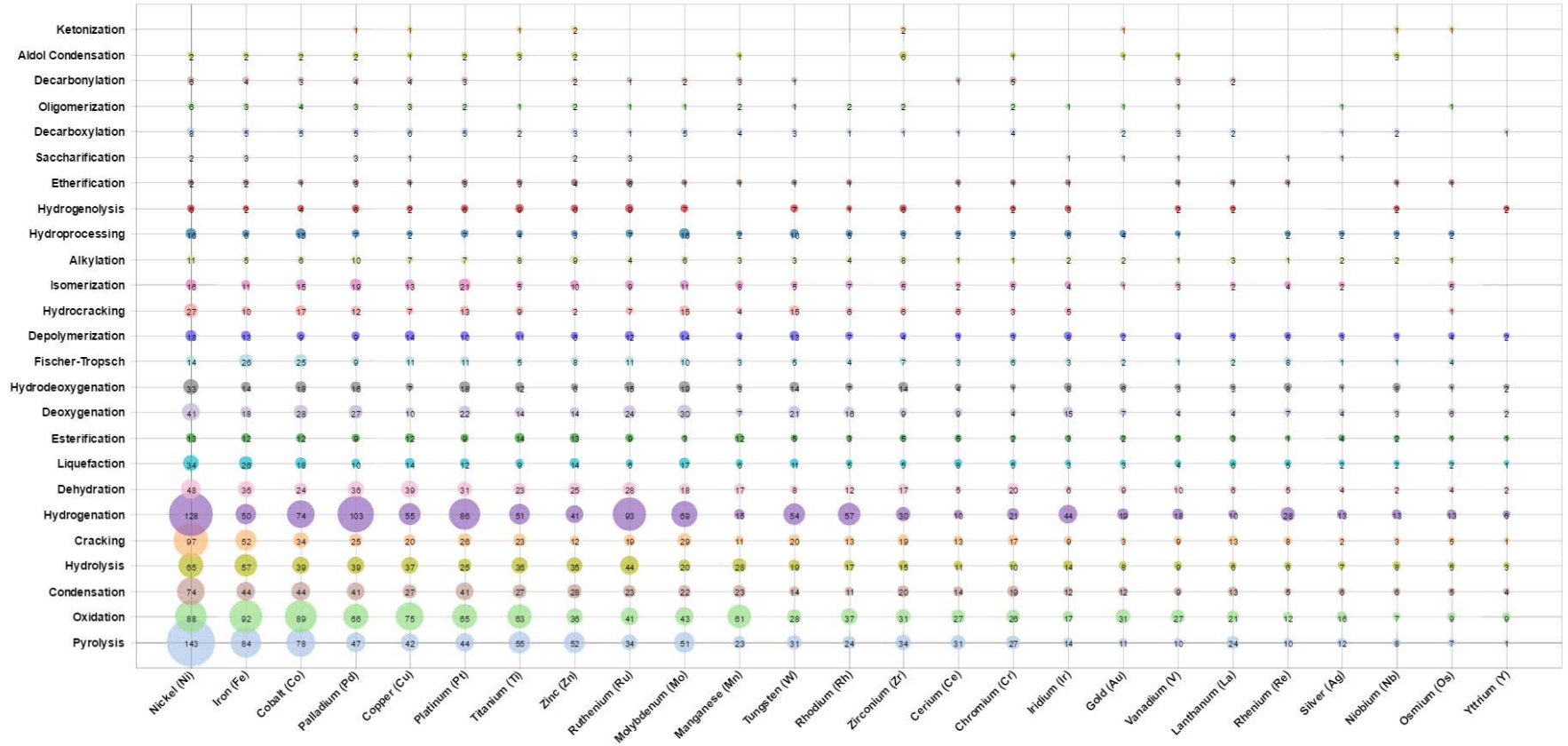

Figure 1.13. The top 25 transition metals which are contained in catalysts (x-axis) versus the top 25 biomass conversion processes (y-axis)

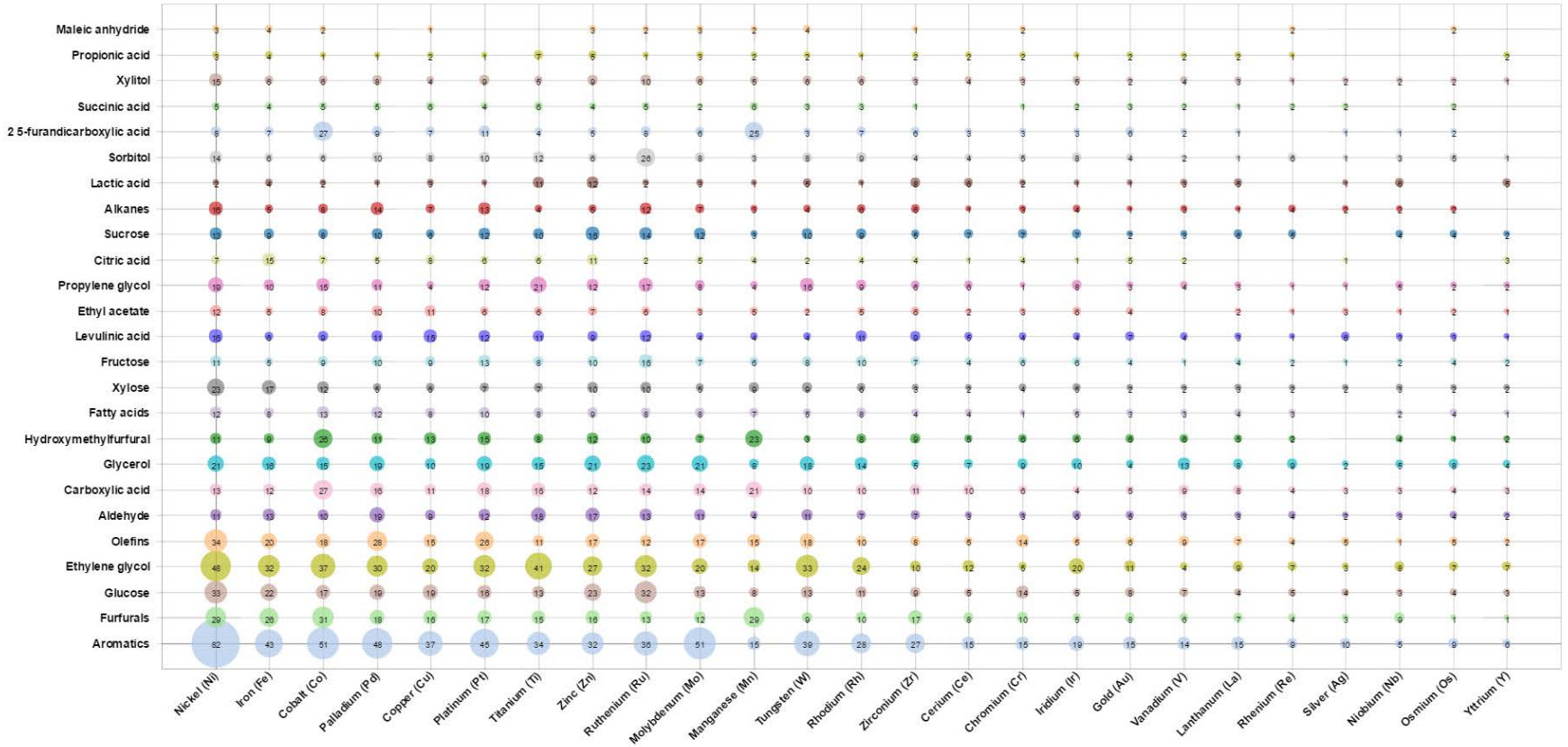

Figure 1.14. The top 25 transition metals which are contained in catalysts (x-axis) versus the top 25 biomass derived products (y-axis)

Hence, Figure 1.13 and Figure 1.14 statistically suggest that the oxidation reaction between HMF and FDCA would be catalyzed by some non-noble transition metals such as Fe, Co, Cu and Mn.

1.3 HMF and its oxidation products

5-hydroxymethylfurfural is an heterocyclic furanic compound with hydroxide and aldehyde functional groups as illustrated in Figure 1.15.[44] Among other primary renewable building blocks, HMF is considered a key versatile platform molecule for the production of for plastics, pharmaceuticals, fine chemicals, and liquid fuel due to its rich chemistry and potential availability from carbohydrates such as fructose, glucose, sucrose, cellulose and inulin.[7],[8]

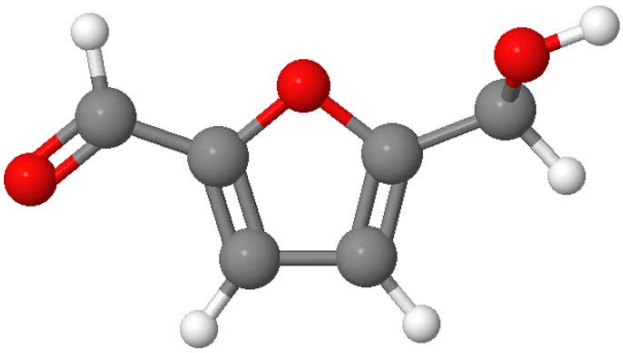

Figure 1.15. Chemical structure of HMF

Having α,ω-bifunctional molecule with substituents in both the 2 and 5 positions allows HMF to be converted to a dicarboxylic acid or a diol by oxidation or reduction reactions and both products can be used for the synthesis of polymers. HMF can also be upgraded to fuel molecules via hydrogenation due to being a relatively unsaturated aromatic compound.[45] Additionally, the heterocyclic structure of furans can be found in an array of biologically active molecules with pharmaceutical applications.

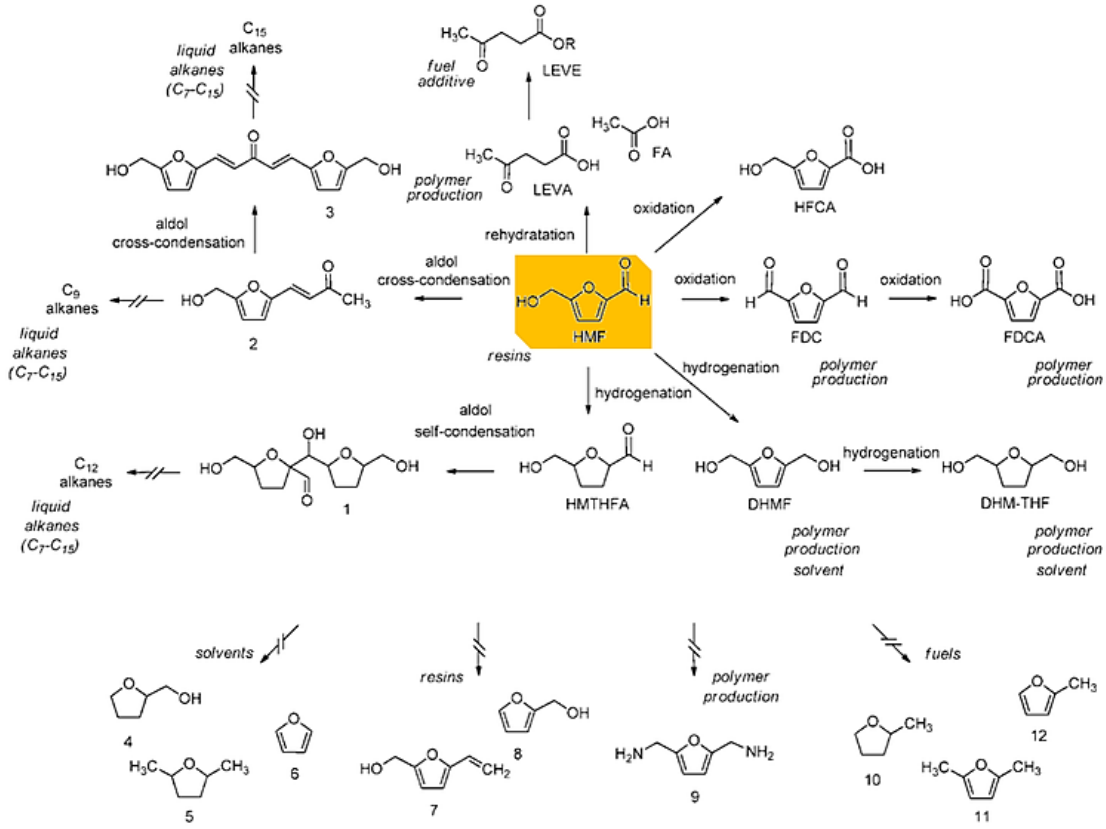

Figure 1.16. As a platform molecule hydroxymethylfurfural and its derivatives [10]

LEVA, levulinic acid; **LEVE**, levulinic ester; **FA**, formic acid; **HFCA**, 5-hydroxymethylfuroic acid; **FDC**, 2,5-furandicarboxyaldehyde; **FDCA**, 2,5-furandicarboxylic acid; **DHMF**, 2,5-di(hydroxymethyl)furan; **DHM-THF**, 2,5-di(hydroxymethyl)tetrahydrofuran; **HMTHFA**, 5-(hydroxymethyl)tetrahydrofuran-2-carbaldehyde; **1**, 2-(hydroxy(5-(hydroxymethyl)tetrahydrofuran-2- yl)methyl)-5-(hydroxymethyl)tetrahydrofuran-2-carbaldehyde; **2**, (E)-4-(5-(hydroxymethyl)furan-2-yl)but-3-en-2-one; **3**, (1E,4E)-1,5-bis(5-(hydroxymethyl)furan-2-yl)penta-1,4-dien-3-one; **4**, tetrahydrofurfuryl alcohol; **5**, 2,5-dimethyltetrahydrofuran; **6**, furan; **7**, 2-hydroxymethyl- 5-vinylfuran; **8**, furfuryl alcohol; **9**, 2,5-di(aminomethyl)furan; **10**, 2-methyl tetrahydrofuran; **11**, 2,5-dimethylfuran; 12, 2-methylfuran) [10]

Figure 1.16 illustrates a diverse portfolio of products obtained from HMF and explains why *Bozell* has published an updated evaluation in which HMF was mentioned among "Top 10+4" as additions to the original list of U.S. Department of Energy's top 12 value added bio-based chemicals that suggests FDCA as one of them.[9],[10],[11]

As 2,5-furandicarboxylic acid can serve as a substitute for petroleum-derived terephthalic acid in the production of poly (ethylene terephthalate) (PET) plastics, due to its similar structure as shown in Figure 1.17, and the market for virgin PET is currently around 50 million tons per year, the oxidation reactions of HMF would be stated as the most important pathway of HMF in particular.[12],[13]

Figure 1.17. Structural similarity in formulas of terephthalic acid and 2,5-furandicarboxylic acid [46]

Figure 1.18 presents the potential products of oxidation reactions of HMF which generate several value added chemicals such as maleic anhydride (MA), 2,5-furandicarboxaldehyde (DFF) and 5-Hydroxymethyl-2-furancarboxylic acid (HMFCA), then 5-formyl-2-furancarboxylic acid (FFCA) and finally FDCA. Aforementioned products can be used for plenty number of different applications. For instance, MA and its derivatives are widely employed to synthesize unsaturated polyester resins, agricultural chemicals, food additives, lubricating oil additives, pharmaceuticals, while DFF is used as a starting material for the synthesis of ligands, drugs, antifungal agents and so forth.[47],[48]

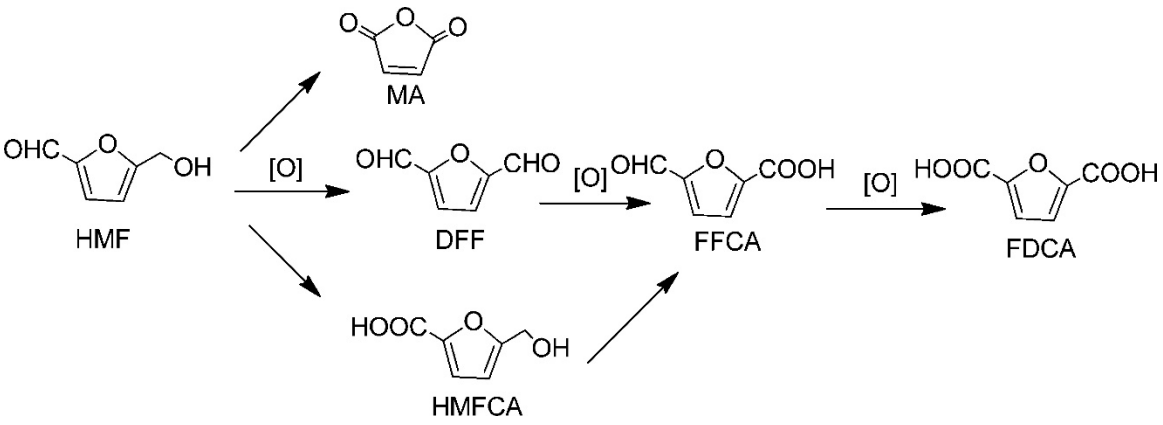

Figure 1.18. Schematic illustration of the potential oxidation products during the oxidation of HMF [47]

Although HMF and its oxidation products are not manufactured in high volumes yet due to their high production costs, the synthesis and utilization of them are being studied extensively owing to their commercial potential in biorefining strategies.[10],[14]

1.4 Spinel oxides catalysis

While several methods have been published, efficient conversion of lignocellulosic materials to fuel and value added biochemicals are still to day a challenging proposition [15],[16]. Thus it is imperative to develop the efficiency of existing processes and supply systems for biomass conversion in order biomass-derived chemicals and fuels to be competitive with the cost of ones derived from petroleum.[17],[18],[19] Biomass conversion processes should follow the 12 principles of green chemistry, such as to utilize waste and by-products as raw materials, increase atom efficiency, utilize as much as possible from the biomass feed, minimize energy consumption, and maximize the selectivity to the desired products.[19] Thus, catalysis is regarded as a key enabling technology for biomass conversion in general.[20] The main goal in the field of catalysis, in terms of green chemistry, is to develop environmentally benign, practical, clean, economical, and efficient processes for catalyst separation and recycling [49].

According to the patent and non-patent literature, HMF can be oxidized to FDCA through DFF, HMFCA and FFCA intermediates via various catalysts similar to the other reactions for lignocellulosicc biomass conversion. Although homogeneous catalysts are effective for this reaction, because of the drawback of homogeneous catalytic systems, heterogeneous catalysts can be employed.[21] In the literature, the use of noble metal based catalysts are more common than non-noble metal catalysts. Nevertheless, more research with non-noble transition metals for the HMF oxidation reactions need to be conducted to understand their catalytic mechanism and also to develop higher performance catalysts with abundant non-noble metals owing to beintheir cheaper price and environmentally benign.

Solid catalysts are quite sophisticated products derived from chemical precursors by several different techniques and procedures.[50] Since specific catalytic properties of heterogeneous catalysts can be strongly affected by every step of the preparation (precipitation, filtration, washing, calcination …etc.) together with the experimental conditions such as pH, temperature as much as quality of the raw materials. The

magnetic particles obtained from magnetic transition metals, which are non-noble, (iron, nickel and cobalt) oxidized readily are more stable against oxidation [51]. For example cobalt ferrite, $CoFe_2O_4$, is an interesting material with an spinel structure that can readily be prepared by co-precipitation method.[52] Inorganic materials with spinel structures with are versatile compounds offering tunable composition, structural stability and possibility for bifunctional redox properties. The general formula for spinel compounds is AB_2O_4, in which A^{2+} metal ions occupy the tetrahedral (t_d) sites while the B^{3+} metal ions occupy the octahedral (O_h) sites within the fcc oxygen sublattices in a cubic crystal system.[22] In Figure 1.19 demonstrates the unit cell of spinel structure contains T_d sites, O_h sites and oxygen atoms are represented by green, yellow and red spheres, respectively. The occupation of metals at T_d and O_h sites have an influence on the spinel properties such as color, magnetic behavior, conductivity, and catalytic activity etc.[23]

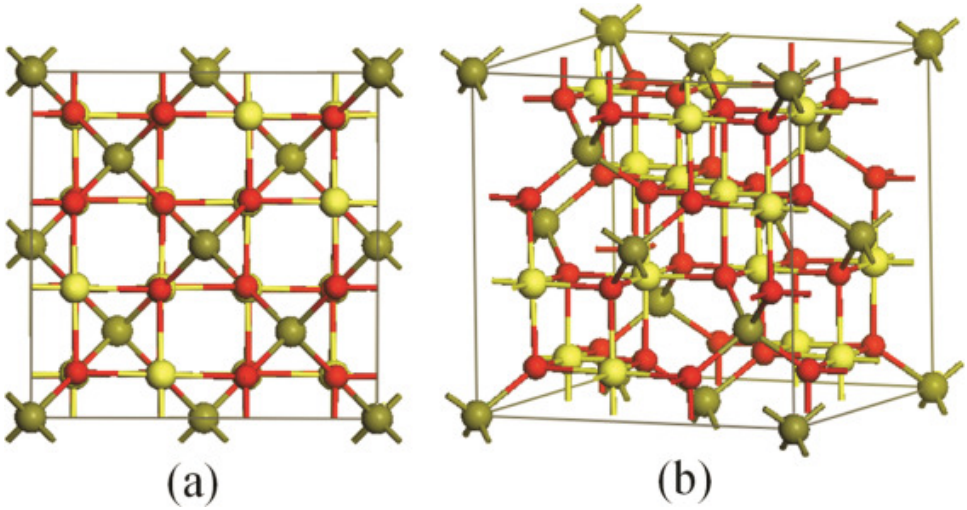

Figure 1.19. The spinel structure projected along (a) [100] direction and (b) a free direction. T_d sites, O_h sites and oxygen atoms are represented by green, yellow and red spheres, respectively[23]

In our work, two series of Co-Fe and Cu-Mn oxide catalysts in $M^1_{3-x}M^2_xO_4$ spinel structure have been synthesized by cost effective co-precipitation method. Each set of catalysts, consist of 5 catalysts and $M^2/(M^1+M^2)$ ratio, have been characterized by various experimental techniques, and employed in the successive oxidation reactions of HMF towards FDCA, as schematized in Figure 1.18.

Chapter 2 The Methods and Materials

2.1 Experimental techniques

X-ray diffraction (XRD)

XRD measurements were carried out at room temperature by a Bruker D8 Advance diffractometer with a Bragg-Brentano configuration and equipped with a Bruker Lynx Eye detector using a Ni-filtered Cu anode as the X-ray source (Kα, λ = 1.5405 Å). The catalysts were analyzed between 5-70° (2θ) with a step size of 0.0197° angle and a step of acquiring time 1 second. The parameters refined were zero shift (2θ), background, cell parameters and peak shape. Crystallite size values were calculated from Williamson-Hall plots[53] for monophasic samples and the Scherrer method[54] for multiphasic samples from the full width at half maximum intensity measurements.

Energy dispersive X-ray (EDX)

EDX analyses were performed by a SEM EDS FEI Quanta 200F, run with 15 kV of accelerating voltage, in which samples were under vacuum conditions (0.38 Torr) at room temperature.

Nitrogen physisorption

N_2 adsorption and desorption volumetry at 77 K were performed by a Micromeritics TRISTAR apparatus with improved vacuum system. The aerogels and oxides were preactivated at, respectively, 50 and 250°C under vacuum (0.5 Pa) for 6 hours to remove the water contained in the solid and free of porosity. The surface area of a sample was evaluated by the Brunauer-Emmett-Teller (BET) analysis method[55] and

the α_S method was used in a search for microporosity. The mesopore size distribution was calculated by a DFT kernel.[56]

Fourier transform infrared spectroscopy (FT-IR)

FT-IR measurements between 400-800 cm^{-1} in transmittance mode were carried on using a Bruker Vector 22 improved by Attenuated total reflection (ATR)[57] apparatus with OPUS software.

Ultraviolet–Visible spectroscopy (UV-VIS)

UV-VIS measurements were carried on using Quartz Hellma 106-QS precision cells with 0.1 mm of light path by a Perkin Elmer Lambda 40 with 250-1100 nm of wavelength range, 60 nm/min of scan speed and 2nm of slit width. $BaSO_4$ was used as the reference. The spectra were converted into the Kubelka-Munkfunction[58] in order to obtain Tauc plot[59] for the determination of band gap energies.[60]

Temperature programmed reduction (TPR)

H_2-TPR measurements were performed by a Micromeritics AutoChem-II 2920 equipped with a TCD detector. The mixture of an oxide catalyst and SiC, in the proper ratio (1:4), was first pretreated with He at 150 ^oC for 90 min prior to the analysis using 5% H_2 in Ar from room temperature to 850 °C with a ramp 20 °C/min.

Transmission electron microscopy (TEM)

Transmission electron micrographs were obtained with a JEOL 1200 EX II.

High performance liquid chromatography (HPLC)

The reaction products were analyzed using a Shimadzu LC-20AD equipped with Bio-Rad 125-0131 Cartridge Holder (30 mm x 4.6 mm) and Bio-Rad Aminex HPX-87H (300 mm × 7.8 mm) pre-packed column. A 0.005 M H_2SO_4 mobile phase was employed as eluent at stabilized 30 °C with a flow rate of 0.6 mL/min for 60 minutes. UV detector at 254 nm was employed. After the injection (2 µl) of each sample, blank measurements have been run in order not only to clean the column but also to verify if it is ready for the next analysis.

2.2 Materials

Cobalt (II) chloride (*$CoCl_2$*) (97.0%), iron (III) nitrate nonahydrate (*$Fe(NO_3)_3{\cdot}9H_2O$*) (98.0%), iron (III) chloride hexahydrate (*$FeCl_3{\cdot}6H2O$*) (98.0%), copper (II) chloride dehydrate (*$CuCl_2{\cdot}H_2O$*) (99.0%), manganese (II) nitrate tetrahydrate (*$Mn(NO_3)_2{\cdot}4H_2O$*) (97.0%), sodium hydroxide (*NaOH*) (97.0%), 5-hydroxymethylfurfural (*HMF*) (98.0%), tert-butyl hydroperoxide (*t-BuOOH*) (purum, ca. 5.5 M in decane over molecular sieves 4 ˚A), acetonitrile (*MeCN*) (99.9%), decane (99.9%), methanol (*MeOH*) (99.8%), maleic anhydride (*MA*) (99.0%), 2,5-furandicarboxylic acid (*FDCA*) (97.0%), 2,5-furandicarboxaldehyde (*DFF*) (97.0%), were purchased from Sigma-Aldrich. 5-Hydroxymethyl-2-furancarboxylic acid (*HMFCA*) and 5-formyl-2-furancarboxylic acid (*FFCA*) were purchased from Abcr and TCI Chemicals, respectively. All the reagents were used without further purification.

2.3 Preparation of catalysts

Two series of mixed oxide catalysts with nominal composition $M^1_{3-x}M^2_xO_4$ have been synthesized with non-noble metals, wherein M^1=Co and M^2=Fe or M^1=Cu and M^2=Mn, by cost effective co-precipitation method as illustrated in Figure 2.1. Each serie consists of 5 catalysts with the cation fractions $M^2/(M^1+M^2)$ of 0, 0.33, 0.50, 0.67, 1.

During preparation of the catalysts, the procedure for the synthesis of nanoparticulate $CoFe_2O_4$ spinel catalysis suggested by *Ballarini et al.* [22] was followed with some minor differences. For $CoFe_2O_4$, where the Fe/(Co+Fe) ratio is 0.67, 50 ml of 0.5 M of $CoCl_2$ and 50 ml of 1 M of $Fe(NO_3)_3{\cdot}9H_2O$ aqueous solutions were mixed then added dropwise into 0.8 M of NaOH at room temperature under 2 hours of stirring. A precipitate was observed on addition of the Fe^{3+} and Co^{2+} solution to NaOH with the color of the solution changing from brown to dark-brown indicative of spinel formation. The solid was isolated by vacuum filtration and washed with demineralized water to remove the Na^+ and NO_3^- then dried in air at 120 °C for overnight and calcined at 450 °C for 6 hours. As NaOH is the precipitation agent, all syntheses carried out in basic media where the pH was kept 12. For Cu-Mn set of catalysts, appropriate amount of $CuCl_2{\cdot}H_2O$ and $Mn(NO_3)_2{\cdot}4H_2O$ precursors have been used. The

stoichiometric calculations have been made, then the procedure mentioned above was applied for other catalysts of the Co-Fe and Cu-Mn series with different Fe/(Co+Fe) or Mn/(Cu+Mn) ratios, in Table 2.1 and Table 2.2.

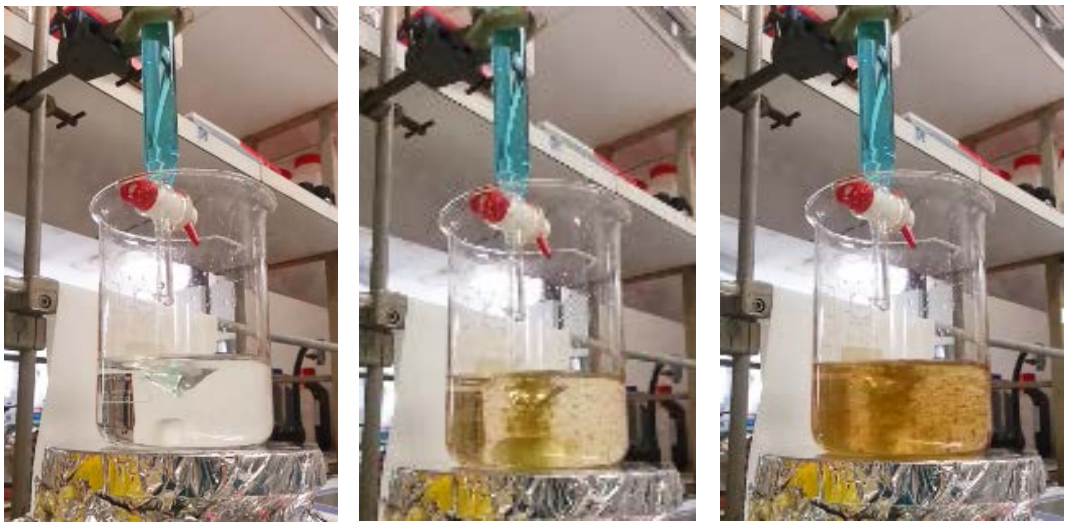

Figure 2.1. Synthesis by coprecipitation method

Table 2.1. The stoichiometric calculations for the catalysts of the Co-Fe serie

Fe/(Co+Fe)	Metal	Precursor	Molarity (mol/L)	Volume (mL)	Mole (mmol)	AW of metal (g/mol)	MM of precursor (g/mol)	Calcination Temperature (°C)
0.00	Co	CoCl2	0.5	150.0	75.0	58.93	129.84	450
	Fe	Fe(NO3)3.9H2O	1.0	-	-	55.85	404.00	
0.33	Co	CoCl2	0.5	100.0	50.0	58.93	129.84	450
	Fe	Fe(NO3)3.9H2O	1.0	25.0	25.0	55.85	404.00	
0.50	Co	CoCl2	0.5	75.0	37.5	58.93	129.84	450
	Fe	Fe(NO3)3.9H2O	1.0	37.5	37.5	55.85	404.00	
0.67	Co	CoCl2	0.5	50.0	25.0	58.93	129.84	450
	Fe	Fe(NO3)3.9H2O	1.0	50.0	50.0	55.85	404.00	
1.00	Co	CoCl2	0.5	-	-	58.93	129.84	450
	Fe	$FeCl_3 \cdot 6H_2O$	1.0	75.0	75.0	55.85	270.30	

Table 2.2. The stoichiometric calculations for the catalysts of the Cu-Mn serie

Mn/(Cu+Mn)	Metal	Precursor	Molarity (mol/L)	Volume (mL)	Mole (mmol)	AW of metal (g/mol)	MM of precursor (g/mol)	Calcination Temperature (°C)
0.00	Cu	$CuCl_2 \cdot 2H_2O$	0.5	75.0	37.50	63.55	170.48	450
	Mn	$Mn(NO_3)_2 \cdot 4H_2O$	0.5	-	-	54.94	251.01	
0.33	Cu	$CuCl_2 \cdot 2H_2O$	0.5	50.0	25.00	63.55	170.48	450
	Mn	$Mn(NO_3)_2 \cdot 4H_2O$	0.5	25.0	12.50	54.94	251.01	
0.50	Cu	$CuCl_2 \cdot 2H_2O$	0.5	37.5	18.75	63.55	170.48	450
	Mn	$Mn(NO_3)_2 \cdot 4H_2O$	0.5	37.5	18.75	54.94	251.01	
0.67	Cu	$CuCl_2 \cdot 2H_2O$	0.5	25.0	12.50	63.55	170.48	450
	Mn	$Mn(NO_3)_2 \cdot 4H_2O$	0.5	50.0	25.00	54.94	251.01	
1.00	Cu	$CuCl_2 \cdot 2H_2O$	0.5	-	-	63.55	170.48	450
	Mn	$Mn(NO_3)_2 \cdot 4H_2O$	0.5	75.0	37.50	54.94	251.01	

2.4 Procedure of HMF oxidation reactions

The oxidation reactions of HMF was carried out using a Parr 5000 Multiple Reactor System, in Figure 2.2, with 6 stainless steel autoclave reactors, equipped with a mechanical stirrer and measurement tools for temperature and pressure. While the initial reaction conditions were inspired by *Hansen et al.*[61], a plenty number of preliminary experiments were carried out at different temperature, for various period of time, and with several solvents for the optimization of reactions. Therefore, 126 mg of HMF (1 mmol) was dissolved in 2 ml of MeCN as solvent. Subsequently 0.1 mmol of catalyst and 2.6 mL of t-BuOOH solution (14 mmol) were added into a reactor. Reactions were conducted for 1 to 3 hours at temperature from 20 to 60 °C under constant magnetic stirring (450 rpm). Blank tests were carried out in the same conditions in the absence of catalyst.

Figure 2.2 Parr 5000 Multiple Reactor System and Control Unit

As a finding of the preliminary experiments, it was decided for the injection of methanol into the reactors as soon as the reaction ended and cooled down to room temperature with the purpose of FDCA extraction and avoiding loss of present solvents inside the reactors by vaporisation. Another advantage of MeOH addition is to retain target products' concentrations within the detection range by diluting the

liquid phase. Due to the poor solubility of FDCA in various solvents (water, acetonitrile and decane), conceivably as a result of available resonance form of its conjugate bases that are not accessible for the other acids, methanol is a good solvent for FDCA, roughly 10 times more soluble than in water.[62] Thus, 10 minutes after adding 1.7 ml of MeOH, the mixture of catalyst and solution was centrifuged using Jouan GR-412 for 10 minutes at 1000 rpm and 20 °C. Then the recovered solution was filtered through a syringe filter (Phenomenex nylon membrane, 0.45µm) prior to analysis by high pressure liquid chromatography, as shown in Figure 2.3.

Figure 2.3. The recovered solutions of different reactions

2.5 Optimization of HPLC analysis conditions

The preliminary HPLC measurements were essentially carried out in order for the detection of potential reaction products and the improvement of their corresponding peaks in the elution diagram; enhancement of quantitative analysis conditions; determination of optimum oven temperature and flow rate.

The pilot tests were evaluated by the refractive index (RI) detector, which would allow an easy quantitative analysis in the case of each standard solution runs individually. However, in the case of analyses of a complex liquid phase that consists of multiple products and solvents as in this work, the use of RI detector has limitations in providing reliable quantitative results due to the peak overlappings at the same retention time and the dominancy of high concentrated solvents over target products with lower concentration as illustrated in Figure 2.4. Altering other parameters such as oven

temperature or flow rate was insufficient even though their retention time shifted as expected. Alternatively, ultra-violet (UV) detector provides the peak detection of target molecules with reasonable intensities, which allow precise area calculations, and a better separation from each other at 254 nm, the optimum wavelength determined by 3D-aided chromatogram, as seen in Figure 2.5.

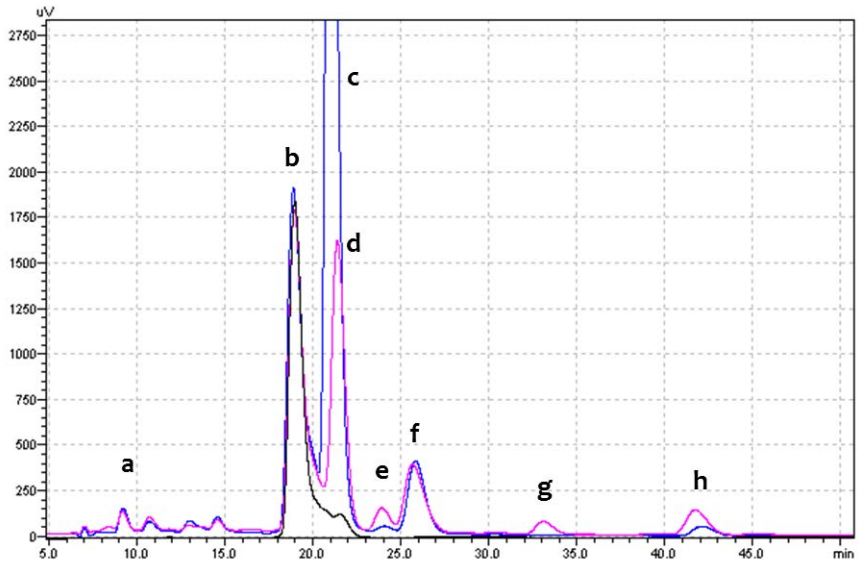

Figure 2.4. HPLC elution diagram of potential oxidation products and HMF by RI detector. The peaks corresponded to MA, t-BuOOH, MeCN/MeOH, FDCA, HMFCA, FFCA, HMF and DFF are represented by a, b, c, d, e, f, g, and h, respectively.

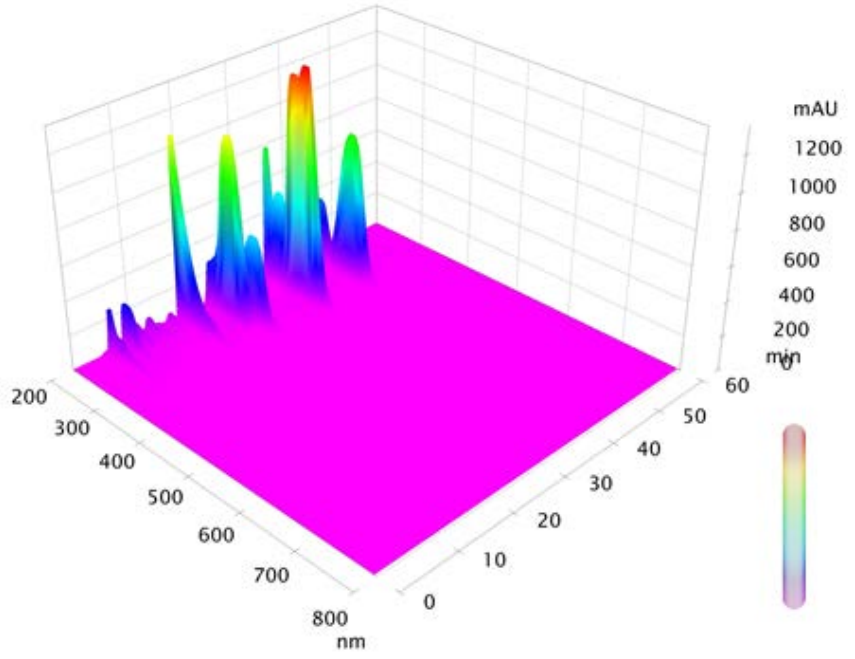

Figure 2.5. 3D Chromatogram of a reaction

The standard solutions in different concentrations (1 mM - 100 mM) belong to HMF and its oxidation products were analyzed by HPLC, not only to define the retention time of their corresponding peaks under optimized analysis conditions but also to obtain reliable calibration curves with high R-squared values (min 0.994) that allows accurate and precise quantitative analysis results which are correlated by corresponding peak area. In Figure 2.6, the HPLC elution diagram of HMF and its potential oxidation products detected by UV detector at 254 nm is illustrated. In addition to HMF and its oxidation products, the peak ***b*** was appeared on the chromatograms of MeOH injected reaction solutions. Hence, it was understood that the peak ***b*** belongs to a MA-derived compound in the presence of MeOH, hereafter called MA*, which might correspond to monomethly maleate[63] as seen in Figure 2.7. Thus on the yield calculations both MA and MA* were taken into account together.

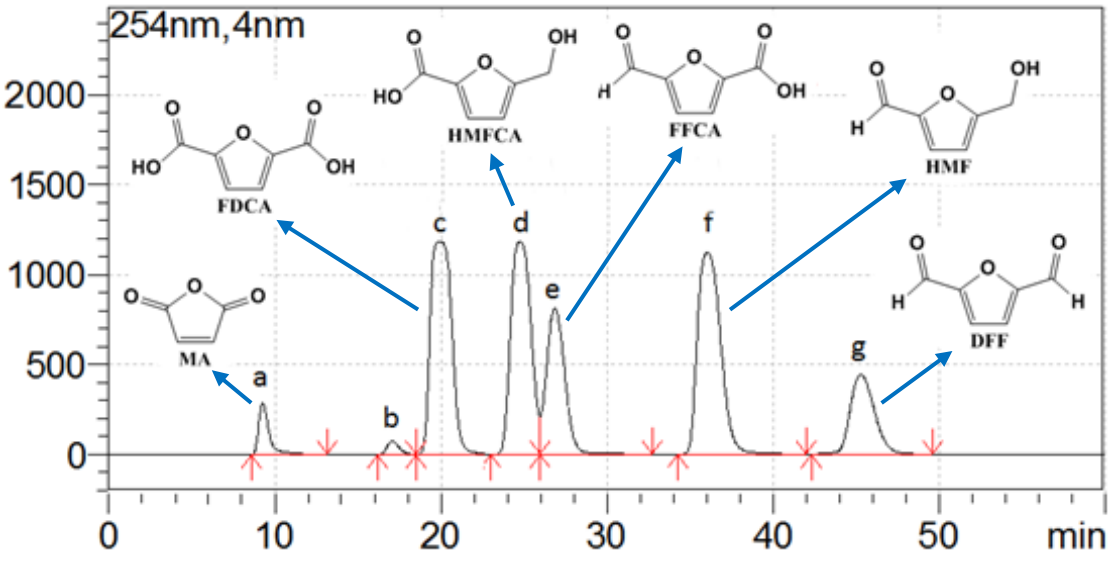

Figure 2.6. HPLC elution diagram of HMF and its potential oxidation products detected by UV detector at 254 nm. The peaks corresponded to MA, MA*, FDCA, HMFCA, FFCA, HMF and DFF are represented by a, b, c, d, e, f, g, respectively.

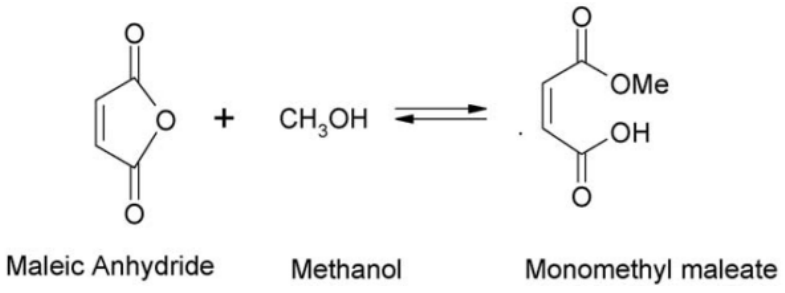

Figure 2.7. Formation of monomethly maleate, a possible correspondence to MA* [63]

Chapter 3 Characterisation of catalysts

3.1 Characterisation of Co-Fe Oxide Catalysts

In Table 3.1, the correlation between aimed and verified Fe/(Co+Fe) ratios is reported. Iron and cobalt contents of samples were retrieved from EDX analysis and for each powder sample 5 different meauserements were performed. The results confirm that the aimed cation ratios for Fe-Co catalysts, synthesized by coprecipitation method, were successfully obtained.

Table 3.1. The Fe/(Co+Fe) ratio confirmed by EDX analysis

Fe/(Co+Fe) [targeted]	**Fe/(Co+Fe) [verified]**
0	0
0.33	0.31 ± 0.02
0.50	0.50 ± 0.16
0.67	0.68 ± 0.14
1	1

Figure 3.1 demonstrates the X-ray diffraction patterns of Co-Fe catalysts. Black, red, blue, green and pink spectra belong to the samples with 0, 0.33, 0.5, 0.67 and 1.0 Fe/(Co+Fe) ratios, respectively. All spectra are shifted on y-axes with the same distance from each other and their relative intensities are conserved. The spectrum belongs to the only cobalt metal containing sample, Fe/(Co+Fe)=0, corresponds to spinel cobalt oxide, Co_3O_4 with cubic crystal system. Additionally, the peak at 2θ angle of 39° indicates the existence of cobalt oxyhydroxide, CoOOH, with tiny amount. In mixed cobalt and iron containing catalysts, which have 0.33, 0.5 and 0.67 Fe/(Co+Fe) ratios, the mixed spinel structure $(Co,Fe)_3O_4$ with cubic crystal system is observed. The characteristic peaks of a spinel positioned around 2θ angles of 19°, 31°, 37°, 39°, 45°, 56°, 59° and 65°, respectively correspond to the planes (111), (220), (311), (400), (511) and (440) as seen in Figure 3.1. However, the pink spectrum illustrates that the catalyst with 1.00 Fe molar fraction has an α-hematite structure, Fe_2O_3, with rhombohedral lattice system and no spinel formation is detected for this sample.

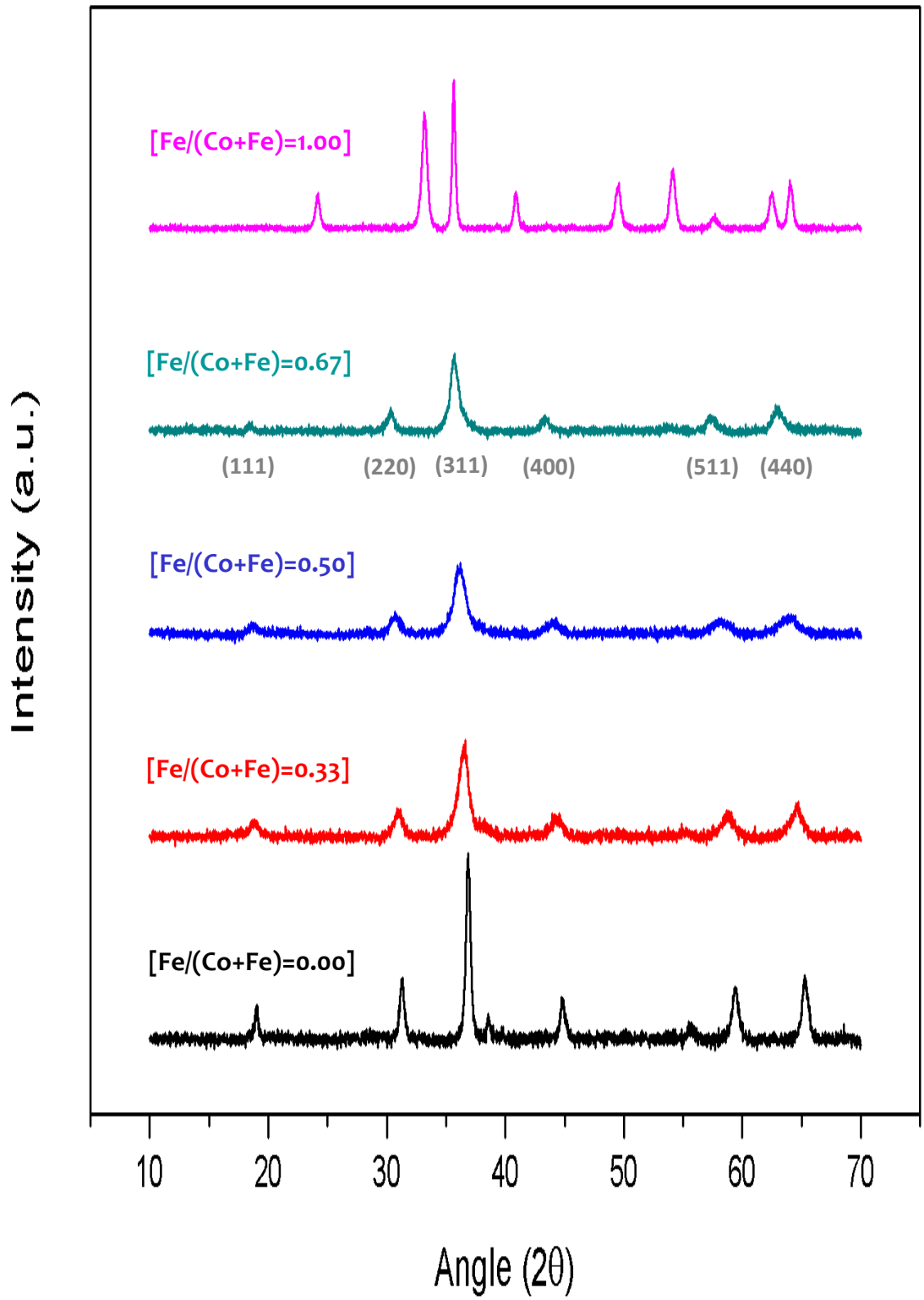

Figure 3.1. XRD spectra of Co-Fe catalysts which are calcined at 450 °C

In Table 3.2, the values of cell parameter and crystallite size of each Co-Fe catalyst are shown. Particle size from Williamson-Hall plots for monophasic samples and by the Scherrer method for multiphasic samples from FWHM intensity measurements.

Table 3.2. Phase and textural characterisation of Co-Fe catalysts

Fe/(Co+Fe)	**Phase**	**Cell size**	**Particle size (nm)**	
		Å	**spinel**	**hematite**
0	spinel	8.09	29	-
0.33	spinel	8.16	7	-
0.50	spinel	8.26	11	-
0.67	spinel	8.36	11	-
1	α-hematite	5.04, 13.76	-	25

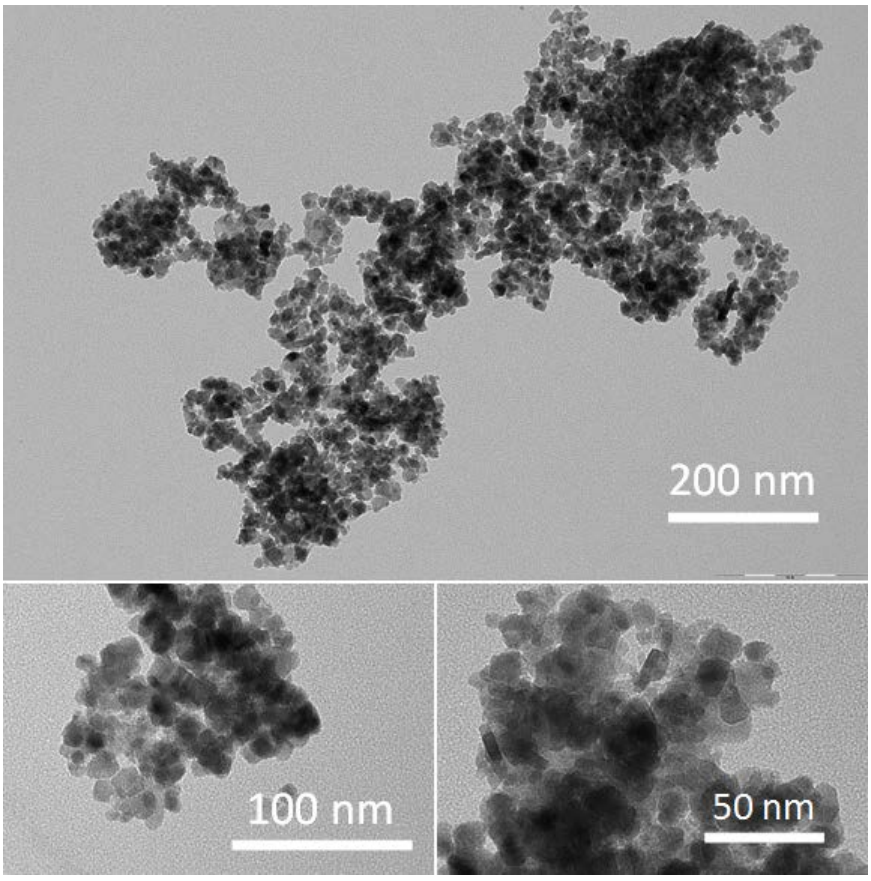

Figure 3.2. Transmission electron micrograph of Co-Fe spinel with 0.5 Fe/(Co+Fe) ratio

In Figure 3.2, TEM images of $Co_{1.5}Fe_{1.5}O_4$ in different magnifications show smooth and roundish crystalline particles with irregular shape with an average size of ∼10 nm; which is a in good agreement with those calculated on XRD patterns.

In Figure 3.3, the nitrogen adsorption-desorption isotherms for Co-Fe oxides are demonstrated. The low-pressure part of the isotherms of hematite and spinel Co_3O_4 are virtually superposed, confirming the similarity of their surface area values, which are 43 and 35 m^2g^{-1}, respectively. Likewise, the mixed spinel catalysts with different cation fractions belong superpositioned isotherms at lower pressure and have similar extension of surface area values, evaluated by the BET method, are reported in Table 3.3. At higher relative pressure, all isotherms present a hysteresis of type IV isotherms that explain the mesoporosity of catalysts. However, their mesoporosities exhibit different distributions. The mixed spinel oxides feature a well-defined condensation steps, vary between 0.7-0.9 p/p°, are observed; whereas single metal containing oxides feature a higher-pressure hysteresis near to p°.

Table 3.3. BET surface area of Co-Fe catalysts

Fe/(Co+Fe)	**S_{BET} (m^2g^{-1})**
0	35
0.33	81
0.50	78
0.67	84
1	43

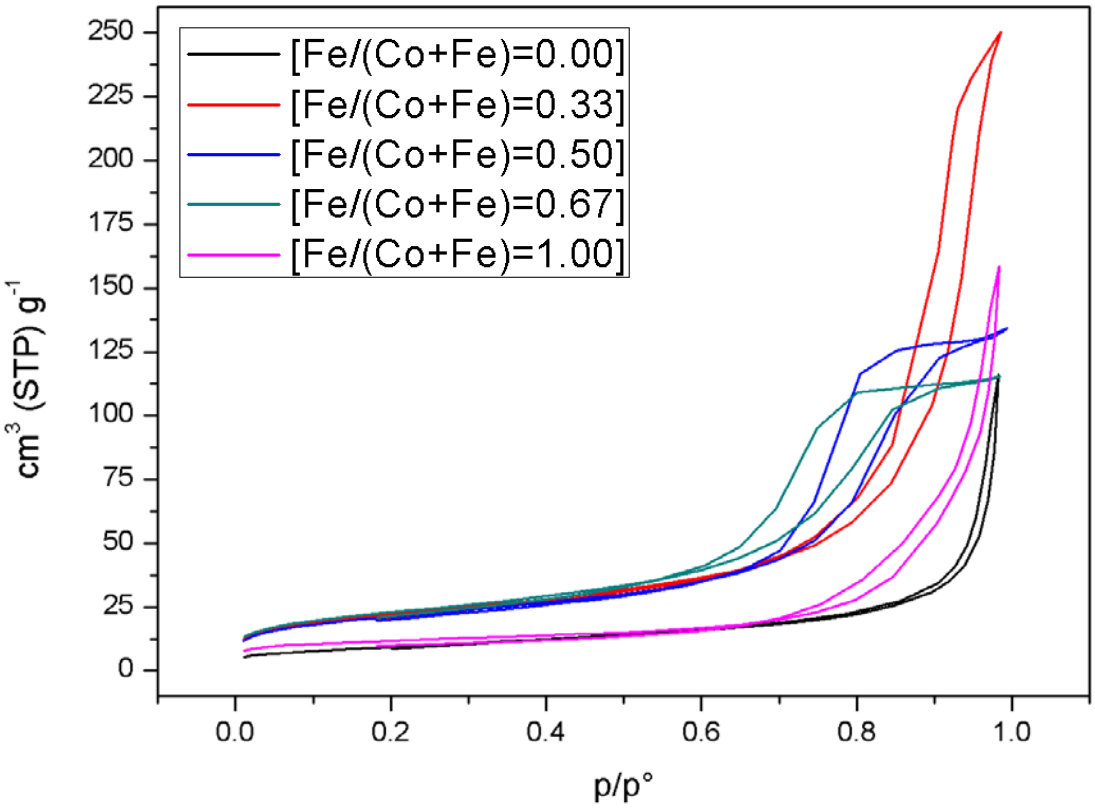

Figure 3.3. N_2 adsorption-desorption isotherms for Co-Fe oxides

The pore size distribution of aformentioned catalysts are compared in Figure 3.4. It is also remarkable to observe that mixed spinels presented a better dispersion than both hematite and spinel Co_3O_4 prepared in the same conditions. Furthermore, this order is correlated with Fe fraction of a mixed spinels. The samples with 0.33, 0.5 and 0.67 Fe/(Co+Fe) ratios, respectively, have more homogenous pore size distribution. Therefore in the series of Co-Fe system, the aggregation of spinel elementary particles affected to form quite monodispersed mesoporosity.

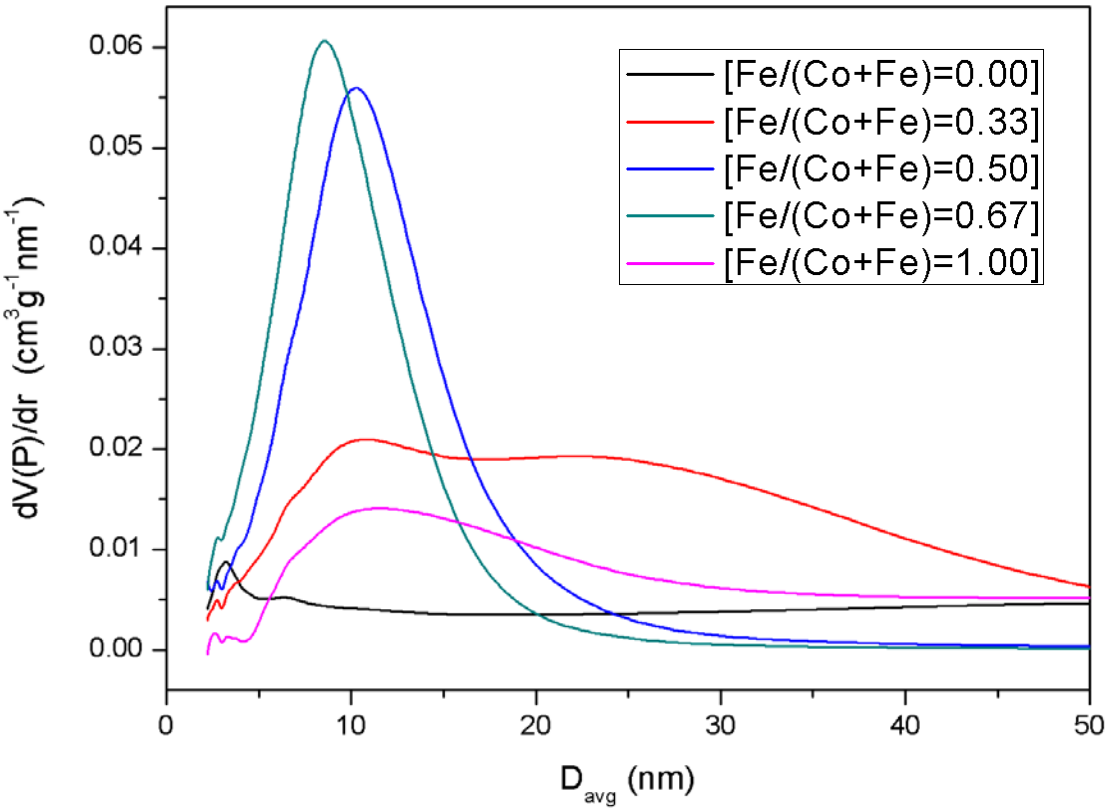

Figure 3.4. Mesoporous size distribution of Co-Fe oxides

According to the textural and phase characterisation of the catalysts, the iron-cobalt system allows the formation of cubic spinel solid solutions on the whole composition domain, with the only exception of the all-iron sample. The cell parameter of spinel evolves with the iron content from 8.09 Å for Co_3O_4 direct spinel to 8.36 Å for the mostly inverted cobalt ferrite $CoFe_2O_4$. The pure iron oxide is α-hematite Fe_2O_3, as expected from the phase diagram in oxidising conditions. The average surface area of the mixed spinels is about 80 m^2g^{-1}, nearly twice the surface area of the cobalt and iron oxides end-terms.

As highlighted in Figure 3.5, the increase of the cell parameter is not linear with the iron fraction. Indeed, the cell size of the samples at Fe/(Co+Fe) ratio 0.33 and 0.5 is much lower than the value expected for a Vegard's law[64] solid solution between cobalt spinel and cobalt ferrite. This effect corresponds to a variation in the distribution of cations in the spinel sites.

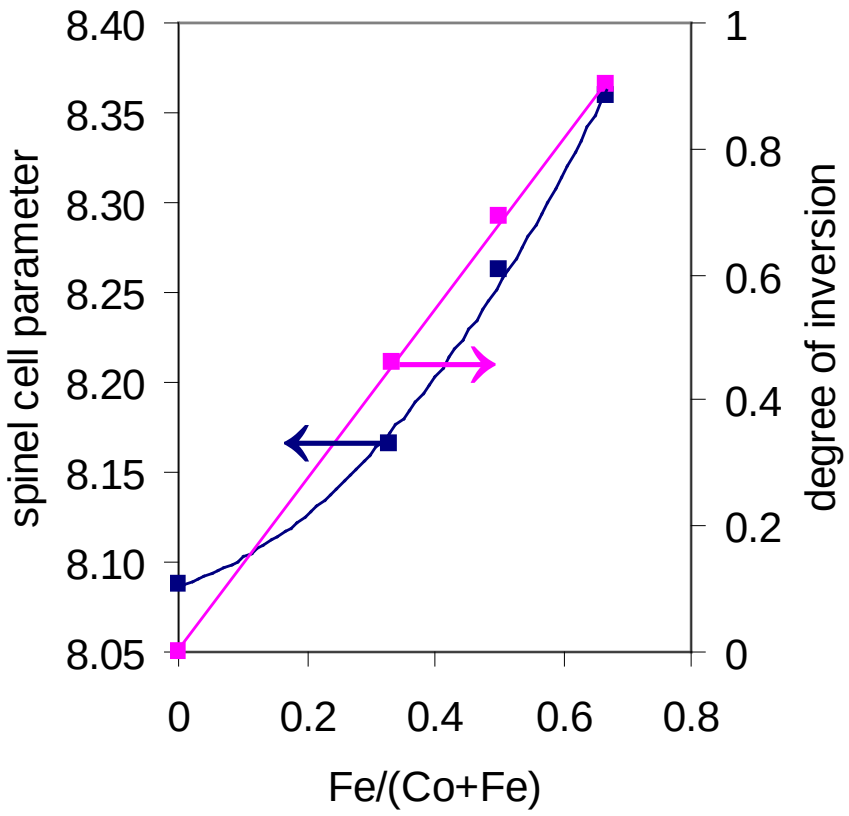

Figure 3.5. Cell size and degree of inversion of the Co-Fe spinels. (The lines are guides for the eye.)

The cation distribution in the spinel phases was evaluated by best-fitting of the cell parameter by the formula;[65],[66]

$$a=(8/(11*3^{0.5}))(5d_{M1\text{-}O}+(33d_{M2\text{-}O}^{2}-8d_{M1\text{-}O}^{2})^{0.5}$$

The M^1-O bond lengths of the tetrahedral site were assumed as 1.865 and 1.975 Å, respectively for Fe^{3+} and Co^{2+}. The M^2-O bond lengths of the octahedral site were assumed as 1.9, 2.025, 2.1, and 2.12 Å, respectively for Co^{3+}, Fe^{3+}, Co^{2+}, and Fe^{2+} [66],[67].

The calculated cation distributions reported in Table 3.4. account for the cell parameters of all Co-Fe spinel samples. A linear variation of the inversion degree, as illustrated in Figure 3.5, is observed between the direct cobalt spinel Co_3O_4 and the largely inverted $CoFe_2O_4$ ferrite, indicating that a lower than expected cell size for the intermediate samples depends on a lower M-O distance in the octahedral site. The Co^{2+}-O and Fe^{2+}-O distances, which are 2.1 and 2.12 Å respectively, in the octahedral

site are nearly equivalent; whereas the Co^{3+}-O distance (1.9 Å) is much shorter than the Fe^{3+}-O distance (2.025 Å). Accordingly, in the samples with Fe/(Fe+Co) 0.33 and 0.5, the average degree of oxidation of cobalt is higher than expected and the degree of oxidation of iron is lower than expected.

Table 3.4. Cation distribution in M_3O_4 spinel phases

Fe/cat	Co^{2+} (T_d)	Fe^{3+} (T_d)	Fe^{2+} (O_h)	Co^{2+} (O_h)	Fe^{3+} (O_h)	Co^{3+} (O_h)
0.00	1	0	0	0	0	2
0.33	0.54	0.46	0.46	0.00	0.08	1.46
0.50	0.31	0.69	0.29	0.40	0.52	0.79
0.67	0.10	0.90	0.12	0.78	0.98	0.12

The TPR profiles of the Co-Fe catalysts are reported in Figure 3.6. The Co_3O_4 sample presents a first reduction peak with onset at 225 °C and maximum at 325 °C. This first reduction corresponds to 22 % of the hydrogen demand for total reduction and corresponds to the reduction of the cobalt spinel to CoO. Reduction of CoO to cobalt metal is completed in a second peak with maximum at 425 °C.

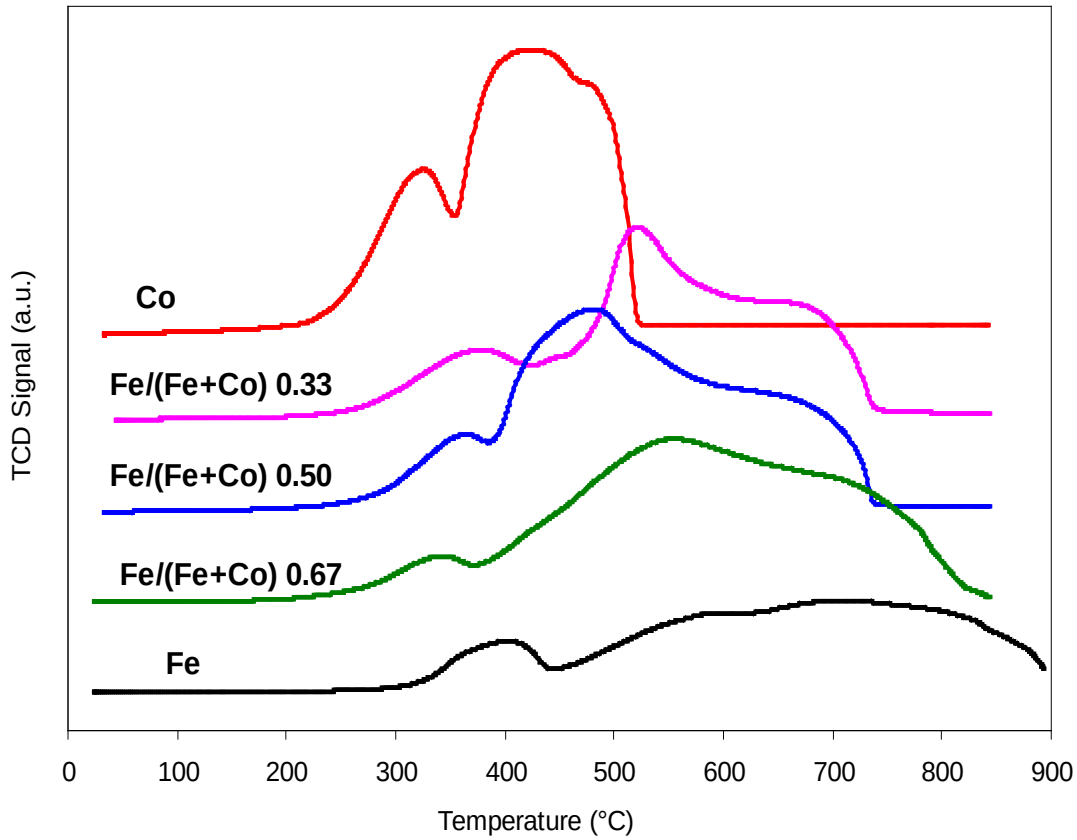

Figure 3.6. TPR profiles of Co-Fe oxide samples

The three mixed spinel samples present an initial reduction step with onset at about 260 °C, corresponding to the reduction of Co^{3+} to Co^{2+}. The maximum temperature of this first peak and the corresponding fraction of consumed H_2 decrease from 14 to 5 % with the decrease of the amount of cobalt in the sample. The reduction of Co^{3+} and the exsolution of CoO destabilize the charge balance of the mixed spinel phase, which decomposes to CoO and a magnetite-like phase. The reduction of CoO to metallic Co and of magnetite to FeO are superposed in a complex way and contribute to a signal with maximum between 480 and 560 °C. The reduction of FeO is completed between 740 and 840 °C.

The reduction of the all-iron oxide follows the literature pattern. A first peak with onset at 300 and maximum at 400 °C consumes 13 % of the total hydrogen and corresponds to the reduction of Fe_2O_3 to Fe_3O_4. A second broad peak with maximum at 590 °C corresponds to the reduction of Fe_3O_4 to FeO and is partially superposed

with the subsequent reduction of FeO to metallic iron. The reduction of the sample is not complete at the final temperature of 900 °C.

Figure 3.7 reveals the Tauc plot of cobalt-iron catalysts for direct band gap energy (Eg) estimation. The controlled variation of Eg in a material is a valuable tool to reflect its performance. It has been demonstrated that metal oxides with low Eg can exhibit good catalytic performance.[60],[68]

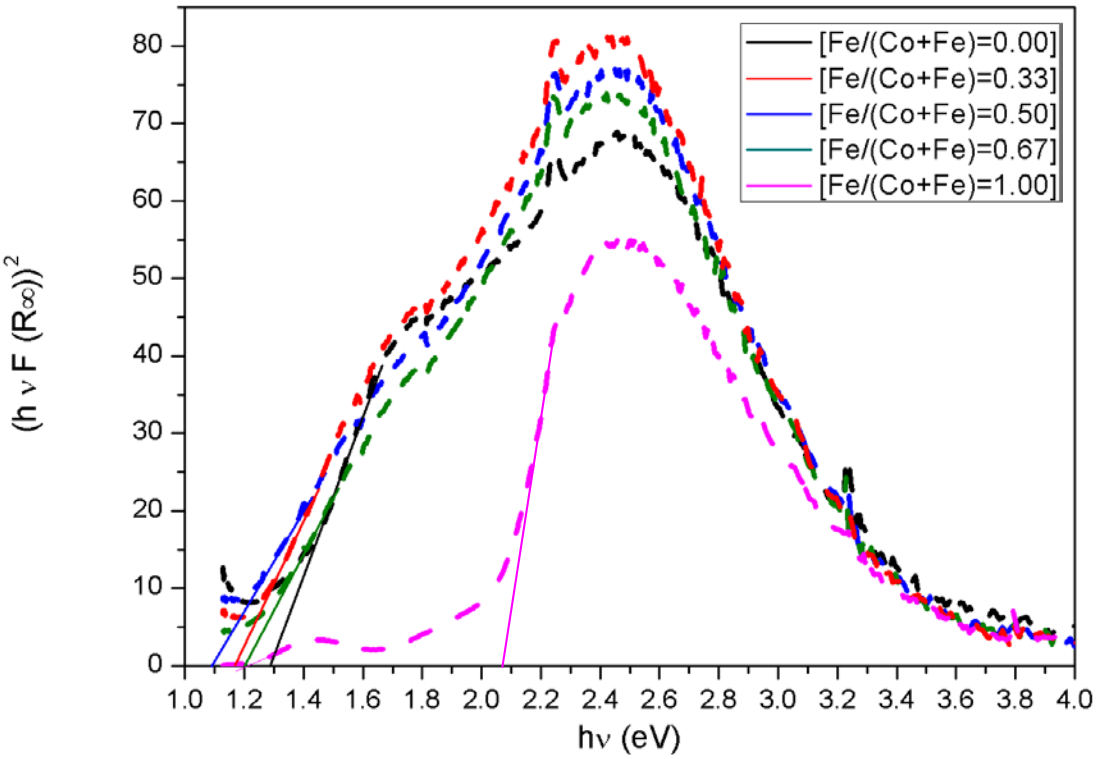

Figure 3.7. Band gap determination of Co-Fe catalysts

In Table 3.5, the band gap values of Co-Fe catalyst are reported. Albeit the Eg values of all spinel catalysts are lower than hematite, no correlation with the Fe content is observed. However, similar trend could be expected from the performance of catalystst with 0.5, 0.33, 0.67, 0.0 and 1.0 Fe/(Co+Fe) ratio.

Table 3.5. Band gap values of Co-Fe catalysts

[Fe/(Co+Fe)]	Eg (eV)
0.00	1.29
0.33	1.17
0.50	1.09
0.67	1.20
1.00	2.09

The evolution from a direct to an inverse spinel structure with the increase of the iron content is confirmed by the FT-IR spectra reported in Figure 3.8. Albeit the similarity between the energies of the Co-O and Fe-O bonds renders the infrared spectra quite insensitive to the isomorphous substitution of Co by Fe in each crystallographic site, the spectra are seriously modified by the degree of inversion of the spinel. Direct Co_3O_4 spinel presented well separated A-O-B_3 and B-O-B_2 stretching vibrations, respectively at 658 and 554 cm^{-1}.[69] The separation between the two peaks was blurred when trivalent cations occupied a significant fraction of tetrahedral sites, until one broad band around 590 cm^{-1} was observed for the mainly inverse spinels with Fe fraction 0.66 or higher.

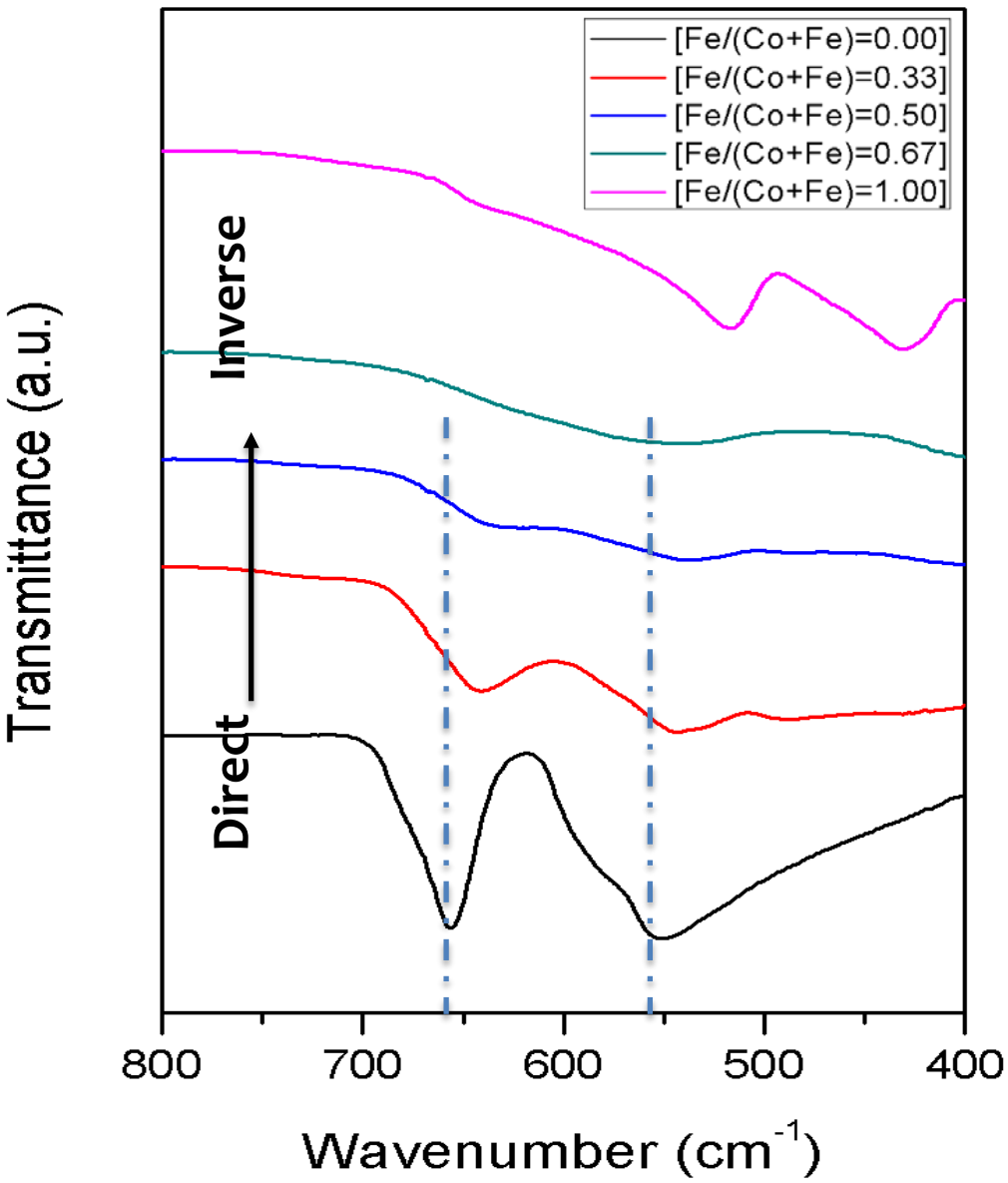

Figure 3.8. FT-IR spectra of Co-Fe oxides

3.2 Characterisation of Cu-Mn Oxide Catalysts

In Table 3.6 the correlation between aimed and verified Mn/(Cu+Mn) ratios is reported. Manganese and copper contents of samples were retrieved from EDX analysis and for each powder sample 5 different meauserements were performed. The results confirm that the aimed cation ratios for Cu-Mn catalysts, synthesized by coprecipitation method, were successfully obtained.

Table 3.6. The targeted Mn/(Cu+Mn) ratios confirmed by EDX analysis

Mn/(Cu+Mn) [targeted]	**Mn/(Cu+Mn) [verified]**
0	0
0.33	0.35 ± 0.11
0.5	0.49 ± 0.12
0.67	0.67 ± 0.16
1	1

Figure 3.9 exhibits the XRD patterns of Cu-Mn catalysts, synthesized by coprecipitation at calcined at 450 °C. Black, red, blue, green and pink spectra belong to the samples with 0.0, 0.33, 0.5, 0.67 and 1.0 Mn/(Cu+Mn) ratios, respectively. All spectra are shifted on y-axes with the same distance from each other and their relative intensities are conserved. The black spectrum belongs to the sample with no manganese reveals 100 % presence of monoclinic CuO tenorite phase. The catalysts with 0.33 and 0.5 Mn molar fraction have mixture of CuO and cubic mixed spinel, $(Cu,Mn)_3O_4$, in different compositions. The composition of different phases can be easily seen, in Figure 3.10, on the TEM images of sample with 0.5 of Mn/(Cu+Mn) ratio. While smooth and roundish spinel oxide particles exhibit a relative agglomeration of the nanoparticles due to their ultra fine size, the CuO oxide particles are present in the form of large aggregated crystals with an average around 25 nm, which is a in good agreement with

XRD patterns. The spectrum belongs to catalyst with 0.67 of Mn/(Cu+Mn) corresponds to completely spinel phase, $CuMn_2O_4$, with cubic crystal system. In all spectra of mixed metal a spinel positioned around 2θ angles of 19°, 31°, 37°, 39°, 45°, 56°, 59° and 65°, respectively correspond to the planes (111), (220), (311), (400), (511) and (440). In the spectrum of Cu-free sample, the mixture of oxides of manganese with different oxidation level, tetragonal Mn_3O_4 and monoclinic Mn_5O_8 phases, were observed. Those phases are the only observed phases in the absence of copper and no traces detected together with spinels, contrary to tenorite. The phase ratios observed for different global compositions of the samples and cell parameters are reported in

Table 3.7. The cell parameters of spinels are quite similar to each other and no dramatic change is detected with the increase of Mn content. The formation of solid solutions with an extended field of continuous variation of composition is not favoured in the copper-manganese system.[70]

Table 3.7. Phase composition of Cu-Mn catalysts

Mn/(Cu+Mn)	**spinel cell *a***	**phase %**			
	Å	**CuO**	**spinel**	**Mn3O4**	**Mn5O8**
0		100			
0.33	8.286	32	68		
0.50	8.290	27	73		
0.67	8.291		100		
1				71	29

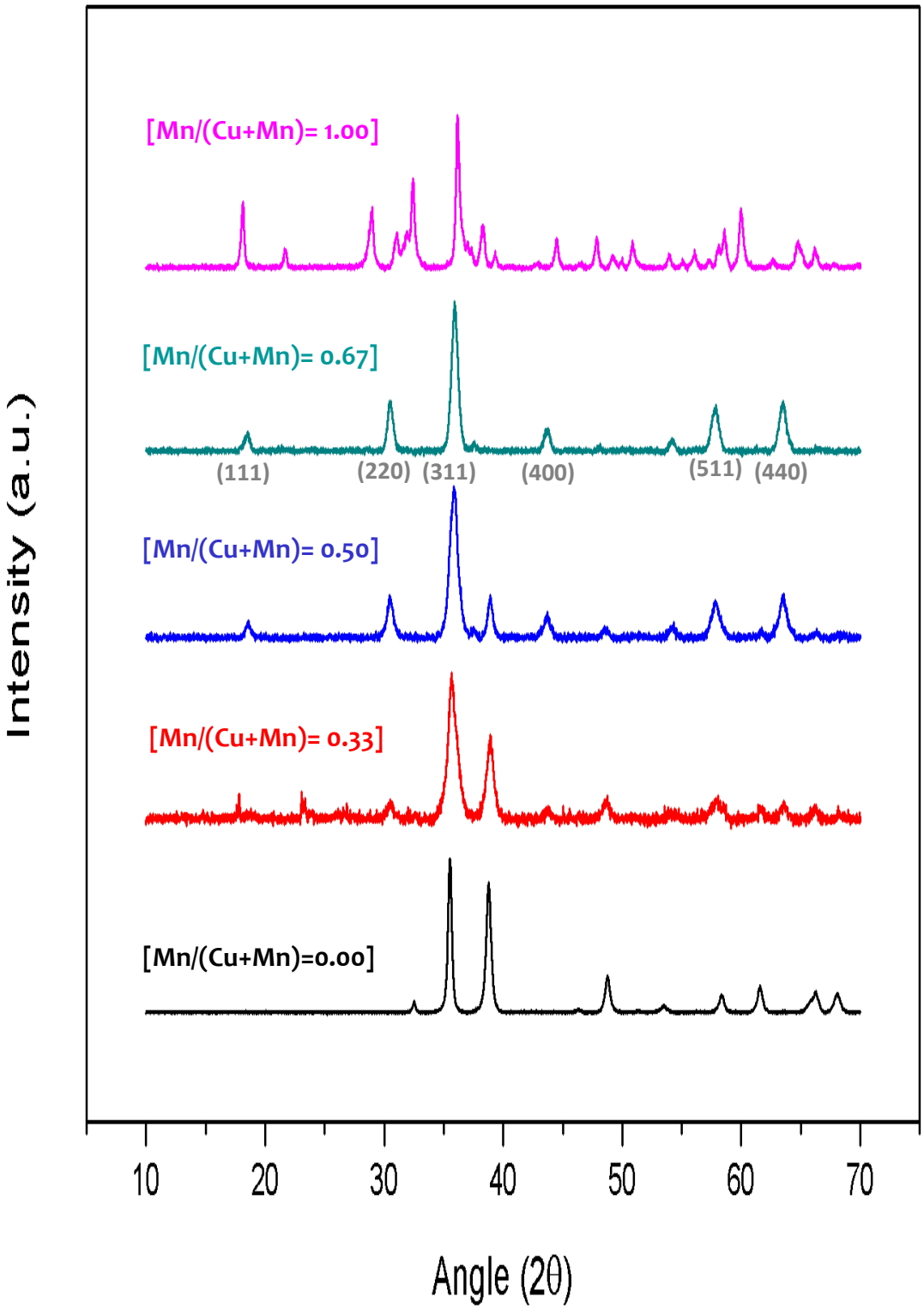

Figure 3.9. XRD spectra of Cu-Mn catalysts which are calcined at 450 °C

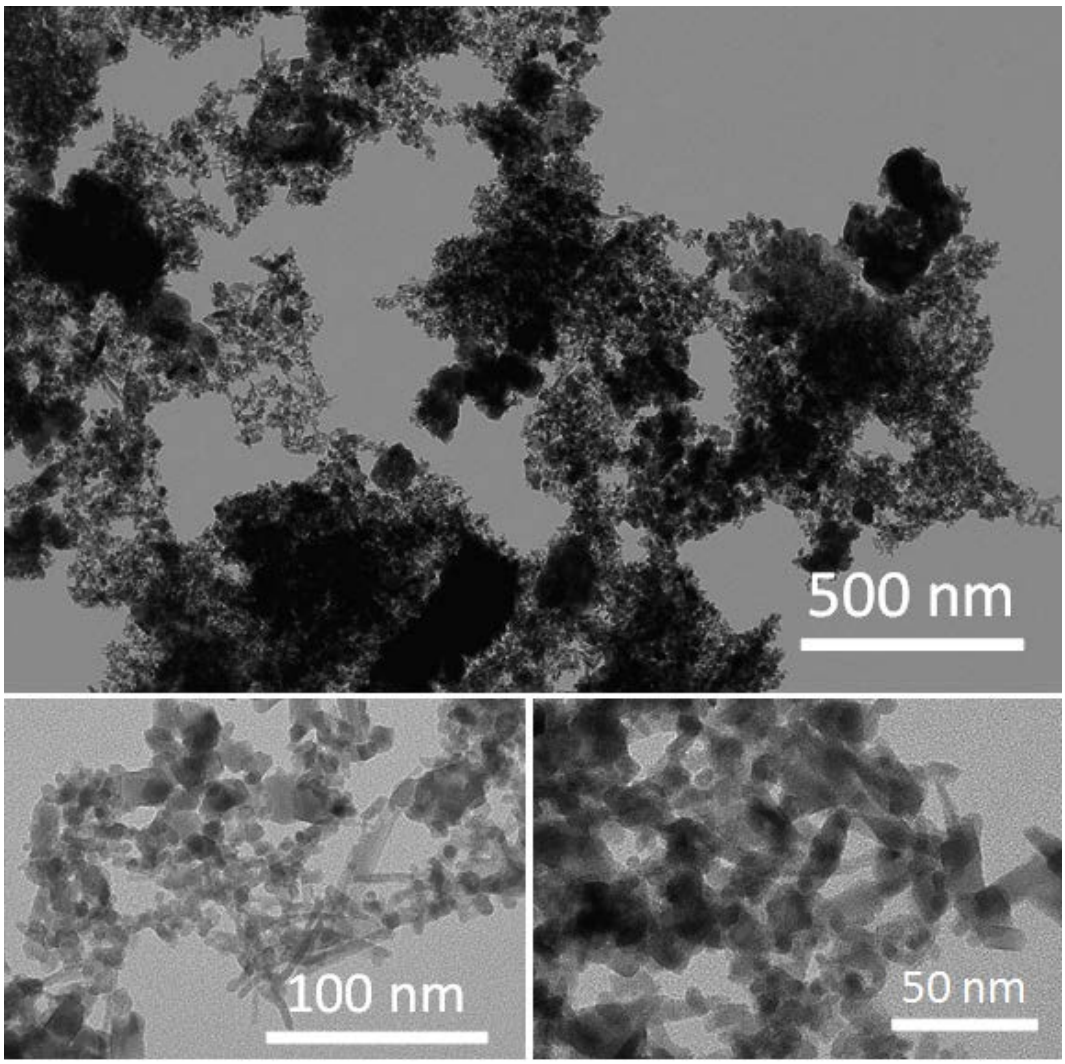

Figure 3.10. Transmission electron micrograph of Cu-Mn spinel with 0.5 Mn/(Cu+Mn) ratio

The cell parameter of spinel presents a very limited variation with the global composition of the sample and it is always consistent with a spinel Mn/(Cu+Mn) ratio 0.51-0.52.[71] It is worth remarking that this composition of the spinel phase is clearly not compatible with the overall copper-manganese balance of the samples. For the samples with global manganese fractions 0.33, 0.50 and 0.67, the phase ratios obtained by the crystallographic data correspond, respectively, to sample cation ratios Mn/(Cu+Mn) 0.16, 0.37 and 0.52. These data indicate a lower than expected amount of manganese in the crystalline phases, which can be easily accounted for by the presence of amorphous manganese oxides in all mixed copper-manganese samples.[72]

In Figure 3.11, the nitrogen adsorption-desorption isotherms for Cu-Mn oxides with with 0.33, 0.5 and 0.67 Mn/(Cu+Mn) ratios are demonstrated. The Cu-rich samples have a higher N_2 capacity than Mn-rich samples. At higher relative pressure, isotherms of aforementioned samples present a hysteresis of type IV isotherms that explain the mesoporosity of catalysts.

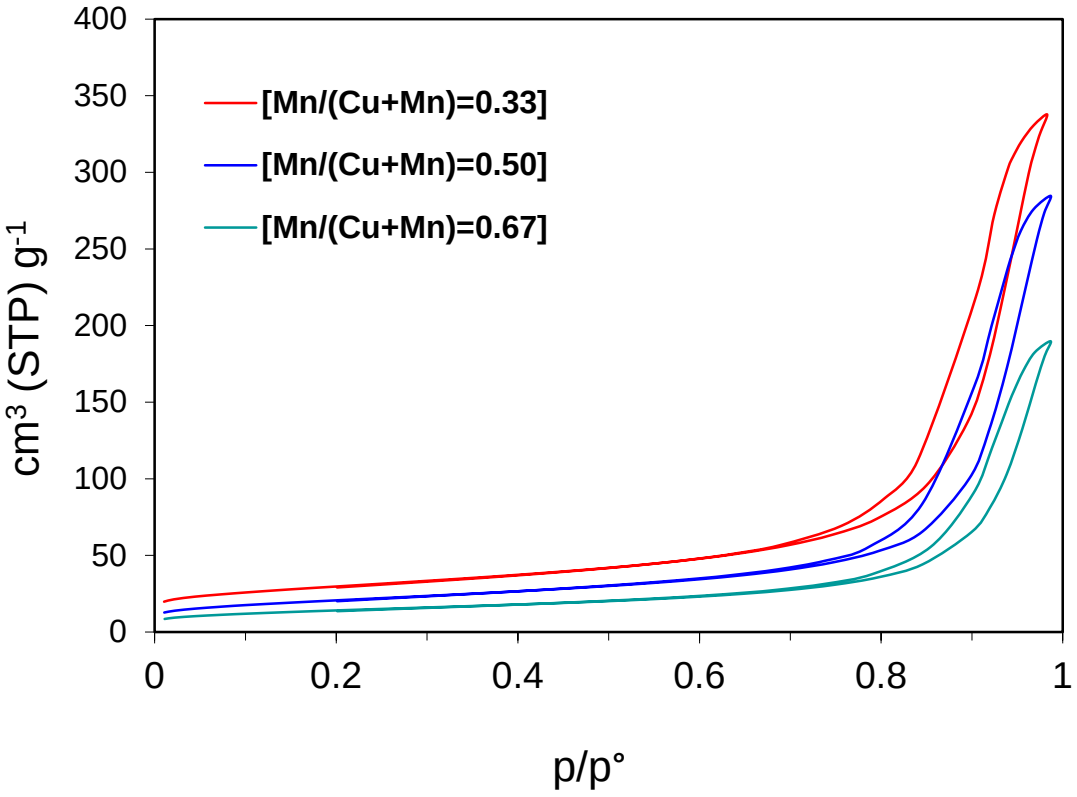

Figure 3.11. N_2 adsorption-desorption isotherms for Cu-Mn oxides with 0.33, 0.5 and 0.67 Mn/(Cu+Mn) ratios

Surface area and grain size of the Cu-Mn samples are reported in Table 3.8. Also in this system, the mixed oxides present higher surface area than the copper and manganese end-terms but the surface area significantly varies with the composition of the oxides. Surface area features a maximum of more than 100 m^2g^{-1} for the Mn fraction 0.33 and steadily decreases for higher Mn contents. The grain size evaluated from the width of the X-ray diffraction lines are very similar for the different phases of every given sample. It is remarkable that the grain size of tenorite is much smaller in the mixed

samples than for CuO crystallised alone. This strongly suggests that the presence of foreign cations increases the ratio between nucleation and growth rates of the oxide.

Table 3.8. Textural characterisation of Cu-Mn catalysts

Mn/(Cu+Mn)	S_{BET}	Particle size (nm)			
	m^2g^{-1}	CuO	spinel	Mn3O4	Mn5O8
0	10	38			
0.33	106	25	11		
0.50	75	21	14		
0.67	51		15		
1	24			22	25

The TPR profiles of the Cu-Mn catalysts are reported in Figure 3.12. The reduction of the CuO sample to metallic Cu begins at nearly 125 °C and is completed at 365 °C after a highly-skewed peak with maximum at 310 °C. In the case of the mixed Cu-Mn samples, an onset of reduction is always observed at nearly 130 °C and develops into a shoulder at about 220 °C, which intensities decreases at decreasing copper content. This initial reduction signal probably includes the reduction of residual CuO the reduction of Mn^{4+} and Mn^{3+} species from spinel phase and amorphous manganese oxides. The maximum temperature of the main peak of reduction of the spinel to metallic Cu and MnO increases from 275 to 305 °C at the increase of the mixed spinel fraction.

The reduction of the all-manganese oxide sample begins at nearly 160 °C and is composed of two peaks with maximum at 315 and 455 °C, which can be attributed to the reduction of, respectively, Mn^{4+} and Mn^{3+} cations to Mn^{2+}.

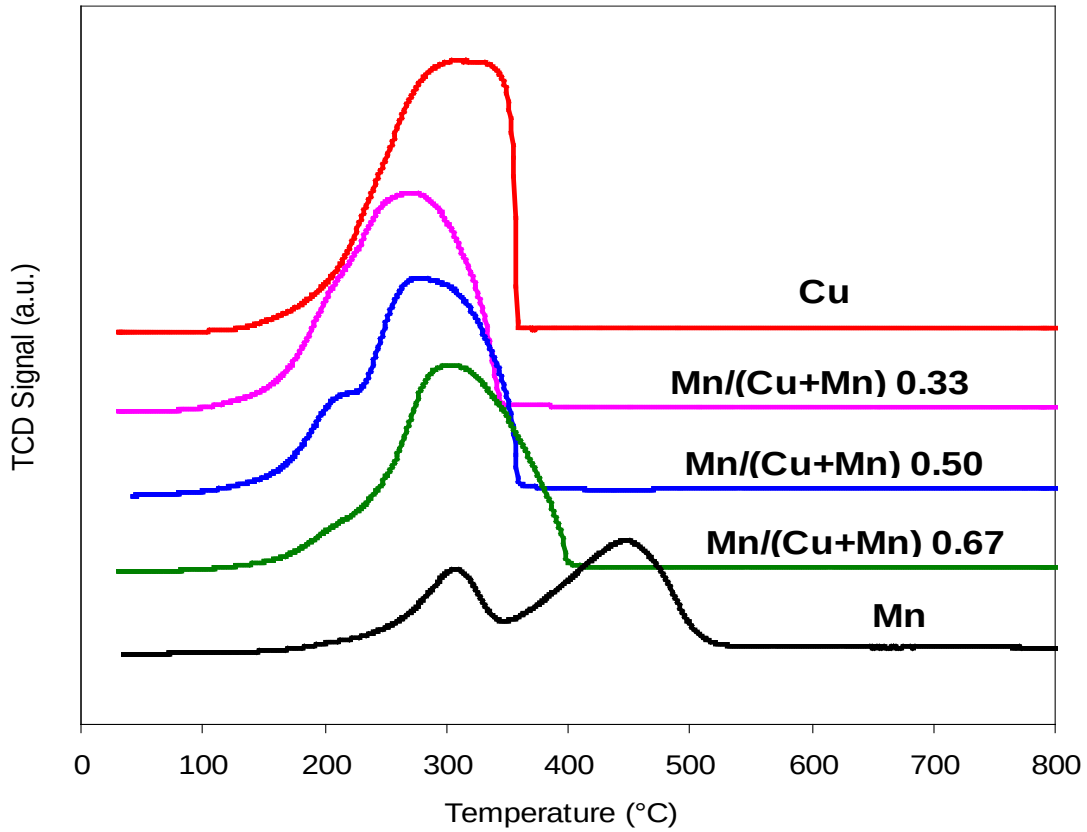

Figure 3.12. TPR profiles of Cu-Mn oxide samples

Chapter 4 The selectivity and kinetics of HMF to FDCA oxidation on mixed oxide catalysts

5-hydroxymethylfurfural (HMF) is a key renewable platform molecules that is convertible to a plenty number of valuable chemicals or fuels via various reactions including 2,5-furandicarboxylic acid (FDCA), which is an alternative molecule to fossil fuel derived terephthalic acid.[44] Successive oxidation reactions of HMF produce FDCA, which allows effective replacement with terephthalic acid in polyesters.[42] Effective catalysts have been proposed, based on noble metals or rare earths; while the interest for alternative catalysts based on oxides of non-noble transition metals has been increasing due to the abundancy thus cheaper price of those metals as well as being environmentally bening. [73],[74],[75]

Co-Fe spinels have been shown to be effective oxidation catalysts, for instance for the oxidation of benzyl alcohol to benzaldehyde[24] and the oxidative decomposition of organic pollutants[25]. Cu-Mn spinels have been proposed as catalysts for oxygenate reforming[26],[27] and water gas shift reaction.[28]

4.1 Analytical methods

In this chapter, the catalytic activity and the results of kinetics study are reported for the successive oxidation reactions of HMF to FDCA through other value-added intermeadiates over the aforementioned two sets of Co-Fe and Cu-Mn oxide catalysts. The materials used, the oxidation reaction and analysis conditions, characterization techniques and conditions are mentioned in the previous chapters.

HMF, DFF, HMFCA, FFCA, FDCA and MA species were analysed. Part of maleic anhydride formed methylated species during the recovery of the products by methanol washing. Also this amount was taken into account in the evaluation of maleic anhydride. Humins and oligomers were evaluated by mass balance difference. Reaction orders were evaluated as the ratio of the logarithms of the variations of reaction rates and initial concentrations. Rate constants were evaluated by best-fit of the activity data in an iterative calculation program. Energies of activation were derived from the variation of reaction rates with temperature of reaction.

4.2 Catalytic activity

The oxidation of HMF to FDCA is a complex cascade process involving several intermediates in parallel or successive reactions. The first step of the process can imply either the oxidation of the alcohol group of HMF to DFF or the oxidation of the carbonyl group to HMFCA. The successive steps are the oxidation of a carbonyl group of DFF or the oxidation of the alcohol group of HMFCA, both reaction forming FFCA, which is later oxidised to FDCA. The main observed reactions in competition with the oxidation to FDCA are the formation of MA or the condensation of oligomers, in some cases qualified as humins.

Several mechanisms have been proposed for the formation of maleic anhydride from HMF. In acidified acetonitrile media the reaction has been suggested to pass through a FFCA intermediate.[47] In our reaction conditions, the formation of maleic anhydride was the fastest in the earliest steps of the reaction, when the concentration of FFCA was lower. This strongly suggests MA to be a primary oxidation product of HMF

through a reaction path independent from the one leading to FDCA. A pathway through a direct oxidative cleavage of C-C bonds with formation of formic acid seems to be the most likely mechanism.[76]

Humins or oligomers are unwanted by-products in most processes involving HMF. It is widely accepted that they are formed by a complex mechanism involving the hydration of the carbon in α to the enol group of HMF, opening of the furanic ring with formation of 2,5-dioxo-6-hydroxy-hexanal (DHH) and keto-enol condensation.[77],[78] It has been suggested that the propagation of the oligomers can occur by condensation of the enol groups of DHH or of the oligomers themselves with any ketone or aldehyde present in the system.[79] Indeed, in our experiments, oligomers are steadily formed from the onset of the reaction up to a high degree of advancement of the oxidation, when the concentration of HMF is no more significant. This suggests that they are formed by condensation not just of HMF but from all carbonyl-bearing molecules involved in the process, namely HMF, DFF and FFCA. A reaction sequence corresponding to these assumptions is represented in Figure 4.1 and has been used in the kinetic modelling of our results.

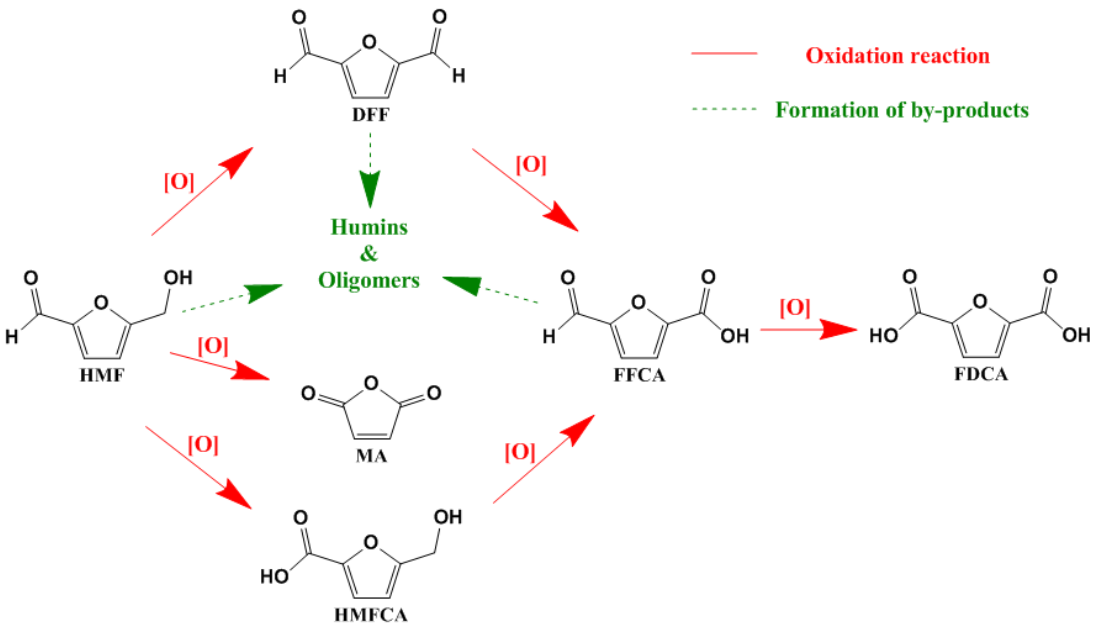

Figure 4.1. Consecutive reactions mechanism of HMF

In the evaluation of the performances of the catalysts, it has to be taken into account that tert-butoxy hydroperoxide is an effective oxidant of HMF also in the absence of a purposely-introduced catalyst. Figure 4.2 illustrates conversions and yields obtained at different temperature by oxidation of HMF by t-BuOOH in the absence of catalyst (left-hand side) and in the presence of a mixed oxide catalyst with ratio Mn/(Cu+Mn)=0.33 (right-hand side). The presence of catalyst significantly increases the conversion of HMF and modifies the distribution of products. In the tests in the absence of catalyst, the degree of advancement of the series of cascade reactions in quite low. As a consequence, the intermediate oxidation products like DFF and HMFCA do not reach high concentration levels and the rates of formation of further oxidation products never reach high values. In the presence of catalyst, a higher concentration of DFF and HMFCA is reached, allowing the formation of significant amounts of FFCA and FDCA.

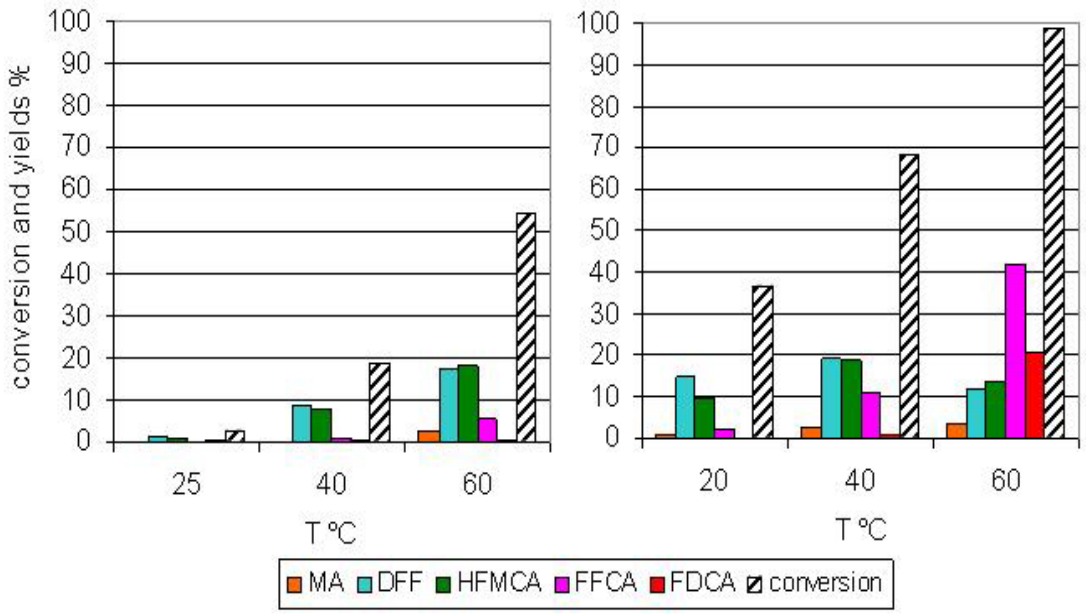

Figure 4.2. Conversion of HMF and yields of MA, DFF, HFMCA, FFCA and FDCA as a function of temperature in the absence of catalyst (left-hand side) and with 30 mg of catalyst Mn/(Cu+Mn)=0.33 (right-hand side). 1 mmol HMF, 1.3 ml t-BuOOH solution in 2 ml MeCN for 3h.

The yields of the reaction intermediates passes through a maximum as the conversion increases at higher temperature. The maximum yield of the primary reaction products, DFF and HFMCA, is observed after the conversion of DFF has passed 50 %, whereas

the secondary oxidation product, FFCA, becomes the main product when the conversion approaches 100 %.

4.3 Activation Energy of reaction steps

Comparison of the reaction rates at 20, 40 and 60 °C on the oxide catalyst with Mn/(Cu+Mn)=0.33 allowed to calculate the energies of activation, reported in Table 4.1. The lowest activation energy, 38 kJ/mol, is observed for the oligomerisation of HMF and other ketone-bearing molecules, a reaction likely controlled by hydration-dehydration steps. A slightly higher activation energy, 46 kJ/mol, is observed for the formation of maleic anhydride, a multiple-steps reaction involving a demethoxylation step. The oxidation of alcohol groups, either in HMF or in HMFCA, presents an activation energy of 49-50 kJ/mol. The oxidation of carbonyl groups presents a higher activation energy, 58-59 kJ/mol in HMF and DFF and 69 kJ/mol for the oxidation of FFCA to FDCA A higher activation energy for the oxidation of aldehyde than for the oxidation of alcohol was classically observed in the gas phase.[80] Our values of activation energy on mixed oxides were comparable with the activation energies between 64 and 77 kJ/mol observed for the oxidation of HMF to DFF on vanadium oxides[81],[82] or the activation energies between 35 and 40 kJ/mol for the oxidation of alcohol groups on gold catalysts.[83],[84]

Table 4.1. Activation energy of reaction steps on the oxide catalyst with Mn/(Cu+Mn)=0.33 in the temperature range 20-60 °C.

Reaction	**Ea (kJ/mol)**
HMF→MA	46
HMF→DFF	50
HMF→HFMCA	59
DFF→FFCA	58
HMFCA→FFCA	49
FFCA→FDCA	69
(HMF+DFF+FFCA)→oligomers	38

Catalytic tests were carried out with different concentrations of oxidant. Conversion and yield of analysed products formed at 60°C with molar ratios t-BuOOH/HMF 7 and 14 are reported in Figure 4.3. In the case of the reaction in the absence of catalyst, doubling the amount of t-BuOOH brings about a very limited increase of conversion and the product distribution is not significantly modified. When a mixed oxide catalyst is present, the conversion being nearly complete at both levels of oxidant, the effect of the amount of t-BuOOH can be observed as an important change of the distribution of products. A strong decrease of the products of primary oxidation, DFF and HFMCA, corresponds to a large increase of the products of secondary and tertiary oxidation, FFCA and FDCA, showing that the degree of oxidation of the products is nearly doubled at the doubling of t-BuOOH amount.

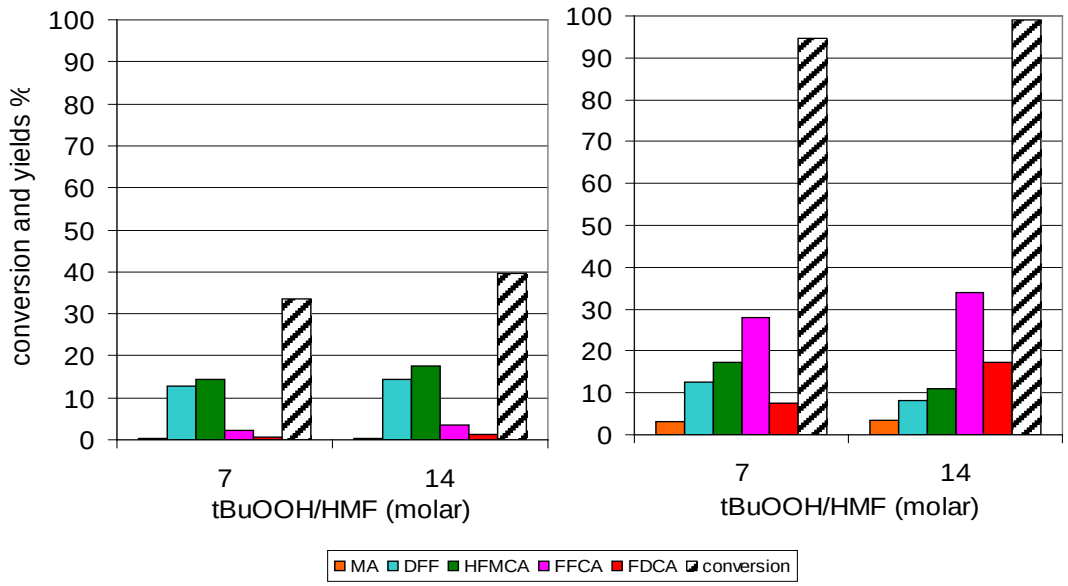

Figure 4.3. Conversion of HMF and yields of MA, DFF, HFMCA, FFCA and FDCA as a function of t-BuOOH amount in the absence of catalyst (left-hand side) and with catalyst Mn/(Cu+Mn)=0.33 (right-hand side), 60 °C for 1h.

The different sensitivity to the concentration of oxidant in the presence or absence of heterogeneous catalyst is reflected by the different orders of reaction with respects to t-BuOOH reported in Table 4.2. In the absence of catalyst, the orders of reaction with respects to t-BuOOH are fractionary and near to zero. This suggests that, at least at the low levels of reactivity observed in the absence of catalyst, t-BuOOH is always in such an excess that the reaction rate only depends on the concentration of the reagent to be oxidised.

Table 4.2. Measured orders of reaction with respects to t-BuOOH in the absence and presence of oxide catalyst

Reaction	**t-BuOOH order of reaction**	
	no catalyst	**Mn/(Cu+Mn)=0.33**
HMF→MA	-0.20	1.01
HMF→DFF	0.27	0.84
HMF→HFMCA	0.39	0.87
DFF→FFCA	0.32	1.08
HMFCA→FFCA	0.32	1.02
FFCA→FDCA	0.31	0.65
(HMF+DFF+FFCA)→oligomers	-0.16	-0.07

In the presence of an oxide catalyst, the oxidation reactions depend on the concentration of t-BuOOH by a reaction order near to unity. Instead, the rate of the unwanted oligomerisation reactions is unaffected by the concentration of oxidant, acid formation can be expected by a process with hydration-dehydration elementary steps.

In the simplified kinetic scheme used for the evaluation of the reaction rate constants, a reaction order one was attributed to all reagents to be oxidised or oligomerised. The order with respects to t-BuOOH was assumed to be zero for the reactions in the absence of catalyst and for the oligomerisation processes, whereas order one was assumed for the oxidation reactions in the presence of oxide catalysts.

4.4 Rate constants

The rate constants measured in blank tests at 60°C in the absence of catalyst are reported in Figure 4.4. All steps of oxidation, both of the carbonyl groups of HMF, DFF and FFCA or of the alcohol groups of HMF and HMFCA, present a very similar rate

constant. Among the unwanted byreactions, the fastest one is the condensation of oligomers, which does not imply any oxidation step but could be easily catalysed by the acids formed by the main oxidation reactions.[85]

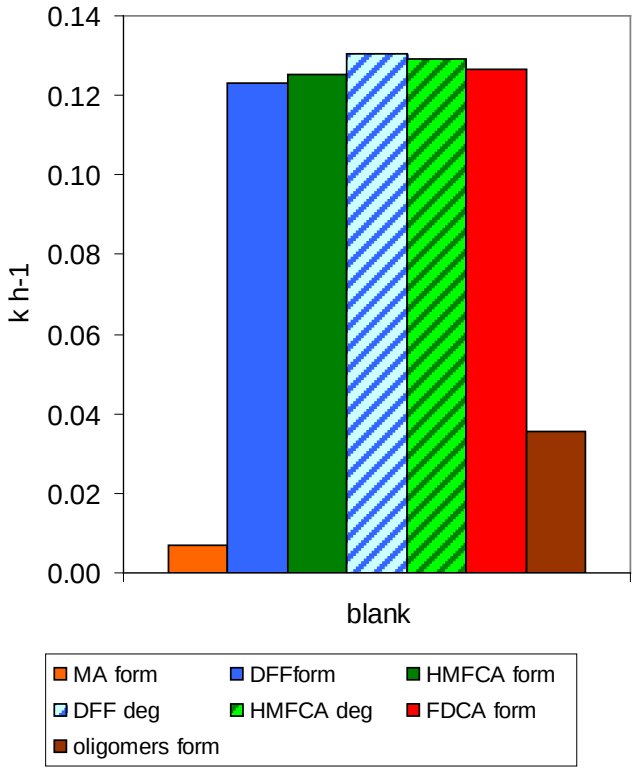

Figure 4.4. Reaction rate constants in the absence of catalyst at 60 °C (form: formation; deg: oxidative degradation)

The composition of the oxide catalysts strongly affected the reaction rates. The reaction rates on the catalysts of the Cu-Mn system are reported in Figure 4.5. The activity of the mixed oxide catalysts was much higher than the activity of the single-component copper or manganese end-terms. If the end-terms are compared, the CuO catalyst was twice more active than the Mn_3O_4 catalyst, despite presenting less than half the surface area of the latter (see Table 3.8. Textural characterisation of Cu-Mn catalysts). Among the Cu-Mn mixed catalyst, the activity was roughly proportional to the surface area, the most active one being the one with Mn/(Cu+Mn) ratio 0.33 and more than 100 $m^2\ g^{-1}$ surface area.

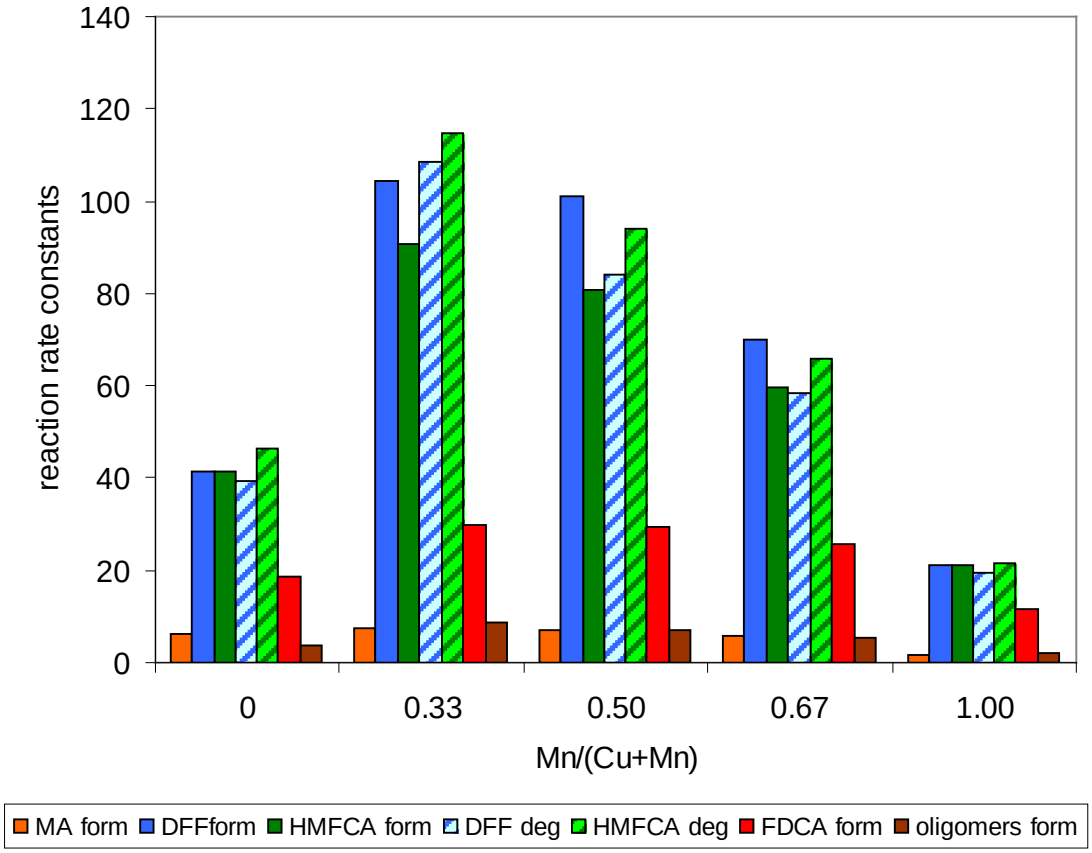

Figure 4.5. Reaction rate constants on Cu-Mn oxide catalysts at 60°C (form: formation; deg: oxidative degradation) (k in dm^3 mol^{-1} h^{-1} g^{-1} for oxidation reactions and h^{-1} g^{-1} for oligomerisation).

Once the differences of activity taken into account, the pattern of selectivity distribution was quite similar for the different catalysts. For each catalyst, the primary and secondary oxidation reactions presented quite similar rate constants. The oxidation of alcohol groups (HMF to DFF and HMFCA to FFCA) were just about 10 % faster than the oxidation of carboxyl groups (HMF to HMFCA and DFF to FFCA). The oxidation of FFCA to FDCA was significantly slower than the primary or secondary oxidation reactions. The rate constants of the slower side reactions leading to maleic anhydride and oligomers also followed the general trend between the activity levels of the different catalysts.

The reaction rates on the catalysts of the Co-Fe system are reported in Figure 4.6. The evolution of the activity with the composition of the catalyst seems to follow a trend similar to the behaviour of the Cu-Mn system, with a low activity of the single-cation

end-terms and the higher activity of the intermediate mixed oxides featuring a maximum for a divalent fraction 0.33. Indeed, the Co/(Co+Fe) 0.33 catalyst presents nearly the same activity per surface area as the catalyst with Mn/(Cu+Mn) 0.33 catalyst, with just a slightly faster oxidation of FFCA to FDCA. Nevertheless, a more detailed analysis reveals some significant peculiarities of the Co-Fe system. Indeed, the three Co-Fe mixed spinels present nearly identical surface areas (see Table 3.3. BET surface area of Co-Fe catalysts). As a consequence, the sharp decrease of activity for Co fractions higher than 0.33 should be attributed to a significant difference of specific activity. It can be observed that supported Co-Fe spinels with equivalent amounts of Fe and Co were shown more active than $CoFe_2O_4$ catalysts also in the reforming of methanol.[86]

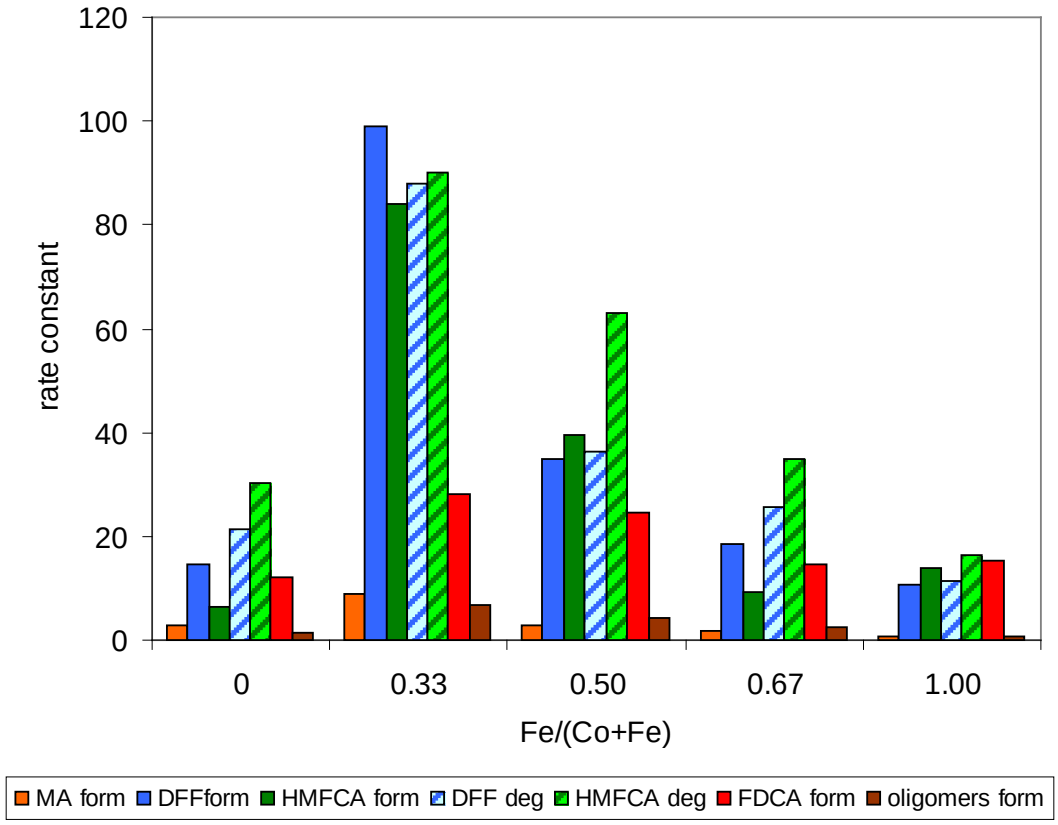

Figure 4.6. Reaction rate constants on Fe-Co oxide catalysts at 60 °C (form: formation; deg: oxidative degradation) (k in dm^3 mol^{-1} h^{-1} g^{-1} for oxidation reactions and h^{-1} g^{-1} for oligomerisation)

The activity of spinels as redox catalysts has been often related to the inversion degree and, more specifically, to the presence of both M^{2+} and Fe^{3+} cations in the octahedral sites, resulting in an inter-valence electron charge transfer between M^{2+}-M^{3+} and Fe^{2+}-Fe^{3+} ion pairs.[87] It is tempting to correlate the highest oxidation activity of the sample with Fe/(Co+Fe) 0.33 to the unusual presence of a significant amount of Fe^{2+} and Co^{3+} cations in the octahedral site.

The selectivities on Co-Fe catalysts can be compared with the ones in the Cu-Mn system. In both cases the oxidation of alcohol groups is slightly faster than the oxydation of carbonyl groups. It can however be observed that in the Co-Fe system secondary and tertiary oxidations are slightly more favoured than primary oxidation reactions.

Conclusion

Two series of mixed oxide catalysts with nominal composition $M^1_{3-x}M^2_xO_4$ have been synthesized with non-noble metals, wherein M^1=Co and M^2=Fe or M^1=Cu and M^2=Mn, by cost effective co-precipitation method. Each serie consists of 5 catalysts with the cation fractions $M^2/(M^1+M^2)$ of 0.00, 0.33, 0.50, 0.67, 1.00. The catalysts have been characterised by various techniques, then employed in the cascade HMF to FDCA oxidation process.

Single-component oxides showed a poor specific activity in our conditions with the exception of CuO, itself hampered by its low surface area. Mixed oxides performed significantly better, confirming the importance of internal redox coupling in oxidation catalysts. In the Cu-Mn system, the $Cu_{1.5}Mn_{1.5}O_4$ spinel proved an effective catalyst but the role of residual CuO and amorphous Mn oxides is worth further investigation. In the Fe-Co system, the high activity of Co-rich mixed spinels is clearly related to their peculiar cation distribution. The comparison of the activation energies of the different steps of the reaction cascade provides suggestions for the optimal conduction of the biorefinery process.

References

[1] P. McKendry, *Bioresour. Technol.* **2002**, *83*, 37–46.

[2] X. Liu, J. Xiao, H. Ding, W. Zhong, Q. Xu, S. Su, D. Yin, *Chem. Eng. J.* **2016**, *283*, 1315–1321.

[3] A. Corma, S. Iborra, A. Velty, *Chem. Rev.* **2007**, *107*, 2411–502.

[4] E. M. Rubin, *Nature* **2008**, *454*, 841–5.

[5] M. J. Climent, A. Corma, S. Iborra, *Green Chem.* **2014**, *16*, 516–547.

[6] K. Triantafyllidis, A. Lappas, M. Stöcker, *The Role of Catalysis for the Sustainable Production of Bio-Fuels and Bio-Chemicals*, Elsevier, Oxford, **2013**.

[7] A. a. Rosatella, S. P. Simeonov, R. F. M. Frade, C. a. M. Afonso, *Green Chem.* **2011**, *13*, 754.

[8] J. Liu, Y. Tang, K. Wu, C. Bi, Q. Cui, *Carbohydr. Res.* **2012**, *350*, 20–24.

[9] T. A. Werpy, J. E. Holladay, J. F. White, *Top Value Added Chemicals From Biomass: I. Results of Screening for Potential Candidates from Sugars and Synthesis Gas*, Richland, WA, **2004**.

[10] M. E. Zakrzewska, E. Bogel-Łukasik, R. Bogel-Łukasik, *Chem. Rev.* **2011**, *111*, 397–417.

[11] J. J. Bozell, G. R. Petersen, *Green Chem.* **2010**, *12*, 539.

[12] B. Wu, Y. Xu, Z. Bu, L. Wu, B.-G. Li, P. Dubois, *Polymer (Guildf).* **2014**, *55*, 3648–3655.

[13] E. de Jong, M. A. Dam, L. Sipos, G.-J. M. Gruter, **2012**, pp. 1–13.

[14] J. Lewkowski, *ARKIVOC* **2001**, *2001*, 17–54.

[15] V. Menon, M. Rao, *Prog. Energy Combust. Sci.* **2012**, *38*, 522–550.

[16] R. J. a. Gosselink, E. de Jong, B. Guran, a. Abächerli, *Ind. Crops Prod.* **2004**, *20*, 121–129.

[17] E. L. Kunkes, D. A. Simonetti, R. M. West, J. C. Serrano-ruiz, C. A. Gärtner, J. A. Dumesic, *Science (80-.).* **2008**, *1381*, 417–421.

[18] Z. Miao, T. E. T. E. Grift, A. C. A. C. Hansen, K. K. C. C. Ting, *Biofuels* **2013**, *4*, 5–8.

[19] P. Anastas, N. Eghbali, *Chem. Soc. Rev.* **2009**, *39*, 301.

[20] J. Zakzeski, P. C. A. Bruijnincx, A. L. Jongerius, B. M. Weckhuysen, *Chem. Rev.* **2010**, *110*, 3552–3599.

[21] R. Sahu, P. L. Dhepe, *React. Kinet. Mech. Catal.* **2014**, *112*, 173–187.

[22] N. Ballarini, F. Cavani, S. Passeri, L. Pesaresi, A. F. Lee, K. Wilson, *Appl. Catal. A Gen.* **2009**, *366*, 184–192.

[23] Y. L. Huang, W. B. Fan, Y. H. Hou, K. X. Guo, Y. F. Ouyang, Z. W. Liu, *J. Magn. Magn. Mater.* **2017**, *429*, 263–269.

[24] E. Hema, A. Manikandan, P. Karthika, S. A. Antony, B. R. Venkatraman, *J. Supercond. Nov. Magn.* **2015**, *28*, 2539–2552.

[25] J. Hao, W. Yang, Z. Zhang, S. Pan, B. Lu, X. Ke, B. Zhang, J. Tang, *Nanoscale* **2013**, *5*, 3078–82.

[26] Y. Tanaka, R. Kikuchi, T. Takeguchi, K. Eguchi, *Appl. Catal. B Environ.* **2005**, *57*, 211–222.

[27] P. Hirunsit, K. Faungnawakij, *J. Phys. Chem. C* **2013**, *117*, 23757–23765.

[28] Y. Tanaka, T. Utaka, R. Kikuchi, T. Takeguchi, K. Sasaki, K. Eguchi, *J. Catal.* **2003**, *215*, 271–278.

[29] Davis, S.C., Hay, Pierce, W., J., *Biomass in the Energy Industry : An Introduction*, **2014**.

[30] U.S. Energy Information Administration, *International Energy Outlook 2016*, **2016**.

[31] G. Centi, P. Lanzafame, S. Perathoner, *Catal. Today* **2011**, *167*, 14–30.

[32] S. Dutta, S. De, B. Saha, *Biomass and Bioenergy* **2013**, *55*, 355–369.

[33] S. Zinoviev, F. Müller-Langer, P. Das, N. Bertero, P. Fornasiero, M. Kaltschmitt, G. Centi, S. Miertus, *ChemSusChem* **2010**, *3*, 1106–1133.

[34] C.-H. Zhou, X. Xia, C.-X. Lin, D.-S. Tong, J. Beltramini, *Chem. Soc. Rev.* **2011**, *40*, 5588–617.

[35] M. Wüstefeld, K. de Groot, *J. Biomed. Mater. Res.* **1989**, *23*, 41–71.

[36] World Intellectual Property Organization, *World Intellectual Property Indicators*, **2016**.

[37] T. Becker, E. Curry, A. Jentzsch, W. Palmetshofer, *New Horizons for a Data-Driven Economy: Roadmaps and Action Plans for Technology, Businesses, Policy, and Society*, **2016**.

[38] S. Rebouillat, F. Pla, *J. Biomater. Nanobiotechnol.* **2016**, *7*, 167–213.

[39] D. Lapray, S. Rebouillat, *Int. J. Innov. Appl. Stud.* **2014**, *7*, 1251–1273.

[40] World Intellectual Property Organization, *Patent Landscape Report : Microalgae-Related Technologies*, **2016**.

[41] J. E. Holladay, J. F. White, J. J. Bozell, D. Johnson, **2007**, *II*.

[42] A. Gandini, *Green Chem.* **2011**, *13*, 1061.

[43] A. Gandini, D. Coelho, M. Gomes, B. Reis, A. Silvestre, *J. Mater. Chem.* **2009**, *19*, 8656.

[44] R.-J. van Putten, J. C. van der Waal, E. de Jong, C. B. Rasrendra, H. J. Heeres, J. G. de Vries, *Chem. Rev.* **2013**, *113*, 1499–597.

[45] T. Wang, M. W. Nolte, B. H. Shanks, *Green Chem.* **2014**, *16*, 548–572.

[46] R. L. de Souza, H. Yu, F. Rataboul, N. Essayem, *Challenges* **2012**, *3*, 212–232.

[47] J. Lan, J. Lin, Z. Chen, G. Yin, *ACS Catal.* **2015**, *5*, 2035–2041.

[48] A. S. Amarasekara, D. Green, E. McMillan, *Catal. Commun.* **2008**, *9*, 286–288.

[49] J. K. Rajput, G. Kaur, *Chinese J. Catal.* **2013**, *34*, 1697–1704.

[50] C. Perego, P. Villa, *Catal. Today* **1997**, *34*, 281–305.

[51] N. D. Kandpal, N. Sah, R. Loshali, R. Joshi, J. Prasad, *J. Sci. Ind. Res.* **2014**, *73*, 87–90.

[52] K. Sreekumar, S. Sugunan, *J. Mol. Catal. A Chem.* **2002**, *185*, 259–268.

[53] G. K. Williamson, W. H. Hall, *Acta Metall.* **1953**, *1*, 22–31.

[54] P. Scherrer, *Nachrichten von der Gesellschaft der Wissenschaften zu Göttingen, Math. Klasse* **1918**, *26*, 98–100.

[55] S. Brunauer, P. H. Emmett, E. Teller, *J. Am. Chem. Soc.* **1938**, *60*, 309–319.

[56] A. V. Neimark, P. I. Ravikovitch, *Microporous Mesoporous Mater.* **2001**, *44–45*, 697–707.

[57] J. Greener, B. Abbasi, E. Kumacheva, *Lab Chip* **2010**, *10*, 1561–1566.

[58] P. Kubelka, F. Munk, *Zeitschrift für Tech. Phys.* **1931**, *12*, 593–601.

[59] J. Tauc, R. Grigorovici, A. Vancu, *Phys. Status Solidi* **1966**, *15*, 627–637.

[60] P. Mountapmbeme Kouotou, H. Vieker, Z. Y. Tian, P. H. Tchoua Ngamou, A. El Kasmi, A. Beyer, A. Gölzhäuser, K. Kohse-Höinghaus, *Catal. Sci. Technol.* **2014**, *4*, 3359.

[61] T. S. Hansen, I. Sádaba, E. J. García-Suárez, A. Riisager, *Appl. Catal. A Gen.* **2013**, *456*, 44–50.

[62] S. M. Payne, F. M. Kerton, *Green Chem.* **2010**, *12*, 1648.

[63] S. Induri, S. Sengupta, J. K. Basu, *J. Ind. Eng. Chem.* **2010**, *16*, 467–473.

[64] A. Denton, N. Ashcroft, *Phys. Rev. A* **1991**, *43*, 3161–3164.

[65] H. S. C. O'Neill, A. Navrotsky, *Am. Mineral.* **1983**, *68*, 181–194.

[66] B. Lavina, G. Salviulo, D. Della Giusta, *Phys. Chem. Miner.* **2002**, *29*, 10–18.

[67] R. J. Hill, J. R. Craig, G. V. Gibbs, *Phys. Chem. Miner.* **1979**, *4*, 317–339.

[68] C. Borgohain, K. K. Senapati, D. Mishra, K. C. Sarma, P. Phukan, *Nanoscale* **2010**, *2*, 2250–2256.

[69] V. C. Farmer, Ed. , *The Infrared Spectra of Minerals*, Mineralogical Society Of Great Britain And Ireland, **1974**.

[70] P. Wei, M. Bieringer, L. M. D. Cranswick, A. Petric, *J. Mater. Sci.* **2010**, *45*, 1056–1064.

[71] a. D. D. Broemme, V. a. M. Brabers, *Solid state Ionics* **1985**, *16*, 171–178.

[72] S. Behar, P. Gonzalez, P. Agulhon, F. Quignard, D. Świerczyński, *Catal. Today* **2012**, *189*, 35–41.

[73] S. Albonetti, A. Lolli, V. Morandi, A. Migliori, C. Lucarelli, F. Cavani, *Appl. Catal. B Environ.* **2015**, *163*, 520–530.

[74] J. Artz, S. Mallmann, R. Palkovits, *ChemSusChem* **2015**, *8*, 672–679.

[75] O. Casanova, S. Iborra, A. Corma, *ChemSusChem* **2009**, *2*, 1138–1144.

[76] Z. Du, J. Ma, F. Wang, J. Liu, J. Xu, *Green Chem.* **2011**, *13*, 554–557.

[77] J. Horvat, B. Klaić, B. Metelko, V. Šunjić, *Tetrahedron Lett.* **1985**, *26*, 2111–2114.

[78] I. van Zandvoort, E. J. Koers, M. Weingarth, P. C. A. Bruijnincx, M. Baldus, B. M. Weckhuysen, *Green Chem.* **2015**, *17*, 4383–4392.

[79] S. K. R. Patil, J. Heltzel, C. R. F. Lund, *Energy and Fuels* **2012**, *26*, 5281–5293.

[80] J. Zhu, S. Lars, T. Andersson, *J. Catal.* **1990**, *126*, 92–100.

[81] C. Moreau, R. Durand, C. Pourcheron, D. Tichit, *Heterog. Catal. Fine Chem. IV Proc. 4th Int. Symp. Heterog. Catal. Fine Chem.* **1997**, *Volume 108*, 399–406.

[82] J. Nie, H. Liu, *Pure Appl. Chem.* **2012**, *84*, 765–777.

[83] Y. Guan, E. J. M. Hensen, *Appl. Catal. A Gen.* **2009**, *361*, 49–56.

[84] L. Ardemani, G. Cibin, A. J. Dent, M. A. Isaacs, G. Kyriakou, A. F. Lee, C. M. A. Parlett, S. A. Parry, K. Wilson, *Chem. Sci.* **2015**, *6*, 4940–4945.

[85] S. K. R. Patil, C. R. F. Lund, *Energy and Fuels* **2011**, *25*, 4745–4755.

[86] I. Genova, T. Tsoncheva, M. Dimitrov, D. Paneva, B. Tsyntsarski, R. Ivanova, Z. Cherkezova-Zheleva, T. Budinova, D. Kovacheva, I. Mitov, et al., *Catal. Commun.* **2014**, *55*, 43–48.

[87] I. Ibrahim, I. O. Ali, T. M. Salama, A. A. Bahgat, M. M. Mohamed, *Appl. Catal. B Environ.* **2016**, *181*, 389–402.

BIOMASS VALORIZATION FOR THE PRODUCTION OF VALUE-ADDED CHEMICALS AND BIO-FUELS

Abstract

Two series of mixed oxide catalysts with nominal composition $M^1_{3-x}M^2_xO_4$ have been synthesized with non-noble metals, wherein M^1=Co and M^2=Fe or M^1=Cu and M^2=Mn, by cost effective co-precipitation method. Each serie consists of 5 catalysts with the cation fractions $M^2/(M^1+M^2)$ of 0.00, 0.33, 0.50, 0.67, 1.00. The catalysts have been characterised using XRD, EDX, N_2 physisorption, FT-IR, UV-VIS, TEM and TPR techniques, then employed in the successive oxidation reactions of biomass derived 5-hydroxymethylfurfural (HMF) to several value added chemicals, which have a diverse portfolio of applications in various industries, including maleic anhydride (MA), 2,5-furandicarboxaldehyde (DFF), 5-Hydroxymethyl-2-furancarboxylic acid (HMFCA), 5-formyl-2-furancarboxylic acid (FFCA) and 2,5-furandicarboxylic acid (FDCA), which can serve as an alternative substitute for fossil fuel derived terephthalic acid in the production of polyethylene terephthalate (PET) plastics. The oxidation reaction products of HMF were analyzed by HPLC then kinetics study has been performed. The ultimate goal is not only to investigate the correlations between physicochemical properties and catalytic performances of the aforementioned catalysts on the complex cascade HMF to FDCA oxidation process but also to make a humble contribution to the scientific literature for a sustainable, renewable and greener world.

Keywords: Biomass, valorisation, 5-hydroxymethylfurfural, HMF, 2,5-furandicarboxylic acid, FDCA, spinel, cobalt-iron, copper-manganese

Riassunto

Due serie di catalizzatori a base di ossidi misti con composizione nominale $M^1_{3-x}M^2_xO_4$ sono stati sintetizzati con metalli non nobili, in cui M^1=Co e M^2=Fe o M^1=Cu e M^2=Mn, con il metodo della co-precipitazione. Ogni serie è composta da 5 catalizzatori con rapporti tra i cationi pari a $M^2/(M^1+M^2)$ 0.00, 0.33, 0.50, 0.67, 1.00. I catalizzatori sono stati caratterizzati attraverso tecniche XRD, EDX, fisisorbimento di N_2, FT-IR, UV-VIS, TEM e TPR, e successivamente testati nelle reazioni di ossidazione del 5-idrossimetilfurfurale (HMF) derivante da biomasse a diversi intermedi ad elevato valore aggiunto, che hanno importanti applicazioni in vari settori dell'industria chimica, tra cui l'anidride maleica (MA), la 2,5-furandicarboxaldeide (DFF), l'acido 5-idrossimetil-2-furancarbossilico (HMFCA), e l'acido 5-formil-2-furancarbossilico (FFCA) e l'acido 2,5-furandicarbossilico (FDCA), che è importante come un sostituto alternativo all'acido tereftalico derivato da materie prime fossili per la produzione di polietilenetereftalato (PET). I prodotti di reazione derivanti dall'ossidazione del HMF sono stati analizzati mediante HPLC ed è stato eseguito un approfondito studio cinetico. L'obiettivo finale è stato non solo quello di trovare una correlazione tra proprietà fisico-chimiche ed attività catalitica dei catalizzatori presi in esame per la complessa trasformazione dell'HMF a FDCA, ma anche quello di dare un contributo consistente ai processi chimici industriali alla base di uno sviluppo sostenibile della società.

Parole chiave: valorizzazione biomassa, 5-idrossimetilfurfurale, HMF, acido 2,5-furandicarbossilico, FDCA, struttura spinello, cobalto-ferro, rame-manganese

Résumé

On a synthétisé deux séries de catalyseurs d'oxydes mixtes de composition nominale $M^1_{3-x}M^2_xO_4$ avec des métaux non nobles, dans laquelle M^1=Co et M^2=Fe ou M^1=Cu et M^2=Mn, par un procédé de co-précipitation rentable. Chaque série se compose de 5 catalyseurs avec les fractions cationiques $M^2/(M^1+M^2)$ de 0,00, 0,33, 0,50, 0,67, 1,00. Les catalyseurs ont été caractérisés en utilisant les techniques de XRD, EDX, physisorption de N2, FT-IR, UV-VIS, TEM et TPR, puis utilisés dans les réactions d'oxydation successives de la 5-hydroxyméthylfurfural dérivée de la biomasse (HMF) vers plusieurs produits chimiques à valeur ajoutée qui ont Un large éventail d'applications dans diverses industries. Ces produits comprennent l'anhydride maléique (MA), le 2,5-furandicarboxaldéhyde (DFF), l'acide 5-hydroxyméthyl-2-furancarboxylique (HMFCA), l'acide 5 formyl-2 furancarboxylique (FFCA) , L'acide 5-furandicarboxylique (FDCA), qui peut servir de substitut alternatif à l'acide téréphtalique dérivé du combustible fossile dans la production de plastiques de poly (éthylène téréphtalate) (PET). Les produits de réaction d'oxydation de HMF ont été analysés par CLHP puis une étude cinétique a été réalisée. Le but ultime est non seulement d'étudier les corrélations entre les propriétés physico-chimiques et les performances catalytiques des catalyseurs mentionnés sur le processus d'oxydation en cascade complexe de HMF à FDCA, mais aussi d'apporter une contribution modeste à la littérature scientifique pour un monde durable, renouvelable et plus vert.

Mots-clés: Biomasse, valorisation, 5-hydroxyméthylfurfural, HMF, acide 2,5-furandicarboxylique, FDCA, spinelle, cobalt-fer, cuivre-manganèse